Structural and kinetic characterization of the mechanism of regulation of phosphoenolpyruvate carboxykinase by anions

by

Sarah Barwell

A thesis

presented to the University of Waterloo

in fulfilment of the

thesis requirement for the degree of

Master of Science

in

Biology

Waterloo, Ontario, Canada, 2019

Author's declaration

I hereby declare that I am the sole author of this thesis. This is a true copy of the thesis, including any required final revisions, as accepted by my examiners.

I understand that my thesis may be made electronically available to the public.

Abstract

Phosphoenolpyruvate carboxykinase (PEPCK) catalyses a reaction that is known to be thermodynamically reversible. In contrast to this thermodynamic reversibility, in eukaryotes, PEPCK is observed to primarily catalyze the forward direction, converting oxaloacetic acid to phosphoenolpyruvate as one of the principle steps in gluconeogenesis. Based upon these seemingly conflicting pieces of data, we hypothesize that there must be an underlying mechanism regulating the kinetic reversibility of the catalyzed reaction *in vivo*.

To this end, we present structural and kinetic evidence for the presence of an allosteric site in PEPCK, which we propose binds negatively charged ions such as chloride which is found in abundance *in vivo*. This allosteric regulation serves to inhibit catalysis in the reverse direction and contribute to the observed unidirectionality in the direction of PEP synthesis *in vivo*. As supporting evidence for this hypothesis, we have collected anomalous diffraction data on several PEPCK crystals that have been exposed to a range of iodide concentrations. From the corresponding anomalous signals at each concentration, we were able to analyze anomalous peak heights and generate binding isotherms for various anion binding sites on PEPCK. Importantly, one of these anion binding sites was observed to titrate with increasing iodide concentration, yielding an apparent binding constant similar to that obtained from our kinetic inhibition studies. This site was in contrast to the others which were shown to not titrate over the same range of iodide concentrations.

The anomalous data in combination with the kinetic data were essential in assigning the allosteric mechanism of regulation as the origin of the observed inhibition. This result was in contrast to preliminary anomalous maps calculated at saturating concentrations of iodide which suggested anions binding to the active site in a purely competitive fashion. This allosteric mechanism of inhibition was further validated through additional anomalous diffraction and kinetic studies on three mutant enzyme variants, giving strong support for the proposed mechanism of regulation, an effect that has interesting biological ramifications for the *in vivo* functioning of PEPCK.

Acknowledgements

I would first like to thank my supervisor, Dr. Todd Holyoak, for allowing me to complete my Masters degree by doing my research project in his lab. I am grateful for the opportunity to attend graduate school, which would not be an option without the funding and guidance provided by Todd. Although busy with his own responsibilities as a professor and an undergraduate advisor, he always made time for us graduate students, and encouraged our progress through weekly meetings with everyone in the lab.

I would also like to thank my committee members, Dr. David Rose and Dr. Elizabeth Meiering, for offering their unique perspectives and advice towards my thesis project, as well as finding time in their schedules to attend meetings, answer emails and read my reports. My thesis would not complete without their feedback and critiques.

Special thanks go to April Wettig, the administrative coordinator of graduate studies for the Department of Biology. She was always quick to answer emails and very easy to approach in person, and was essential in ensuring I met degree requirements on time.

Acknowledgements would not be complete without a nod towards my fellow graduate students, both in the Holyoak lab as well as the Rose lab, our sister lab next door. They were quick to lend a hand explaining new techniques and how to use laboratory equipment when I first began my degree, and we still bounce ideas off each other to this day. My peers were essential in creating a friendly and supportive environment, and it was a wonderful experience attending monthly coffee hours and other social events run by the BGSA.

Dedication

I dedicate my thesis to my mother, for her support and enthusiasm towards the sciences. Though she has passed, I know she would be proud of how far I've come.

Table of Contents

List of Figures

List of Tables

List of Acronyms & Abbreviations

Å	angstroms
A_{280}	absorbance at 280 nm
A_{340}	absorbance at 340 nm
ADP	adenosine diphosphate
AI	auto-induction
ASU	asymmetric unit
AMP	adenosine monophosphate
ADP	adenosine diphosphate
ATP	adenosine triphosphate
BL21 (DE3)	competent *E. coli* expression cell line
C-PEPCK	cytosolic phosphoenolpyruvate carboxykinase
CCP4	Collaborative Computational Project #4
CuKα	rotating copper anode – source of incident x-ray beam
dNTP	deoxynucleoside triphosphate
DTT	dithiothreitol
Ɛ	molar extinction coefficient
FFT	Fast Fourier Transform
GDP	guanosine diphosphate
GTP	guanosine triphosphate
HEPES	4-(2-hydroxyethyl)-1-piperazineethanesulfonic acid
His_6	hexa-histidine tag
IMAC	immobilized metal affinity chromatography
IPTG	isopropyl β- D-1-thiogalactopyranoside
Kan	kanamycin
kDa	kilodaltons
keV	kiloelectron volts
K_I	inhibition constant
K_M	Michaelis constant
LB	lysogeny broth
LB-Kan	bacterial growth media containing lysogeny broth and kanamycin

LDH	lactate dehydrogenase
MAD	multi-wavelength anomalous dispersion
MDH	malate dehydrogenase
M-PEPCK	mitochondrial phosphoenolpyruvate carboxykinase
MW	molecular weight
NADH	nicotinamide adenine dinucleotide, reduced
Ni-NTA	nickel nitrilotriacetic acid, a type of metal affinity resin
NPS	nitrogen, phosphate and sulphate salts
OAA	oxaloacetic acid
OD_{600}	optical density or absorbance at 600 nm
P6DG	polyacrylamide 1000 - 6000 MW fractionation range desalting gel
PCR	polymerase chain reaction
PDB	Protein Data Bank
PEG	polyethylene glycol
PEP	phosphoenolpyruvate
PK	pyruvate kinase
PP_i	pyrophosphate
rcPEPCK	rat cytosolic phosphoenolpyruvate carboxykinase
rpm	rotations per minute
RT	ambient/room temperature – approximately 21°C
SAD	single-wavelength anomalous dispersion
SDS-PAGE	sodium dodecyl sulphate-polyacrylamide gel electrophoresis
SEC	size exclusion chromatography
SUMO	small ubiquitin-like modifier
TCEP	tris(2-carboxyethyl)phosphine
TS	transition state of a chemical reaction
V_{max}	maximum velocity
WT	wildtype
WT rcPEPCK	wildtype rat cytosolic phosphoenolpyruvate carboxykinase
XL1-blue	competent *E. coli* cloning cell line

Chapter 1: Introduction

1.0 Background of PEPCK

Glucose metabolism is tightly regulated through two distinct metabolic pathways that are not simply the reverse of one another, but act to achieve opposite goals – the breakdown of glucose or the generation of glucose (Figure 1). The catabolic pathway, known as glycolysis, begins in the cytosol with glucose gradually being broken down into a smaller molecule, pyruvate, by a series of glycolytic enzymes through several intermediate reactions. Pyruvate is then converted to acetyl-CoA and then to citrate as it cycles through the citric acid cycle (located in the mitochondria), generating ATP as a source of biochemical energy to be used by the cell.[1]

The anabolic pathway, or gluconeogenesis, is one of the pathways responsible for replenishing the body's energy storage. Through a series of enzymatic reactions, pyruvate is converted into glucose. Similar to glycolysis, the majority of the gluconeogenic pathway occurs in the cytosol, with the exception of the first few steps. In eukaryotes, the conversion of pyruvate to oxaloacetate (OAA) occurs within the mitochondria, while the enzymes needed to catalyze the reactions from phosphoenolpyruvate (PEP) onwards are located in the cytosol.[1] The enzyme that catalyzes the formation of PEP from OAA is phosphoenolpyruvate carboxykinase.

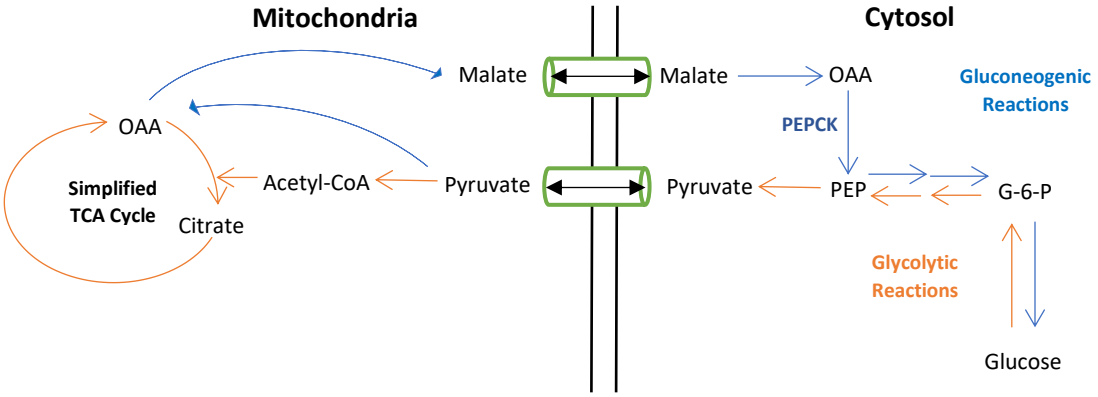

Figure 1: Simplified reaction map of glucose metabolism in the cell. Glycolytic and gluconeogenic reactions, labelled in orange and blue respectively, occur partially in both the mitochondrial matrix (left) and the cytosol (right). Pyruvate crosses the mitochondrial membrane via specialized transport proteins shown as a green cylinder.

Phosphoenolpyruvate carboxykinase (EC 4.1.1.32), known by its acronym PEPCK, is a key enzyme in the regulation of glucose metabolism. In most higher eukaryotes, PEPCK catalyzes the reaction of oxaloacetic acid (OAA) to phosphoenolpyruvate (PEP), by using guanosine triphosphate (GTP) as a phosphoryl donor.

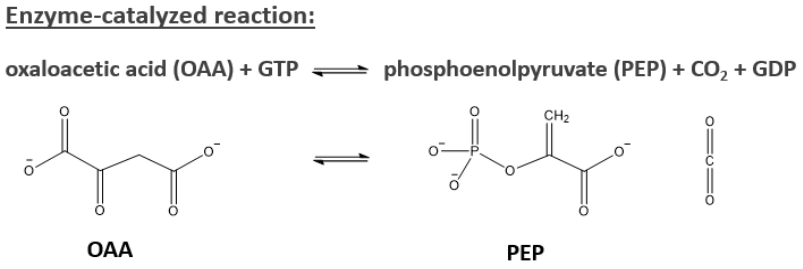

Figure 2: PEPCK-catalyzed reaction. A diagram of the PEPCK-catalyzed reaction, written in from left to right in the physiological direction of gluconeogenesis. The GTP/GDP nucleotide structure is not shown.

It is of interest to note that some prokaryotic organisms and other eukaryotes, including fungi and plants, use adenosine triphosphate (ATP) or even pyrophosphate (PPi) as a source of phosphate instead.[2] To further complicate things, PEPCK can be further divided into cytosolic and mitochondrial isoforms known as cPEPCK and mPEPCK respectively.[3]

mPEPCK is the lesser understood of the two PEPCK isoforms, and not much is known mechanistically aside from that fact that mPEPCK's structure is nearly identical to that of cytosolic PEPCK, with high sequence conservation. cPEPCK is well studied and is known for its integral role in gluconeogenesis and glyceroneogenesis, as well as its more recently discovered role as a cataplerotic enzyme involved in the recycling of amino acid skeletons.[4,5] It was previously thought that regulation of PEPCK and its role in glucose metabolism could be attributed to changes in gene expression as it has been demonstrated that transcription of the PEPCK gene is stimulated by cyclic AMP and the hormone glucagon and inhibited by insulin.[6–8] More recent research however, suggests control of PEPCK at the protein level, involving posttranslational crosstalk of acetylation, ubiquitination and phosphorylation of PEPCK contributing to the regulation of cataplerotic versus anaplerotic reactions.[9,10]

Although PEPCK primarily catalyzes the reaction of OAA to PEP, the PEPCK-catalyzed reaction is actually thermodynamically reversible, in that the reaction can proceed in either direction.[11]

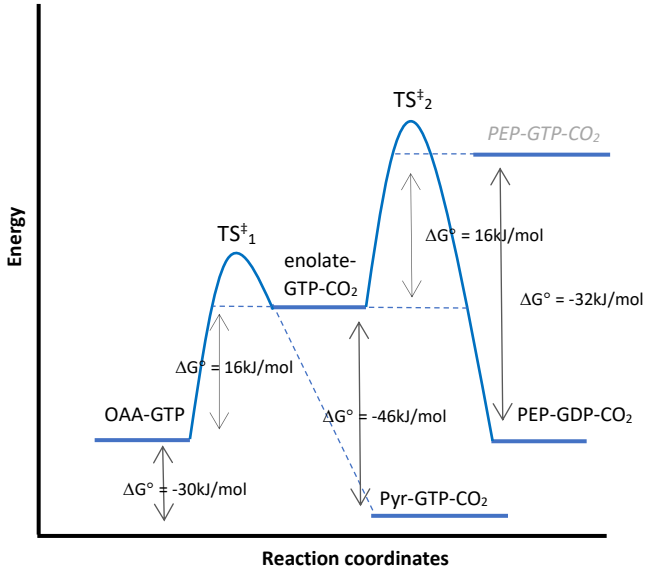

Figure 3: Reaction coordinates for the PEPCK-catalyzed reaction. A diagram showing the thermodynamic reversibility of the PEPCK-catalyzed reaction.[11]

This phenomenon of thermodynamic reversibility seemingly conflicts with the earlier statement that C-PEPCK unidirectionally catalyzes the OAA→PEP reaction, which we can call the forward direction, or the physiological direction necessary for gluconeogenesis.

Standard kinetic assays for PEPCK activity demonstrate this reaction reversibility *in vitro*. Given the ideal conditions needed to optimize activity, cPEPCK is able to catalyze the conversion of PEP to OAA, albeit with a lower maximum activity when compared to a standard activity assay performed in the forward direction.[12]

Table 1: Kinetic parameters for the PEPCK-catalyzed reaction *in vitro*.[12]

	k_{cat} (s^{-1})	k_{cat}/K_M (M^{-1} s^{-1}) (OAA/PEP)	k_{cat}/K_M (M^{-1} s^{-1}) (GTP/GDP)
OAA → PEP	52 ± 1	1.0×10^6	9.5×10^6
PEP → OAA	19 ± 1	3.7×10^4	9.2×10^4

Previous kinetic studies trying to determine the reason behind lower enzyme activity in the reverse direction have focused on the required carbon dioxide (CO_2) substrate. After assaying for enzyme activity at high concentrations of CO_2, it was concluded that there was substrate-mediated inhibition (Figure 4).[13]

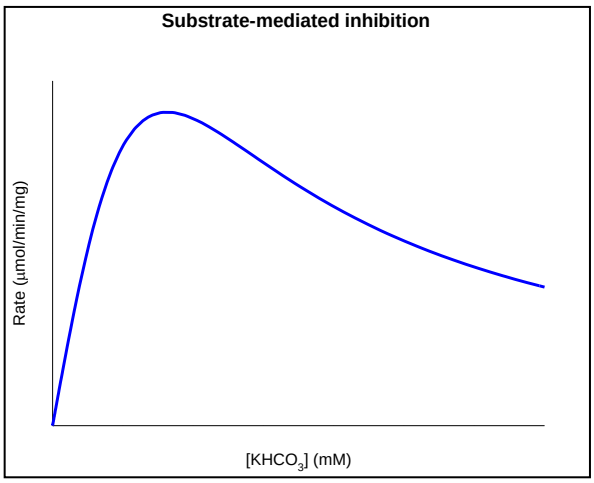

Figure 4: Substrate-mediated inhibition of PEPCK. Apparent inhibition of PEPCK activity at high concentrations of $KHCO_3$, the source of CO_2 *in vitro*.

However, our recent research suggests that this observed inhibition is not substrate-mediated, but rather due to the anionic nature of the dissolved bicarbonate anion, a source of CO_2 but not PEPCK's true substrate.

$$H_2CO_3 \rightleftharpoons HCO_3^- + H^+ \rightleftharpoons CO_2 + H_2O$$

Figure 5: Equilibrium of dissolved bicarbonate in water. A schematic of bicarbonate ion dissolved in water. By bubbling in gaseous CO_2, you can shift the equilibrium towards PEPCK's true substrate.

Investigation into the potential regulatory properties of anions is necessary in order to determine the underlying cause behind the unidirectionality of the PEPCK-catalyzed reaction *in vivo*. It is important to note that through the optimization of standard activity assays *in vitro*, the majority of salts that would be found in biological systems are removed. It is therefore accurate to say that cPEPCK would be subjected to much higher concentrations of various anionic species *in vivo*, which could have an adverse effect on enzyme function.

1.1 Enzyme Kinetics

In order to understand the effects of anionic inhibition, the enzyme kinetics of the PEPCK-catalyzed reaction must be analyzed. Enzyme kinetics refers to the study of reaction rates and substrate-binding affinities, as well as inhibitory effects on reaction rate and enzyme turnover. The reaction rate, denoted by the symbol ***v***, can be plotted against substrate concentration **[S]** to generate a plot with a distinct hyperbolic shape (Figure 6). This plot is called a Michaelis-Menten curve, named after two scientists who made significant contributions to enzyme kinetics.[14]

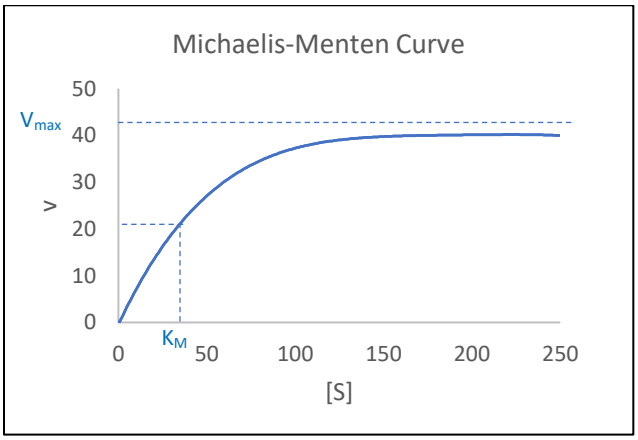

Figure 6: A basic Michaelis-Menten curve. The plot represents the rate of enzyme catalysis, *v*, as a function of substrate concentration, [S]. From this plot, the Michaelis-Menten constant, or K_M, can be derived as the substrate concentration at one half V_{max}.

Michaelis-Menten kinetics allows us to determine the maximum reaction rate, $\mathbf{V_{max}}$, and the Michaelis-Menten constant, or $\mathbf{K_M}$. The $\mathbf{K_M}$ can be calculated as the substrate concentration at half the $\mathbf{V_{max}}$, representing the enzyme's affinity for that particular substrate. However, this is often only an apparent affinity, as many other factors affect the $\mathbf{K_M}$, and may be masking the true binding affinity of the substrate to the enzyme. A more accurate definition of the Michaelis constant is the concentration of substrate at which the time required for substrate capture is equal to the time for product release.[15] The addition of an inhibitor can affect both the $\mathbf{V_{max}}$ and the $\mathbf{K_M}$, depending on the type of inhibition and mechanism of inhibitor binding.[16]

Enzyme inhibition can be categorized into three different classes: competitive, uncompetitive, or mixed inhibition, which is sometimes referred to as non-competitive inhibition in certain cases where the inhibitor can bind equally to the enzyme or enzyme-substrate complex. Inhibitors are classified into these different groups by the mechanism in which they interact with the enzyme or enzyme-substrate complex (Figure 7).

Competitive inhibitors only bind to free enzyme without substrate bound, lowering the apparent substrate affinity or $\mathbf{K_M}$ while leaving the overall reaction rate ($\mathbf{V_{max}}$) unchanged.[1] The effect on apparent $\mathbf{K_M}$ requires adding additional substrate to the assay mix to ensure saturating substrate concentrations. Uncompetitive inhibitors bind to the enzyme-substrate complex, due to a conformational change that occurs upon the substrate binding, therefore adding additional substrate has no effect. Both the apparent $\mathbf{V_{max}}$ and $\mathbf{K_M}$ are affected. Mixed inhibitors have the properties of both competitive and uncompetitive inhibition, in that the inhibitor binds to both the free enzyme and the enzyme-substrate complex.[1]

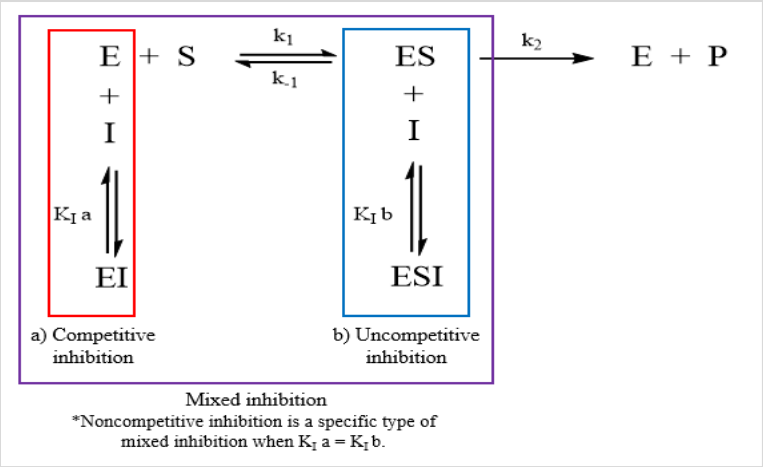

Figure 7: Types of enzyme inhibition classified by enzyme-inhibitor interactions.

Uncompetitive inhibitors can be allosteric in nature, meaning they only bind to the enzyme at a secondary site away from the catalytic active site. Competitive inhibitors generally bind at the active site where substrates would bind, but can also act in an allosteric fashion, provided the enzyme-inhibitor complex does not allow for substrate binding.

The term 'allosteric' was first coined in 1961 from the prefix '-allo' meaning 'other' and 'steric' referring to the spatial arrangement of a molecule.[17] In other words, allostery refers to a mechanism of binding where the inhibitor is not a steric analogue of the substrate. Allosteric binding was historically understood to occur in multimeric enzymes, where binding to one subunit would cause a conformational change affecting the activity of the entire enzyme. Today allostery is also understood to occur in monomeric enzymes, and recent research has suggested that allosteric binding may occur without an observable conformational change, due to the intrinsic dynamic nature of proteins.[18,19] Allosteric binding can be either inhibitory or activating in nature, and can be thought of as an ON/OFF switch.

Enzymes that are controlled by allosteric regulation are classified as either K-type, if the allosteric effector alters the K_M for the substrate, or V-type, if there is a change in their maximum enzyme activity. Most allosteric enzymes are K-type: binding of an effector to the allosteric site causes a conformational change resulting in an apparent change in affinity for the substrate at a different site.[20]

Multiple kinetic studies have already shown various different types of substrate-analogues can act as competitive inhibitors of cPEPCK and related enzymes.[21,22] Only a few allosteric inhibitors of PEPCK have been identified, including 3-mercaptopicolinate, previously identified only as an active site inhibitor.[23–25] Michaelis-Menten curves can be used to show the various forms of enzyme inhibition, in this case competitive inhibition. Through a series of kinetic inhibition assays, an inhibition constant, or K_I, can be calculated, which is a representation of the inhibition strength of that compound. An inverse relationship exists between the K_I and the strength of the inhibitor, such that the lower the K_I, the stronger the inhibitor and vice versa.

For this study on the regulation of PEPCK activity, enzyme inhibition can be studied kinetically using simple halides to represent the anionic conditions of the intracellular environment. Chloride is one of the most prevalent anions in a biological system, ranging from 10 mM up to 100 mM or higher, depending on the type of cell and organism.[26,27] Inhibition of PEPCK can be examined by performing an activity assay under increasing chloride concentrations, to mimic the physiological conditions found *in vivo*. Such inhibition assays can be performed in the 'forward' or physiological direction of catalysis by adding OAA and GTP substrates (Figure 8a). Similarly, inhibition of the 'reverse' direction of catalysis can be analyzed by adding PEP and GDP to the kinetic assay (Figure 8b).

a) Forward Direction

$$OAA + GTP \rightarrow PEP + CO_2 + GDP$$

b) Reverse Direction

$$PEP + CO_2 + GDP \rightarrow OAA + GTP$$

Figure 8: Directional PEPCK-catalyzed reactions. The PEPCK-catalyzed reaction is written as separate unidirectional reactions. The "forward" direction corresponds to the physiological direction of gluconeogenesis in biological systems, while the "reverse" direction is only observed in kinetic assays performed *in vitro.*

1.2 X-ray Crystallography

Enzyme function can also be analyzed through a structural approach, using protein crystallography. Crystallography involves the growth of protein crystals large enough to be viewed under a microscope, ideally a couple hundred microns (μm) in length. Growing crystals is a delicate process typically performed using vapour diffusion to achieve a slow and gradual removal of water from the protein sample, moving from soluble to crystalline on the protein solubility curve without causing the protein to precipitate out of solution.

The resulting crystal consists of millions of protein subunits stacked together in such a structure that has different axes of symmetry depending on the type of crystal packing. The simplest repeating unit in the crystal structure is called the Unit Cell, which is stacked in three dimensions to form the macroscopic crystal. Even smaller still is the aptly named Asymmetric Unit, or ASU, the smallest repeating component of the crystal which can contain one or more protein subunit. Applying symmetry operations to the ASU generates the unit cell (Figure 9).[28]

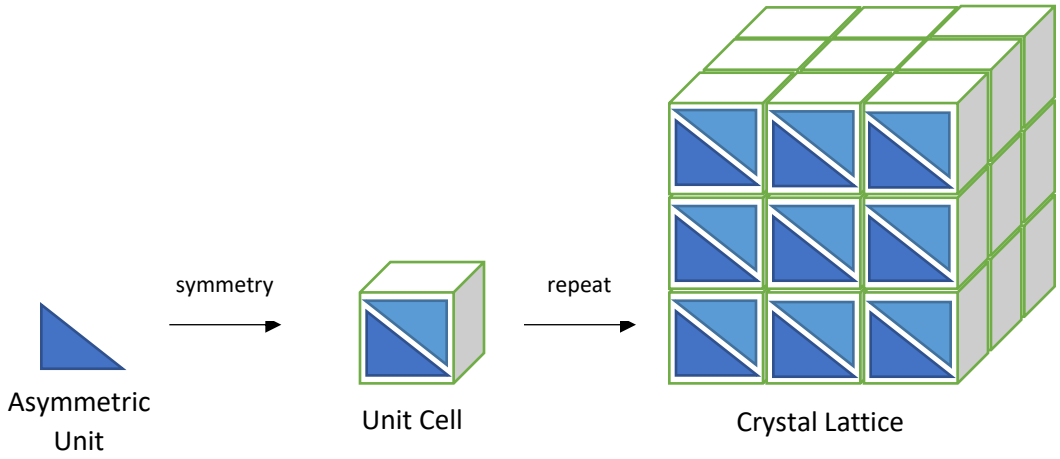

Figure 9: Assembly of unit cells into a complete crystal structure. Asymmetric units are shown as blue triangles and unit cells are shown as cubes.

To analyze protein structure, we can use a technique involving X-ray Diffraction. By subjecting a crystal to X-rays, the incident beam will diffract through the crystal, interacting with the electrons that comprise the different atoms of the peptide structure. The crystal itself acts as an amplifier to increase the diffraction signal picked up by the detector on the other side of the mounted crystal. The detector measures a series of spots or reflections that represent diffracted x-rays that are in-phase with each other, resulting in constructive interference. The resulting diffraction pattern of spots (Figure 10) gives us the intensity of the diffracted x-rays, dependent upon the exposure time the crystal is subjected to.

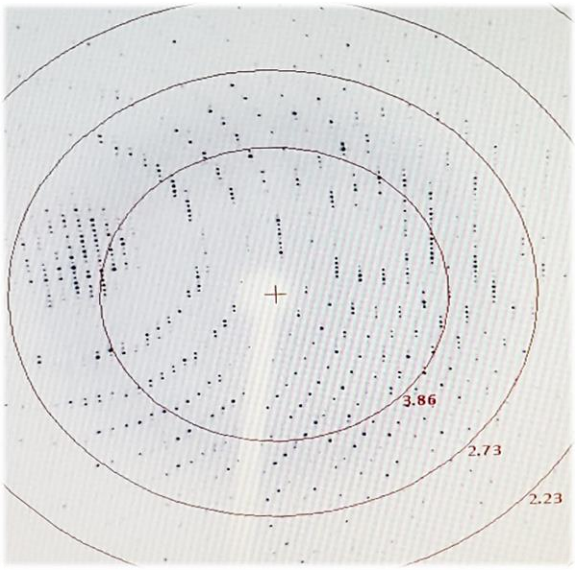

Figure 10: Example of a series of spots that make up an x-ray diffraction pattern. Multiple high-resolution images taken at 360° around the crystal make up a complete dataset that must be indexed, integrated and scaled. Resolution in Å is denoted by red circles, with high resolution data in the corners.

At this point, only the X-ray amplitudes are known, but in order to determine electron density of the atoms in the protein crystal, the phase information of the diffracted X-rays is required. Molecular replacement is a common technique that uses another crystal structure with sufficient homology to that of the protein structure being studied to obtain the phases.[29] Using the obtained phase information combined with the intensities from the diffraction pattern, we can generate electron density maps and fit amino acid residues to the electron density, provided we know the primary sequence of our protein.

When trying to solve a new crystal structure, often the PDB database will not contain any structures with sufficient homology to the protein being studied. In this case, molecular replacement is not an option, and another solution to the phase problem must be determined.

A specialized technique using isomorphous replacement followed by multi-wavelength (MAD) or single-wavelength anomalous diffraction (SAD) is another solution sometimes used to obtain phase information.[30–33] Isomorphous replacement involves the addition of heavy atoms to the protein crystal, often through soaking experiments. Anomalous diffraction or anomalous scattering is a phenomenon that occurs when an atom is hit with enough energy to excite one of its electrons, causing it to transition into a higher energy electron shell. When the electron returns to its original shell, it releases the energy with a phase shift compared to that of the incident X-rays (Figure 11). The wavelength at which the energy corresponds with an atom's ionization potential is known as an absorption edge, a sharp spike in that atom's absorption spectrum. From the anomalous phases and the intensities of the diffracted X-rays, the electron densities can be determined.

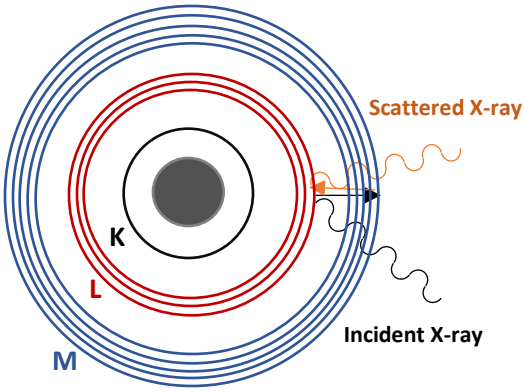

Figure 11: A schematic showing anomalous scattering of X-rays. Anomalous dispersion of x-rays occurs when the wavelength of the incident beam (shown in black) corresponds with the energy of the K, L or M shells (labelled and coloured black, red and blue respectively). The energy absorbed by an electron causes it to excite to a higher shell, eventually releasing the energy (shown in orange) and falling back to its original shell.

1.3 PEPCK Crystal Structure

The structure of rat cytosolic PEPCK, the isoform of PEPCK that we study in the lab, is already well characterized, and its structure with several ligands bound can be found on the PDB database. rcPEPCK is a 622 amino acid monomer with a globular structure, with 3 dynamic loops involved with catalytic function found at the enzyme's active site (Figure 12).[34] One of the aforementioned loops, the Ω-loop, is named for its characteristic fold in the distinct shape of the Greek omega symbol. It acts as a lid to protect reaction intermediates from unwanted chemistry, and is thus sometimes referred to as the Ω-loop lid.[35] The other two loops found within the active site are the P- and R-loops, responsible for the coordination and positioning of the GTP/GDP nucleotide and the OAA/PEP substrates respectively.[36]

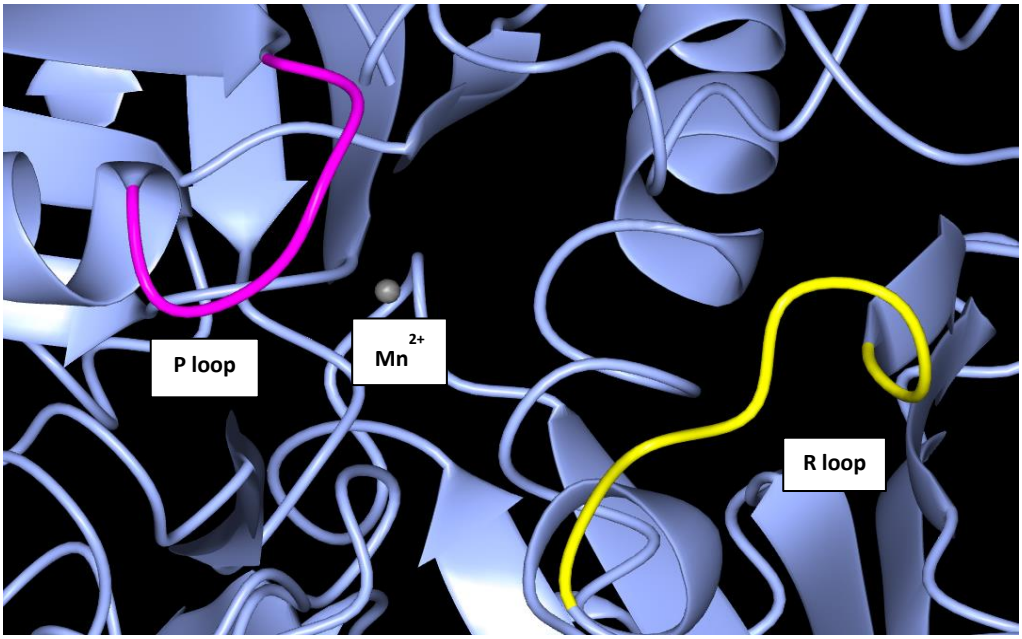

Figure 12: Ribbon structure of PEPCK's active site. PDB ID: 2QEW. The catalytically active loops, the R-loop and the P-loop, are labelled and coloured yellow and pink respectively. A single M1 manganese cation is labelled and depicted as a small grey sphere. All graphics were generated using CCP4MG.[37]

The P- and R-loops undergo conformational changes necessary for enzyme catalysis upon substrate binding.[36] This transition from a disordered to an ordered state is what allows the reaction to proceed, and any extrinsic force that prevents this transition negatively affects enzyme function.

1.4 Structural and Kinetic Analysis of PEPCK Regulation

Now that the two different approaches of enzyme characterization have been introduced, we can proceed to ask the question: although thermodynamically reversible, what factors may contribute to the typically observed unidirectionality of the PEPCK-catalyzed reaction *in vivo*? Our objective is to use a combined structural and kinetic approach to determine the possibility of the regulation of PEPCK activity *in vivo* by anions.

From kinetic data found in the literature, as well as previous kinetic assays done in our lab[38,39], it can be observed that PEPCK is catalytically active in both directions *in vitro*, which seemingly conflicts the aforementioned statement that only the "forward" direction is catalyzed in biological systems. Interestingly, although kinetic assays performed in the lab indeed show activity in the "reverse" direction, the maximum rate of catalysis is significantly lower, roughly by a factor of two when compared to assays performed in the "forward" or physiological direction of catalysis.[12]

From the aforementioned study[13], we hypothesized that anionic inhibition was occurring in the reverse direction of catalysis, leading to the observed decrease in reaction rate in that direction. Logically, this inhibitory effect would be greater *in vivo*, where PEPCK is subjected to higher concentrations of salts. Chloride is an obvious choice to study enzyme inhibition *in vitro*, due to its physiological relevance and abundance in biological systems.

For a structural approach, iodide was chosen as the inhibitor instead of chloride, due to its unique anomalous properties (Table 2). Of all of the halides we had at our disposal in the laboratory, iodide has the closest absorption edge to the wavelength generated by our home source's rotating copper anode (**CuKα = 1.54Å**). Iodide has an absorption edge around 2.4Å, or 5.2 keV, corresponding to its L-I shell.[40] Based on these intrinsic properties, we can use single-wavelength anomalous dispersion (SAD) to detect where iodide, as our anionic inhibitor, is binding to PEPCK.

Table 2: Absorption edges of various halides.[40]

X-ray Absorption Edge Iodine	keV	Å	X-ray Absorption Edge Bromine	keV	Å
K	33.1694	0.3738	K	13.4737	0.9202
L – I	**5.1881**	**2.3898**	L – I	1.7820	6.9576
L – II	4.8521	2.5553	L – II	1.5960	7.7684
L – III	4.5571	2.7207	L – III	1.5499	7.9995
M	1.0721	11.5646	**X-ray Absorption Edge Chlorine**	**keV**	**Å**
CuKα	**8.0509 keV**	**1.54 Å**	K	2.8224	4.3929

Data was generated using the web-form at http://skuld.bmsc.washington.edu/scatter/AS_form.html.

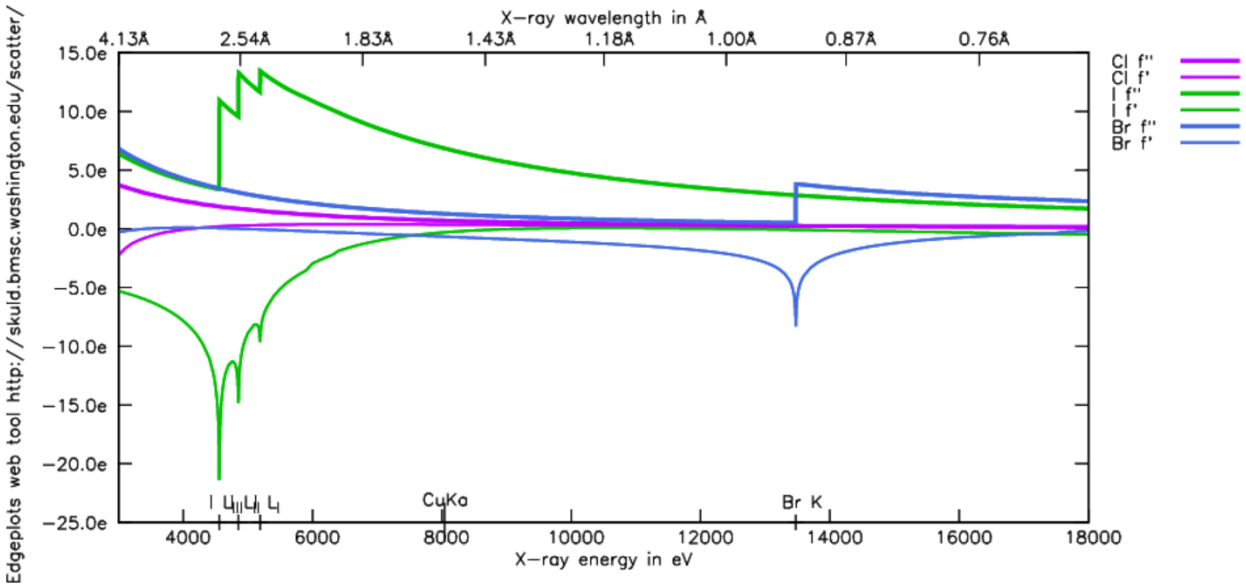

Figure 13: Absorption edge plot of common halides. The absorption spectrum of chlorine (**purple**), iodine (**green**) and bromine (**blue**), showing their various absorption edges, as well as the wavelength of the CuKα home source. The edge plot was generated using the web-form at http://skuld.bmsc.washington.edu/scatter/AS_form.html.

Combining the data from the kinetic assays with the structural information obtained using X-ray crystallography and anomalous diffraction, we can demonstrate how PEPCK is regulated to catalyze the OAA to PEP reaction in a unidirectional manner in biological systems. In this way, we can provide evidence for how the cellular environment may affect regulation of metabolic pathways at a structure-function level.

Chapter 2: Experimental Procedures

2.1 Materials

GDP and ADP were purchased from Combi Blocks and BioShop respectively. GTP, PEP, and NADH were purchased from Chem-Impex International, and OAA was purchased from Millipore Sigma (CalBioChem). Co-NTA resin was purchased from UBP Bio and regenerated in the laboratory as Ni-NTA resin. P6DG and Chelex resin were purchased from BioRad. TCEP and DTT reducing agents were purchased from GoldBio.

2.2 Enzymes

The enzymes used in the coupled-enzyme assay for PEPCK activity, pyruvate kinase, lactate dehydrogenase and malate dehydrogenase, were used as provided by the supplier (Calzyme). The plasmid expressing His_6-SUMO protease was a gift from C. Lima (Sloan-Kettering Institute, New York, NY). The SUMO protease was expressed and purified via the protocol below.

A 50 mL culture of BL21 *E. coli* cells containing the His_6-SUMO plasmid was grown overnight at 37°C and 225 rpm in LB media containing 50 µL of 50 mg/mL kanamycin. The overnight culture was added to inoculate 1L of fresh LB-Kan media. The culture was incubated at 37°C until the OD_{600} reached 2.0. The incubation temperature was lowered to 30°C and expression was induced by adding IPTG to a final concentration of 0.75 mM (10 mL of 75 mM IPTG). Cells continued to grow under these conditions for an additional 4 hours, then were spun down at 6000 rpm, room temperature for 15 minutes. The supernatant was discarded and the resulting cell pellet was resuspended in buffer containing 25 mM HEPES pH 8.0, 350 mM NaCl, 2 mM TCEP and 20 mM imidazole. The resuspended cells were lysed via two passes through a French Press, then centrifuged at 12 000 x g for 30 minutes at 4°C. The pellet was discarded and the supernatant was incubated for 1 hour at 4°C with Ni-NTA resin that had been pre-equilibrated with the same resuspension buffer. The Ni-NTA resin was washed with buffer until the flow through reached an $A_{280} < 0.1$. The SUMO protease was then eluted from the resin using an elution buffer containing 25 mM HEPES pH 8.0, 350 mM NaCl, 2 mM TCEP and 400 mM imidazole. The eluate was

concentrated to 5 mg/mL (ε_{280} = 1.18 mL mg^{-1}) and 50% glycerol was added to a final volume of 25% (v/v). The final protease solution (2.5 mg/mL) was flash-frozen in small aliquots by immersion in liquid nitrogen and stored at -80°C.

2.3 Cloning and transformation of the WT rcPEPCK DNA sequence into an expression vector

The gene encoding for WT rat cytosolic PEPCK was cloned into a pSUMO-star expression vector as previously described.[35] The entire plasmid was then subsequently transformed using heat shock into the BL21 *E. coli* cell line, and stored at -80°C as a common laboratory cell stock.

The WT rcPEPCK plasmid was purified using a High-Speed Plasmid Mini Kit by Geneaid. The miniprep protocol was followed as provided by the supplier, and the purified plasmid was stored at -20°C. The purified plasmid was used as the template sequence for PCR mutagenesis.

2.4 PCR mutagenesis of rcPEPCK

Forward and reverse primers were designed to introduce the F284H and F284W mutations into the PEPCK DNA sequence. An *E. coli* codon usage chart was used to determine the ideal single-base pair substitution to mutate the phenylalanine residue at position 284 into a histidine or a tryptophan. The resultant mutant DNA primers were subsequently synthesized by Sigma-Genosys (Table 3).

Table 3: Mutant Primer Design for F284H and F284W rcPEPCK enzyme variants*

Primer Name	**Length (nt.)**	**T_m (°C)**
t993c_t994a forward	27	79.46
t993c_t994a reverse	27	79.46
Mutation	atacctggcagcagcc**ttc**cccagtgcctgtgg 3'-ggaccgtcgtcgg**gtg**gggtcacggac-5' 5'-cctggcagcagcc**cac**cccagtgcctg-3' tatggaccgtcgtcgg**aag**gggtcacggacacc	
F284H		
Primer Name	**Length (nt.)**	**T_m (°C)**
t994g_c995g forward	27	79.46
t994g_c995g reverse	27	79.46
Mutation	atacctggcagcagcc**ttc**cccagtgcctgtgg 3'-ggaccgtcgtcgg**acc**gggtcacggac-5' 5'-cctggcagcagcc**tgg**cccagtgcctg-3' tatggaccgtcgtcgg**aag**gggtcacggacacc	
F284W		

The codons in **blue represent the changes in the wildtype DNA sequence for mutagenesis.*

PCR mutagenesis was performed using 1 µL of each of the mutant primers at 100 ng/µL, 0.5 µL of Phusion high fidelity polymerase (Thermo Scientific), 5 µL of dNTPs, 10 µL of 5X reaction buffer (Thermo Scientific), and 5 µL the WT PEPCK SUMOstar expression vector (100 ng/ µL) as the DNA template. The thermocycler parameters were set as shown in Table 4. After amplification, the PCR products were digested with Dpn1 for 1 hour to degrade the WT plasmid template.

Table: 4: Cycling Parameters for PCR Mutagenesis

Segment	**Cycle No.**	**Temperature**	**Time**
1	1	95°C	1 min
2	1	95°C	30 s
3	1	60°C*	1 min
4	1	72°C	8 min 30 s
5	2-18	Repeat segment 2 - 4	
6	18	72°C	10 min
7	18	4°C	HOLD

**The annealing temperature was set as a gradient with an average temperature of 60°C ± 5°C.*

The PCR products were run on an agarose gel to confirm successful DNA amplification, then transformed into chemically-competent XL1 *E. coli* cells via heat shock.[41,42] The resultant cell culture was plated onto LB-Kanamycin agar plates using the streak-plate method. Colonies that successfully grew on the kanamycin plates were harvested and used to inoculate new LB-Kan media, and stored at -80°C as mutant PEPCK cell stocks. The mutant rcPEPCK plasmids were miniprepped using the same procedure as the WT plasmid miniprep, then sent to Robarts Research (London, ON, Canada) for sequencing to confirm the mutation of the corresponding codons and absence of unintended mutation of the remaining gene.

2.5 Wildtype and Mutant rcPEPCK expression and purification

The cell stock of BL21 *E. coli* containing the expression vector was used to inoculate four Erlenmeyer flasks of 50mL of LB-kanamycin media, which were left to incubate at 37°C while mixing overnight. The culture flasks were then each added to four separate flasks of 950mL autoinduction media, for a total of 4L culture volume. The autoinduction media contains 50 µg/mL of kanamycin for antibiotic selection of pSUMO-star-containing cells. Autoinduction media also contains $MgSO_4$, NPS salts, trace elements, glucose and lactose sugars for induction of the T7 lac promoter on the expression vector.[43] The autoinduction flasks were incubated for 20-24 hrs at 20°C to induce expression of the His_6-SUMO-rcPEPCK fusion protein.

The autoinduction media was then centrifuged at RT, 5000 x g for 15 minutes and the supernatant was discarded. The resulting cell pellet was resuspended in wash buffer containing 10% glycerol, 300 mM NaCl, 10 mM imidazole, 25 mM HEPES pH 7.5, and 2 mM TCEP-HCl. The resuspended cells were then lysed via two passes through a French Press, then spun down at 4°C, 12 000 x g for 1 hour. All protein purification from this point onwards was performed at 4°C. The protein-containing supernatant was added to Ni-NTA affinity resin that had been pre-equilibrated with 200 mL of wash buffer, and incubated with gentle shaking for a minimum of 1 hour.

After incubation, the Ni-NTA column was washed with approximately 600 mL of wash buffer to remove non-specifically bound proteins, until the flow-through reached an A_{280} of zero. At this point, the fusion protein was eluted off the column and collected in 10 mL aliquots (Figure 14), using an elution buffer composed of 300 mM imidazole, 25 mM HEPES pH 7.5, and 2 mM TCEP-HCl. Aliquots with an A_{280} > 0.3 were then pooled together and concentrated to a final volume less than 10 mL via a 30 kDa filter and N_2 gas concentrator. The concentrated eluate was added to a P6DG resin SEC column for buffer exchange that was pre-equilibrated with a second wash buffer containing 25 mM HEPES pH 7.5 and 2 mM TCEP-HCl. The P6DG column was washed while collecting aliquots of 10 mL (Figure 14). Aliquots with an A_{280} > 0.1 were pooled together and SUMO protease was added to cleave the His_6-SUMO tag from the fusion protein. The SUMO digest was left at 4°C with gentle mixing overnight.

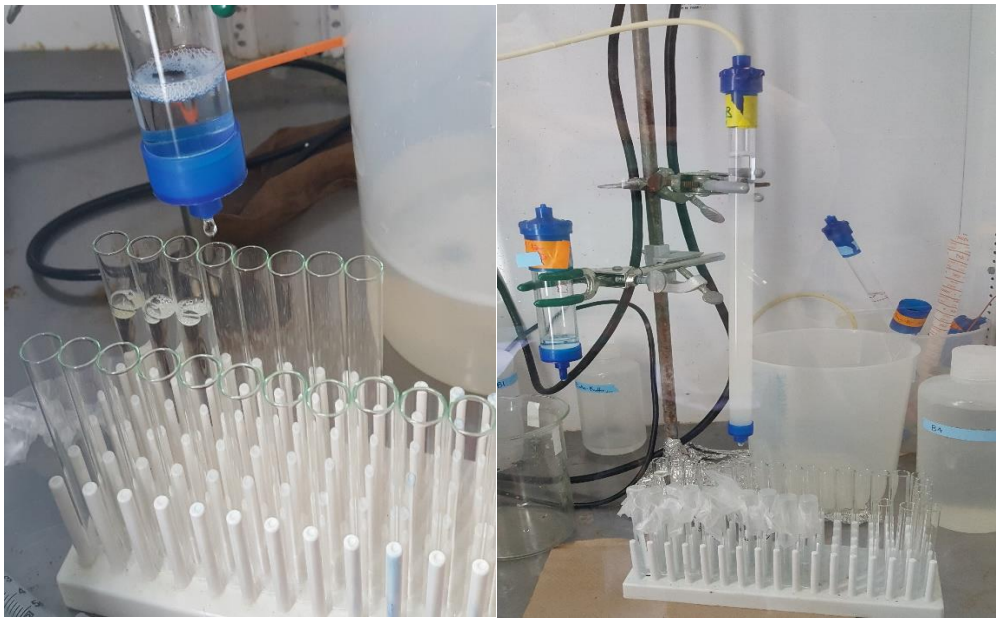

Figure 14: Nickel Affinity (left) and Size-Exclusion (right) chromatography columns for protein purification. Chromatography columns are equilibrated with buffer and then incubated with cell lysate containing the protein of interest. The His_6-SUMO-PEPCK fusion protein binds to the Ni-NTA column and is eluted from the column after several washes. The SEC column is used for buffer exchange between steps. Incubating the protein eluate with SUMO protease removes the His_6-SUMO tag so the protein can be concentrated and flash-frozen in liquid N_2.

The SUMO-digested sample was then added to the Ni-NTA column, pre-equilibrated with 200 mL of wash buffer. The protein sample flowed through the column while the cleaved His_6-SUMO tag remained bound to the column. Aliquots of 10 mL were collected once more, pooled together if $A_{280} > 0.1$, and concentrated to a final volume of less than 10 mL via a 30 kDa filter and N_2 gas concentrator. The concentrated protein sample was added to a P6DG resin SEC column that had been pre-equilibrated with the final buffer, containing 25 mM HEPES pH 7.5 and 10 mM DTT for long-term stability and storage of the protein at -80°C. Aliquots containing protein were collected from the P6DG column, pooled together if $A_{280} > 0.1$, and concentrated to a final concentration of 10 mg/mL via 30 kDa filter centrifugation at 4°C, 3500 x g, at 10 minute intervals. Protein concentration was determined using a NanoDrop spectrophotometer and an $\varepsilon_{280} = 1.7$ mL mg^{-1}, using the final storage buffer as a blank.

The final concentrated rcPEPCK sample was flash-frozen into 25 µL aliquots by pipetting directly into a liquid nitrogen-containing vial, and then storing the entire sample (roughly 1 to 1.5 mL total volume) at -80°C, leaving the nitrogen to evaporate overnight.

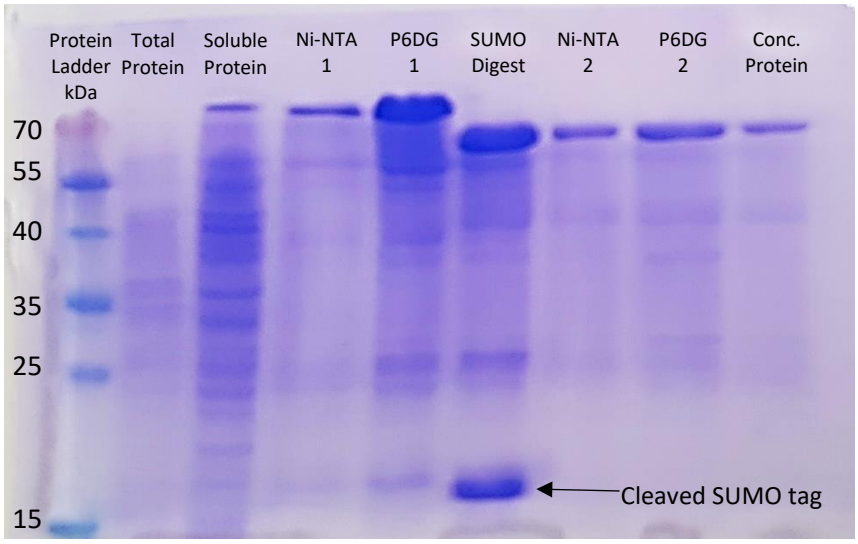

Figure 15: SDS-PAGE results for a representative WT rcPEPCK protein purification. 25 µL of sample was taken after each step of the purification protocol and loaded onto a 12% SDS PAGE gel after adding Coomassie Brilliant Blue dye. The total protein sample has been diluted 1/50, and the P6DG and SUMO digest samples were overloaded. The concentrated protein sample was diluted to ~0.1 mg/mL and appears on the far right.

2.6 Wildtype rcPEPCK crystallization and anion soaking

WT PEPCK crystals were grown using both sitting-drop and hanging-drop vapour diffusion methods, at 14 – 24% PEG 3350, 75 mM $MnCl_2$, 100 mM HEPES pH 7.5, and 10 mg/mL protein. Crystals grew within a few days, with a rod-shaped morphology, and were harvested up to three days post crystallization as it was observed that the diffraction quality would begin to deteriorate with older crystals.

WT PEPCK crystals were incubated in cryoprotectant containing a solution identical to the mother liquor, with the addition of 10% PEG 400 and potassium iodide ranging from 0 to 500 mM. Starting with 0 mM KI, the protein crystals were instantly dipped into 20 µL of cryoprotectant in a gradual, step-wise fashion to prevent cracking progressing through a range of: 0 mM, 10 mM, 25 mM, 50 mM, 100 mM, 250 mM, and 500 mM KI with the final KI concentration reflecting the final concentration of the salt the crystals were exposed to. Regardless of the final KI concentration, the crystals were incubated in the final KI solution for precisely 10 minutes. After incubation, the crystals were cryocooled by direct immersion in liquid nitrogen and mounted on the diffractometer. Our home source uses a rotating copper anode (CuKα = 1.54Å) to generate incident X-rays, and a Rigaku detector to read the resulting diffraction patterns.

The detector was set roughly 160 mm away from the mounted crystal, and the crystal was centered in the X-ray beam and cryostream through careful adjustment of the goniometer. Each of the crystals were exposed to X-rays for 120 seconds, and diffraction patterns were collected at 1° intervals around the crystal, for a complete 360° dataset. Six different datasets were collected, one for each crystal soaked at each of the above listed KI concentrations.

Each of the datasets were indexed as a primitive monoclinic Bravais lattice, integrated and scaled both anomalously and non-anomalously in a $P2_1$ spacegroup using HKL-2000.[44] The resulting scalepack files were converted into .mtz files using CCP4[45], with only one PEPCK molecule in the ASU. The non-anomalous datasets were used for structure solution as follows: molecular replacement was done via the MOLREP program using the WT rcPEPCK structure found on the PDB database (PDB ID: 2QEW).[46] Refinement was done using both CCP4 and Coot.[47] Lastly, anomalous difference maps were generated by

scaling the diffraction data in an anomalous fashion and generating the resultant anomalous data file using CCP4. The anomalous data within this .mtz file was combined with amplitudes and phases from the refined structure, using the CAD program in CCP4 to merge the two files. Subsequently, this .mtz file was used as the input data for the FFT program to perform a Fourier transform, generating the anomalous difference map. The FFT program also has an option called 'Peak Search' that calculates anomalous peak heights above a certain intensity and lists them in a .pdb file. Using Coot to visualize the anomalous difference maps and the peak heights in the .pdb file, anomalous peak heights were assigned to PEPCK's allosteric site for each dataset, corresponding to the allosteric anion occupancy for PEPCK crystals soaked at each iodide concentration. An allosteric binding isotherm was created by plotting the anomalous peak heights against the KI concentration.

F284H and F284W rcPEPCK crystals were grown under the same crystallization conditions as the WT rcPEPCK crystals, with the additional step of seeding. A seed stock was created from a WT rcPEPCK crystal, and further seed stocks were created via serial dilutions of this initial solution. The seed stocks were created using a stabilizing solution of PEG 3350, PEG 400, HEPES and $MnCl_2$ to mimic the reservoir solution. Mutant rcPEPCK crystals were grown at lower protein concentration ranging from 2 – 6 mg/mL, and seeded with seed stocks diluted between 10^3 - 10^4. Mutant rcPEPCK crystals were subjected to the same iodide soaking protocol as the WT, albeit only a 250 mM potassium iodide dataset was collected on each of the mutant crystals.

2.7 Wildtype rcPEPCK kinetic activity and inhibition assays

A standard enzyme activity assay was performed in both directions of the PEPCK-catalysed reaction. A Cary 100 UV-Vis dual-beam spectrophotometer was used to perform the assays. PEPCK activity was determined via a coupled assay using PK and LDH in the forward direction and MDH in the reverse direction (Figure 16). Reaction rates were measured spectrophotometrically at A_{340}, corresponding to the depletion of NADH via coupled-enzyme kinetics.

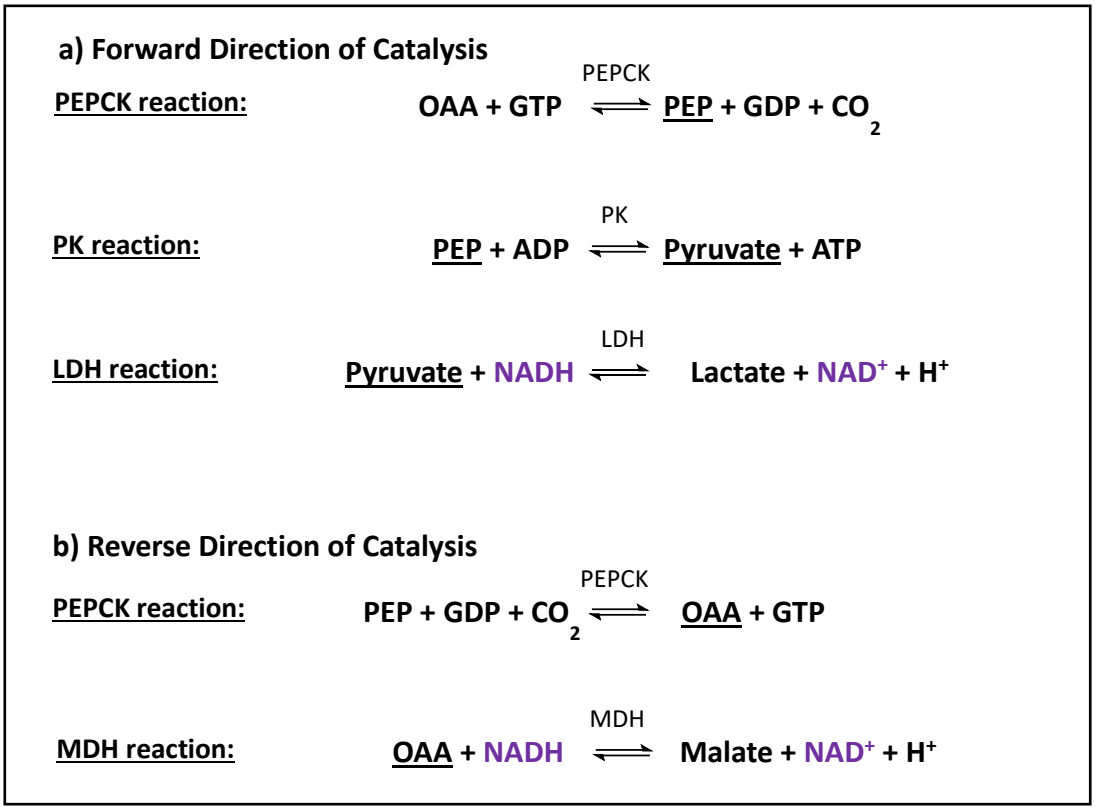

Figure 16: Coupled-enzyme reactions for the a) forward direction and b) reverse direction assays. The forward assay uses both PK and LDH coupling enzymes. The reverse assay uses MDH as a coupling enzyme. Underlined products represent substances that are used as substrates for the coupled reaction. The coupled-enzyme assay allows for the spectrophotometric detection of reaction rate via NADH depletion at 340 nm. NADH and NAD^+ are shown in purple.

The assay mix in the forward direction contained 100 mM HEPES pH 7.5, 10 mM DTT, 4 mM $MgCl_2$, 100 µM $MnCl_2$, 0.5 mM GTP, 1 mM ADP, 300 µM NADH, and 350 µM OAA, as well as 10 U of PK, 30 U of LDH, and 2.5 µg of PEPCK at 0.5 mg/mL. The total assay volume was 1 mL. For the 'reverse' direction assay, concentrations of HEPES, DTT, NADH, $MgCl_2$, $MnCl_2$ and PEPCK remain the same, while 1 mM GDP, 4 mM PEP, 500 mM $KHCO_3$ and 10 U of MDH are added instead.

Assays were performed while varying each of the 4 possible substrates and keeping the rest of the substrates at a fixed and saturating concentration (at least 5 times the K_M value). For the 'forward' direction, Michaelis-Menten curves were generated for both the OAA substrate and the GTP nucleotide, while curves for the 'reverse' direction were created for the PEP substrate and the GDP nucleotide. Anionic inhibition assays were also performed on WT PEPCK, by adding increasing amounts of potassium chloride. A series of five inhibition curves were plotted, one for each KCl concentration: 0 mM, 5 mM, 15 mM, 25 mM, and 40 mM KCl in the 'forward' direction assay, and 0 mM, 10 mM, 25 mM, 40 mM, and 100 mM KCl in the 'reverse' direction assay. The same anionic inhibition assay was repeated on the wildtype in the 'reverse' direction using iodide for comparison of the two anionic inhibitors. SigmaPlot's Enzyme Kinetics module was used to generate the Michaelis-Menten curves, as well as calculate kinetic parameters including V_{max}, K_M and K_I.

2.8 Mutant rcPEPCK kinetic activity and inhibition assays

F284H and F284W rcPEPCK were characterized to determine new kinetic parameters for the nucleotides in both reaction directions as due to the proximity of the mutation to the nucleotide binding site it was possible that the K_M value may have been increased in these enzyme variants. A standard activity assay as described above for the WT enzyme was performed in both the forward and reverse direction of catalysis, varying nucleotide concentration while keeping the other substrates constant (with the exception of $MgCl_2$, which was kept at a 4:1 ratio with the varied nucleotide to form the metal-nucleotide substrate complex). Once the ideal concentration of GTP or GDP nucleotide was determined for maximum enzyme activity, inhibition assays were performed as described above for WT rcPEPCK. The chloride inhibition was determined for the F284H and F284W mutant isoforms up to a maximum concentration of 200 mM KCl.

2.9 Kinetic re-plots for analysis of anionic inhibition data

For the anionic inhibition studies, the kinetic data were fit nonlinearly to the standard Michaelis-Menten equation using SigmaPlot to determine K_M and V_{max} values corresponding to each inhibitor concentration (equation 1).[1] The resulting K_{Mapp} values were re-plotted against the inhibitor concentration to calculate the K_I value for chloride from a linear fit to equation 2.[39] Non-specific effects of high salt concentration were determined using a similar approach by plotting V_{max} against inhibitor concentration (equation 3).

Equation 1: $$v = \frac{V_{max} \times [S]}{K_M + [S]}$$

Equation 2: $$\frac{K_{Mapp}}{V_{max\,app}} = \frac{K_M}{V_{max} \times K_I} \times [I] + \frac{K_M}{V_{max}}$$

Equation 3: $$\frac{1}{V_{\max\,app}} = \frac{1}{V_{max} \times K_I} \times [I] + \frac{1}{V_{max}}$$

In equations 1-3, v is the initial velocity, V_{max} is the maximal velocity, [S] is the concentration of substrate, K_M is the Michaelis constant, [I] is the inhibitor concentration, and K_I is the inhibition constant. For the data analysis V_{max} is represented as the maximal specific activity of PEPCK.

Chapter 3: Results

3.1 WT rcPEPCK Enzyme Kinetics

WT rcPEPCK enzyme activity was measured both in the OAA → PEP direction and the PEP → OAA direction (Appendix B). Activity in the forward direction, as measured by k_{cat}, was found to be 1.5-fold greater than that in the reverse direction. The same assay was performed by varying GTP/GDP, and a similar trend was observed (Table 5).

Table 5: Kinetic characterization of WT rcPEPCK at 25°C.

a) OAA + GTP → PEP + GDP + CO_2					
	K_M (µM)			**k_{cat}/K_M (M^{-1} s^{-1})**	
enzyme	**OAA**	**GTP**	**k_{cat} (s^{-1})**	**OAA**	**GTP**
WT rcPEPCK	39.6 ± 4.8	54.6 ± 6.0	22.3 ± 0.7	$5.6x10^5$	$4.1x10^5$
b) PEP + GDP + CO_2 → OAA + GTP					
	K_M (µM)			**k_{cat}/K_M (M^{-1} s^{-1})**	
enzyme	**PEP**	**GDP**	**k_{cat} (s^{-1})**	**PEP**	**GDP**
WT rcPEPCK	206.3 ± 17.2	85.9 ± 9.3	15.0 ± 0.3	$7.3x10^4$	$1.8x10^5$

All kinetic experiments were performed at 25°C. PEPCK activity was determined in the a) forward direction and b) reverse directions of catalysis via a coupled-enzyme assay.

The K_M for the PEP substrate is greater than that of the OAA substrate by 5-fold. This translates to an order of magnitude between the catalytic efficiency (k_{cat}/K_M) in the forward and reverse directions of catalysis. Although not as large a difference, the affinity for the nucleotide in the forward compared to reverse directions follows the same trend: the K_M for GDP nucleotide is greater than that of GTP by about 1.5-fold.

3.2 WT rcPEPCK Inhibition Kinetics

Inhibition assays were performed on WT rcPEPCK as detailed in **Section 2.7**. A K_I for chloride was determined for WT rcPEPCK in both the forward and reverse directions of catalysis (Table 6).

Table 6: Chloride inhibition constants for wildtype rcPEPCK calculated from the kinetic re-plots (Appendix H)

a) OAA + GTP → PEP + GDP + CO_2		
Variable Substrate	**K_M/V_{max} K_I (mM)**	**$1/V_{max}$ K_I (mM)**
OAA	120.5 ± 0.43	757.1 ± 0.43
b) PEP + GDP + CO_2 → OAA + GTP		
Variable Substrate	**K_M/V_{max} K_I (mM)**	**$1/V_{max}$ K_I (mM)**
PEP	14.1 ± 3.7	290.3 ± 0.01

All kinetic experiments were performed at 25°C. Chloride inhibition was determined in the a) forward direction and b) reverse directions of catalysis via a coupled-enzyme assay. Error associated with the KI's were obtained from a linear regression of the kinetic data using the LINEST function in Excel.

An inhibition assay performed in the reverse direction demonstrated a strong inhibitory effect of chloride ions on the wildtype enzyme (Table 6b), yielding a competitive K_I of 14.1 ± 3.7 mM. Conversely, exposing WT rcPEPCK to increasing concentrations of chloride in the forward direction of catalysis gives a competitive K_I of 120.5 ± 0.43 mM (Table 6a). Chloride inhibition in the reverse direction is 9-fold greater than that of the forward or physiological direction of gluconeogenesis. 1/V effects of the inhibitor on the enzyme were also observed, but these had a lesser effect on inhibition than K/V. The K/V effect was 6-fold and 20-fold greater than the 1/V effect in the forward and reverse directions respectively.

3.3 WT rcPEPCK Crystallization

WT rcPEPCK crystals were grown using both the sitting and hanging-drop vapour diffusion methods. Crystal conditions were optimized to obtain the largest and most robust crystals (Figure 17) to achieve the best diffraction quality possible at our home source. The crystal quality and size were found to be highly dependent on the concentration of the PEG 3350 precipitant with an optimal concentration range of 18-20% (Figure 17B).

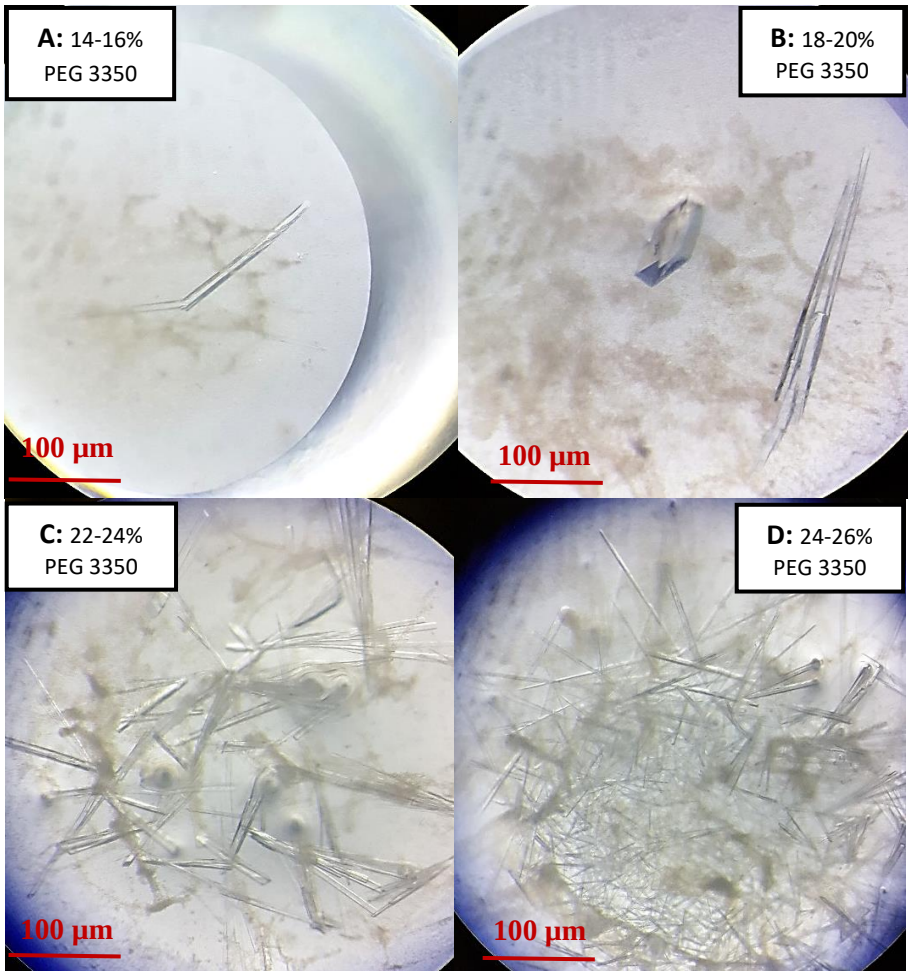

Figure 17: Optimizing crystallization conditions for WT rcPEPCK. Crystal morphology when grown at 14-16% PEG 3350 (A), 18-20% PEG 3350 (B), 22-24% PEG 3350 (C) and 24-26% PEG 3350 (D). All crystals were observed using an Olympus SZX16 microscope.

Crystals with optimal morphology were harvested and incubated in cryoprotectant containing iodide as outlined in **Section 2.6** (Figure 18). Soaking into increasing concentrations of iodide was performed in a step-wise manner to avoid deterioration of crystal structure (See **Section 2.6** for anion soaking).

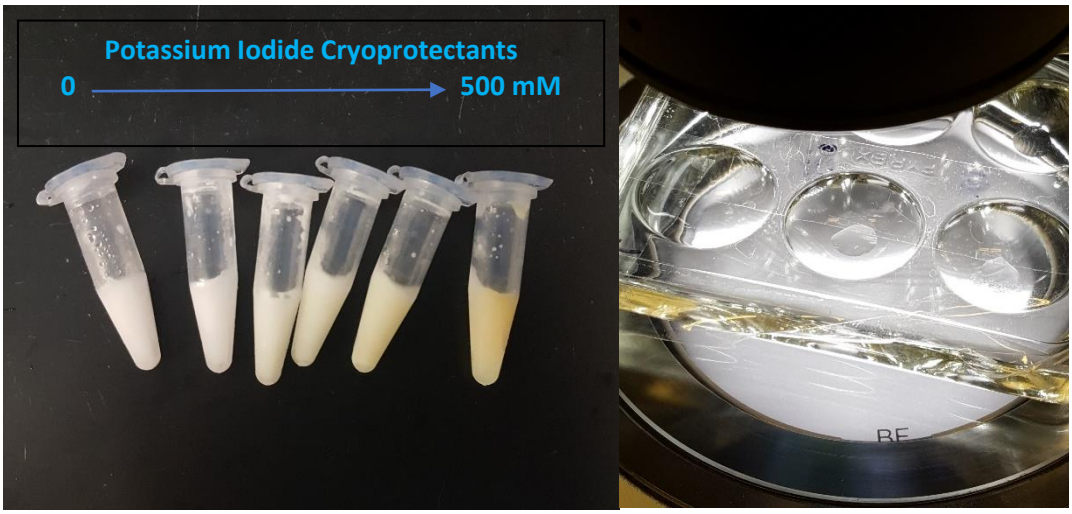

Figure 18: Iodide soaking of WT rcPEPCK crystals. Cryoprotectants (left) contained a solution identical to the reservoir solution of the crystals, with the addition of PEG 400 and potassium iodide (0-500 mM). Crystals were incubated with cryoprotectant (right) before flash cooling in liquid N_2.

3.4 Structure solution of WT rcPEPCK and determination of anion binding via the anomalous diffraction of iodide

Analysis of an initial WT rcPEPCK crystal soaked in 500 mM iodide revealed the presence of iodide bound to the active site. Comparing the location of the anomalous signal to a structure of WT rcPEPCK with substrate bound at the active site (PDB ID: 4GNP) demonstrates that iodide binds competitively to PEPCK at the OAA/PEP binding site (Figure 19).[34]

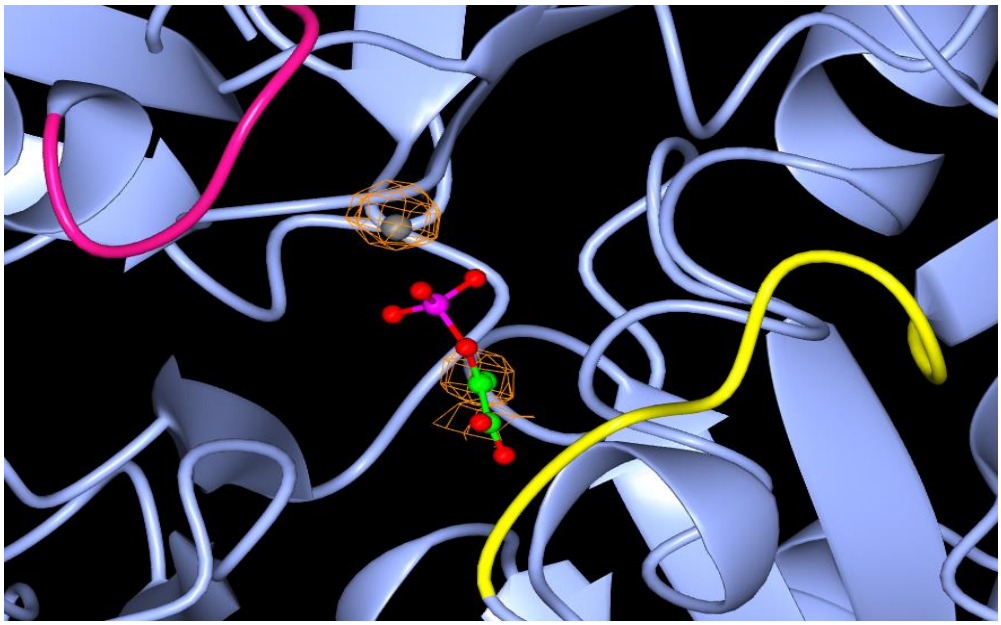

Figure 19: Superimposition of anomalous signal onto WT rcPEPCK structure with PEP substrate (PDB ID: 4GNP). Two catalytically important mobile loops in the active site, the R-loop (residues 85-92) and the P-loop (residues 284-292) are coloured yellow and pink respectively. PEP is rendered as a stick model coloured by atom type, and the M1 manganese ion is shown as a grey sphere. Anomalous signal is shown as an orange electron density. All graphics were generated using CCP4MG.[37]

Further soaking of multiple PEPCK crystals over a range from 10 mM to 500 mM potassium iodide showed anomalous signal at another site located behind the P-loop (Figure 20). In contrast with the active site signals, this anomalous signal was unique because it appeared to titrate over the range of iodide concentrations used (Figure 21). The range of iodide used for crystal soaking was determined from the observed K_I for the kinetic inhibition phenomenon observed above (10-500 mM). These new data led us to hypothesize that anion binding to this putative allosteric site was the source of the observed inhibition rather than a competitive mechanism of inhibition from anion binding to the active site. See **Appendix I** for a complete list of all iodides bound to PEPCK.

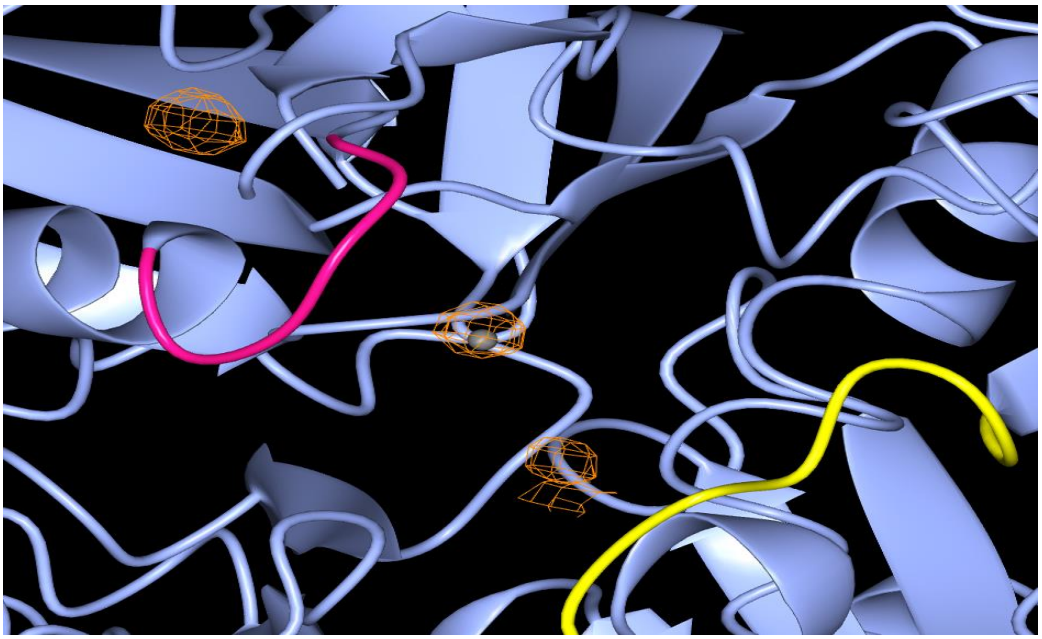

Figure 20: Allosteric site and active site binding sites of WT rcPEPCK. Two catalytically important mobile loops in the active site, the R-loop (residues 85-92) and the P-loop (residues 284-292) are coloured yellow and pink respectively. The M1 manganese ion is shown as a grey sphere, and the anomalous signals are represented as orange electron density. All graphics were generated using CCP4MG.[37]

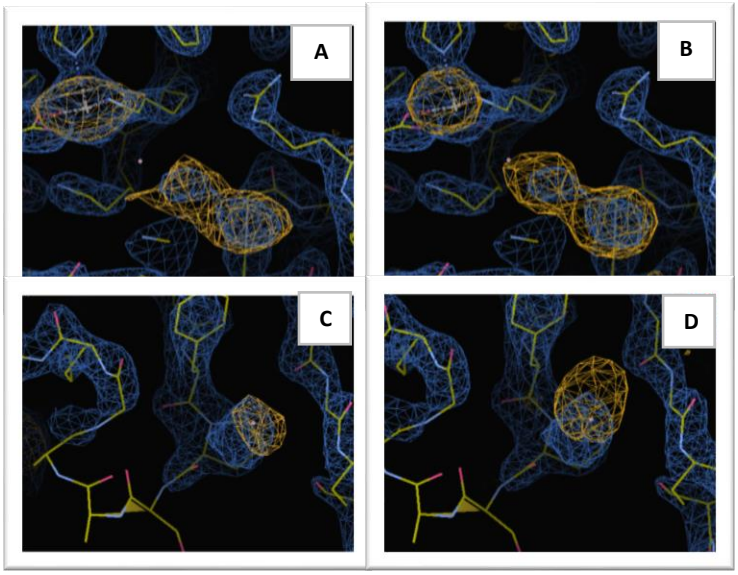

Figure 21: Titration of anomalous signal over the range of iodide soaking. Anomalous signal at the active site remains constant from low (A) to high (B) concentration of iodide used. Anomalous signal at the putative allosteric site titrates from low (C) to high (D) concentrations of iodide. Due to weak electron density, the P-loop was not modelled in the final structure. Anomalous difference map is represented as orange electron density.

Through the quantification of the anomalous signal found at the allosteric site, we can begin to understand the role anions play in the regulation of PEPCK activity. Plotting the anomalous peak height of iodide against the concentration of iodide used in each crystal soak, a type of binding isotherm can be generated for the allosteric site (Table 7, Figure 22).

Table 7: Anomalous peak height at the allosteric site corresponding to each potassium iodide soak

[Iodide] (mM)	Mn^{2+} Anom. Peak Height ($e^-/Å^3$)	Allosteric Anom. Peak Height ($e^-/Å^3$)	*Norm. Anom. Peak Height ($e^-/Å^3$)
10	16.23	6.26	**0.386**
25	17.28	10.41	**0.602**
50	15.8	11.54	**0.730**
100	11.56	10.72	**0.927**
250	11.26	12.02	**1.067**
500	13.7	13.68	**0.999**

**Peak heights were normalized by dividing by the anomalous peak height of their corresponding Mn cations.*

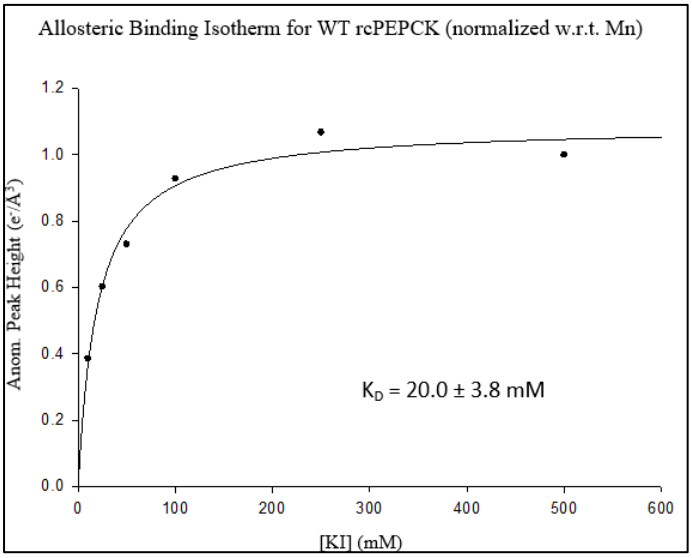

Figure 22: WT rcPEPCK allosteric binding isotherm for iodide. Normalized anomalous peak height values were calculated by dividing the allosteric anomalous peak height by that of the Mn (M1) cation, and then fit hyperbolically (See Section 2.9, Equation 1) against the range of iodide concentration used for anion soaking. This plot was generated using SigmaPlot 11.

The K_D for iodide bound to the allosteric site was determined to be 20.0 ± 3.8 mM. This value is on the same order of magnitude as the chloride inhibition constant for WT rcPEPCK in the reverse direction of catalysis (K_I of 14.1 ± 3.7 mM), despite using iodide as the inhibitor.

3.5 Structural analysis of the allosteric site

Looking closer at the putative allosteric site, we observe that it is in close proximity to the P loop, and as such many of the amino acids contributing to iodide binding also play in role in nucleotide binding (Figure 23). Consistent with the mM binding constant observed for chloride, iodide is found to be coordinated in the allosteric 'pocket' by numerous weak interactions that are all greater than 4Å away.

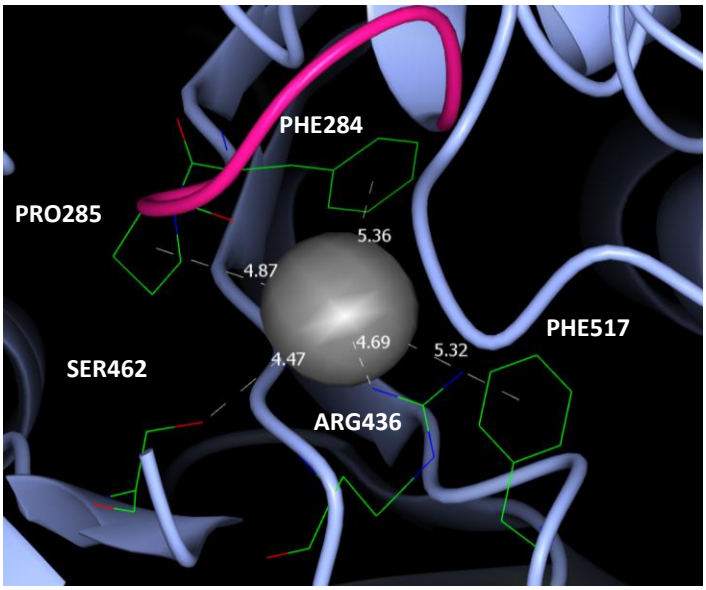

Figure 23: Putative allosteric site of WT rcPEPCK. The P-loop is coloured pink and iodide ion is shown as a large grey sphere. Residue side chains are labelled and coloured by atom type, and the distances between them and the iodide ion are listed in Angstroms. All graphics were generated using CCP4MG.[37]

It is important to note that when anions are not present in high concentration, the pocket occupies a closed conformation, but upon anion binding, the P-loop undergoes a conformational change that is unfavourable for catalytic function (Figures 24 & 25). In this anion-bound state, the P-loop is observed to be in a disordered and therefore difficult to model conformation, due to the resultant weak electron density from the disordered loop element.

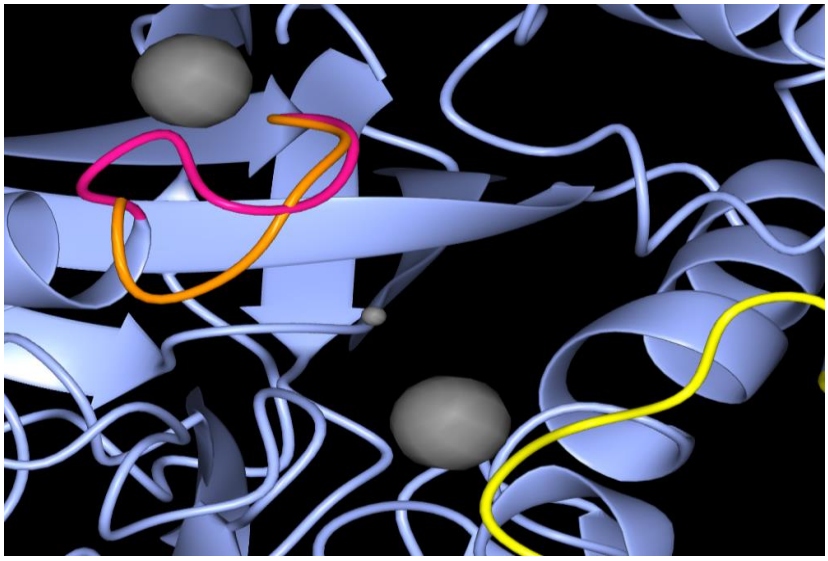

Figure 24: Conformational change of the P loop upon iodide binding. The R-loop is coloured yellow, and the unbound and anion-bound conformations of the P-loop are coloured pink and orange respectively. The M1 manganese cation is shown as a small grey sphere in the centre of the active site. Iodide ions are represented as larger grey spheres. All graphics were generated using CCP4MG.[37]

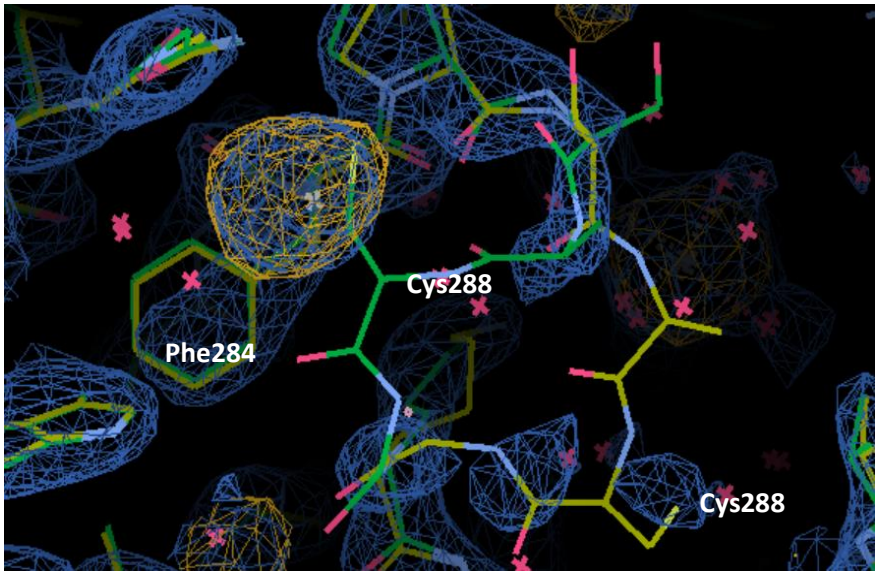

Figure 25: Superimposition of iodide-bound and unbound structures of WT rcPEPCK. The P-loop undergoes a conformational change upon binding iodide to the allosteric pocket. The sulfhydryl group of Cys288 occupies the allosteric site in the absence of iodide. The unbound structure is coloured green, while the iodide-bound structure is coloured yellow by default. Electron density of the iodide-bound structure is shown in blue, and the corresponding anomalous difference map for the 250 mM KI structure is shown in orange. The residue Cys288 is labelled on both structures. All graphics were rendered in Coot.[47]

Table 8: Crystallographic Data and Model Statistics

	0mM Iodide	10mM Iodide	25mM Iodide	50mM Iodide	100mM Iodide	250mM Iodide	500mM Iodide
Wavelength (Å)	1.54	1.54	1.54	1.54	1.54	1.54	1.54
Space Group	P1 21 1	P1 21 1	P1 21 1	P1 21 1	P1 21 1	P1 21 1	P1 21 1
Unit Cell Dimensions	a = 45.3 b = 118.9 c = 61.2 α = γ = 90.0° β = 108.5°	a = 45.4 b = 118.4 c = 61.3 α = γ = 90.0° β = 108.7°	a = 45.4 b = 118.6 c = 61.2 α = γ = 90.0° β = 108.5°	a = 45.5 b = 118.5 c = 61.4 α = γ = 90.0° β = 109.2°	a = 45.1 b = 118.9 c = 60.8 α = γ = 90.0° β = 110.9°	a = 45.5 b = 118.6 c = 61.1 α = γ = 90.0° β = 110.8°	a = 45.5 b = 118.8 c = 61.1 α = γ = 90.0° β = 111.0°
Resolution Limits (Å)	41.58 – 1.95	41.56 – 2.00	41.52 – 2.10	34.83 – 2.10	42.19 – 2.45	42.02 – 2.27	34.58 – 2.25
No. of unique reflections	37512	36219	32344	32543	20753	26351	27035
Completeness (%)	88.5 (31.9)	92.0 (47.5)	95.4 (61.6)	95.5 (66.5)	99.2 (91.6)	99.4 (93.8)	99.0 (87.6)
Redundancy	6.8 (3.4)	6.8 (3.3)	7.1 (4.7)	6.9 (3.5)	6.6 (5.0)	6.8 (4.8)	6.3 (4.1)
I/sigma	23.4 (2.1)	19.3 (1.6)	20.4 (1.9)	16.1 (1.7)	19.1 (2.0)	15.8 (1.7)	11.1 (1.4)
R_{merge}	0.07 (0.39)	0.07 (0.43)	0.07 (0.49)	0.08 (0.48)	0.07 (0.62)	0.11 (0.57)	0.15 (0.66)
No. of ASU molecules	1	1	1	1	1	1	1
R_{free}	0.24 (0.38)	0.26 (0.39)	0.27 (0.38)	0.25 (0.41)	0.27 (0.47)	0.25 (0.44)	0.27 (0.35)
R_{work}	0.19 (0.36)	0.21 (0.37)	0.22 (0.35)	0.21 (0.33)	0.21 (0.36)	0.20 (0.33)	0.21 (0.34)
Average B factor (Å^2)							
protein	41.9	52.5	51.2	50.6	58.9	52.5	51.9
Mn, Na	43.9	46.3	43.3	45.1	61.1	48.3	48.2
waters	40.0	47.1	43.6	43.1	50.1	49.2	49.1
I	-	76.7	77.4	69.2	86.1	81.0	71.9
Estimated coordinate error based on maximum likelihood (Å)	0.135	0.176	0.198	0.176	0.269	0.200	0.221
Bond length rmsd (Å)	0.006	0.005	0.006	0.005	0.002	0.003	0.003
Bond angle rmsd (deg)	1.364	1.356	1.389	1.360	1.232	1.264	1.241
Molprobity statistics (score, percentile, no. of Ramachandran outliers)	1.17, 100th, 2	1.56, 95^{th,} 2	1.72, 93th, 1	1.56, 97th, 1	1.61, 99th, 1	1.59, 98th, 5	1.52, 99th, 5

**Values in parentheses represent those in the highest resolution shell.*

3.6 Design of Allosteric Mutants

To investigate allosteric regulation, PEPCK mutants were created in order to perturb anion binding. F284 was chosen for mutagenesis as one of the only residues of the allosteric pocket that does not have a direct role in substrate binding, or an integral part of a dynamic loop (Figure 23).

Two different PEPCK mutants were created, both with variations of residue 284: F284H and F284W (Figure 27). In order to retain proper protein folding, the mutations introduced needed to have the same properties as the wildtype, so histidine and tryptophan were chosen for their non-polar aromatic side chains. Tryptophan is a much larger aromatic residue than histidine or phenylalanine, so it was hypothesized to have the greatest perturbation of the allosteric site.

The same kinetic and structural experiments were performed on the allosteric mutants for comparison to the wildtype enzyme to investigate allosteric regulation of PEPCK.

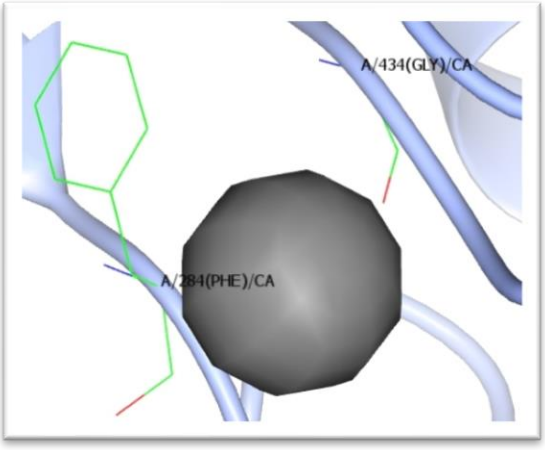

Figure 26: F284 of WT rcPEPCK. Phenylalanine was chosen for mutagenesis. The phenylalanine side chain is coloured by atom type, and iodide is represented as a large grey sphere.

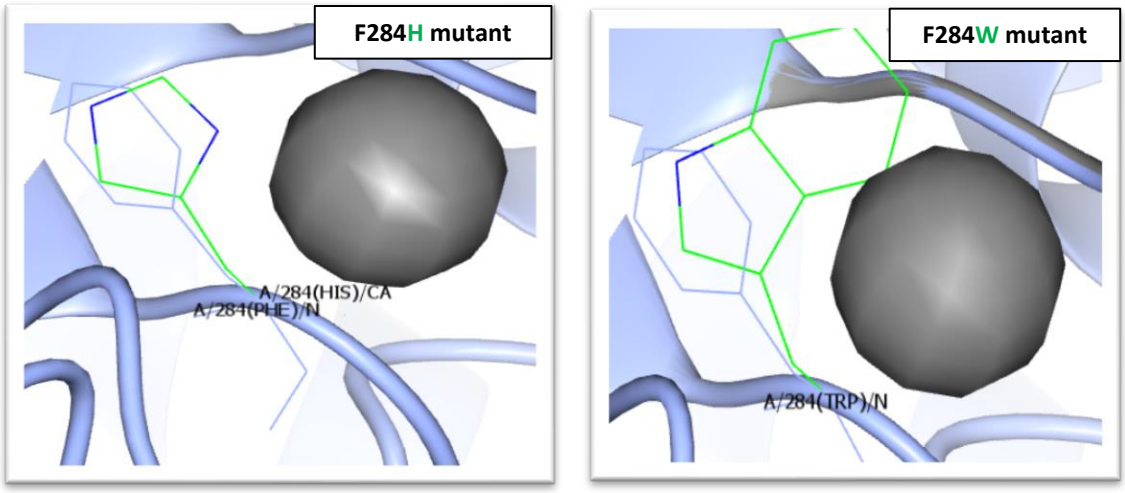

Figure 27: Superimposition of PEPCK mutants onto the wildtype enzyme. The WT phenylalanine residue is coloured light blue, while the histidine (left) and tryptophan (right) residues are coloured by atom type. Iodide is represented as a large grey sphere. All graphics were generated using CCP4MG.[37]

3.7 Mutant PCR Mutagenesis, Transformation and Protein Expression

Mutant strains of rcPEPCK were created using specially designed primers to introduce the mutation via PCR mutagenesis (see **Section 2.4**), using the P-SUMOstar expression vector containing the WT rcPEPCK DNA sequence as the template. PCR products were run on an agarose gel for confirmation (Figure 28), transformed into the XL1 *E. coli* cloning cell line for plasmid replication (Figure 29), and then into the BL21 *E. coli* expression cell line for PEPCK expression (Figure 30). After sequencing to ensure successful mutagenesis of the allosteric site, the F284H and F284W mutants were expressed and purified using the same protocol as described in **Section 2.5**.

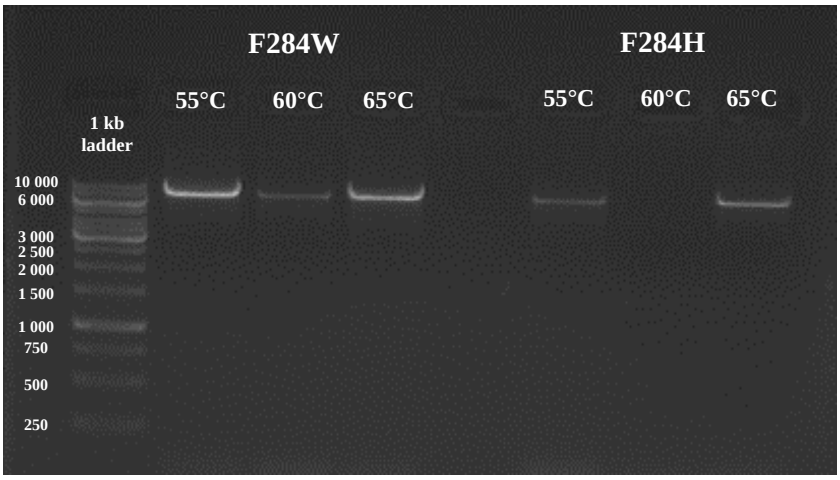

Figure 28: Agarose gel results of PCR mutagenesis for F284H and F284W mutants. Each mutant PEPCK pSUMO star vector is loaded onto the gel in triplicate, corresponding to the annealing temperature during PCR. The mutant rcPEPCK plasmid is ~8.4 kb in size.

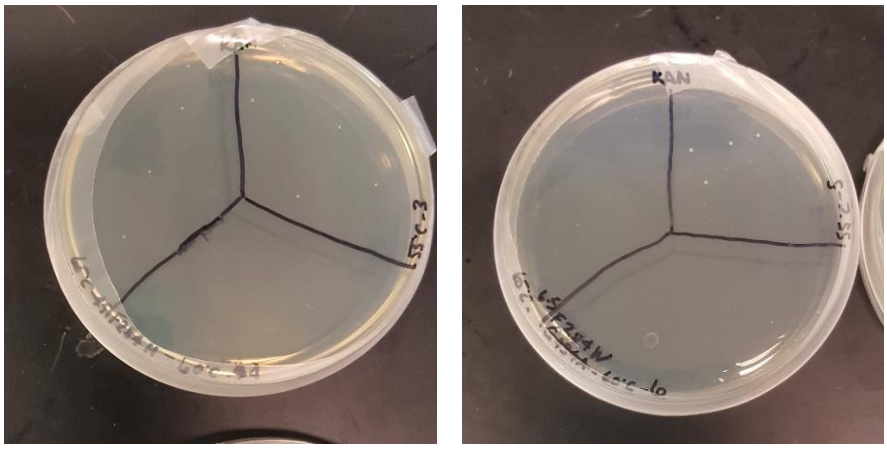

Figure 29: Transformation of the F284H and F284W PEPCK plasmids into XL1 *E. coli* cloning cell line. PCR products were transformed into the XL1 cloning cell line via heat shock. The streak-plate method was used along with kanamycin selection to find colonies that had successfully taken up the plasmid.

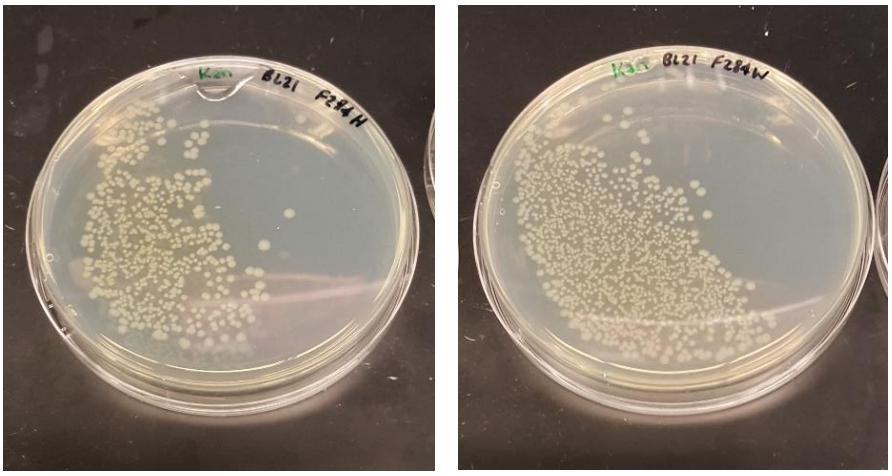

Figure 30: Transformation of F284H (left) and F284W (right) rcPEPCK plasmids into BL21 *E. coli* expression cell line. The streak-plate method was again used along with kanamycin selection, resulting in colonies with a round, opaque, beige coloured morphology.

3.8 Mutant rcPEPCK Protein Purification and Crystallization

Mutant rcPEPCK was purified using the same protocol as the WT rcPEPCK enzyme. Initially the WT rcPEPCK crystallization conditions were used, however, both the F284H and F284W mutant isozymes of rcPEPCK proved difficult to crystallize. These mutant crystals were smaller, appeared cracked or fractured (Figure 31), and were more two-dimensional instead of the 3-D rod morphology of the wildtype enzyme. Of the two mutant isoforms, the tryptophan mutant, F284W was the most difficult to crystallize.

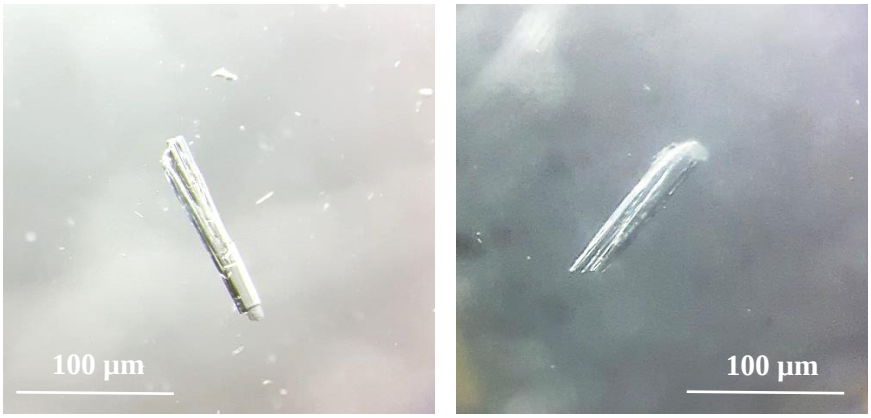

Figure 31: Mutant crystals harvested and soaked in cryoprotectant. F284H and F284W rcPEPCK crystals appear cracked and fractured in comparison to the wildtype crystals. Crystals were observed using an Olympus SZX16 microscope.

In attempt to grow crystals with better morphology and diffraction quality, crystal seeding was performed. Mutant rcPEPCK was grown at lower protein concentrations ranging from 2 to 6 mg/mL instead of the standard 10 mg/mL, and was seeded 24 hrs after equilibration of the protein drop at 21°C. Crystal seeding encouraged nucleation and mutant rcPEPCK crystals formed.

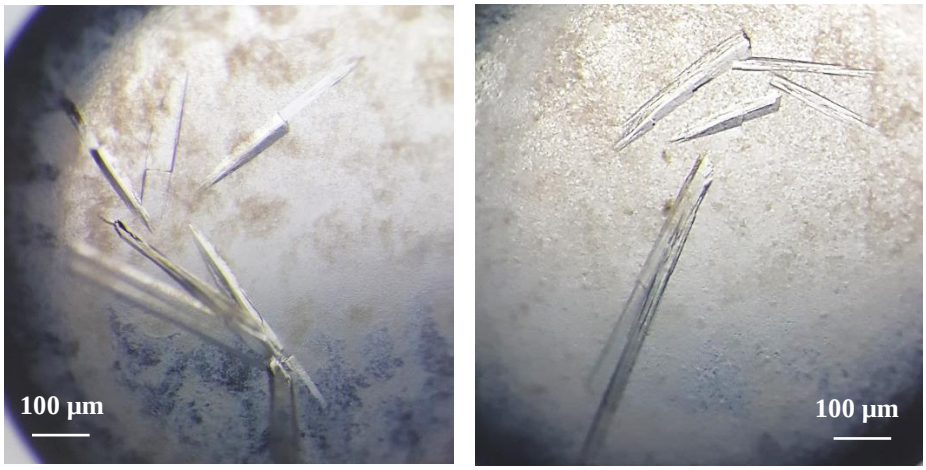

Figure 32: F284H (left) and F284W (right) rcPEPCK crystals after seeding. F284H crystals have a two-dimensional sheet-like morphology (left) and F284W crystals have an irregular rod-shaped morphology (right).

Mutant crystals were harvested and soaked in cryoprotectant containing 250 mM potassium iodide using the same protocol as described in **Section 2.6**. These crystals were diffracted at our home source (Table 9), and the anomalous signal was analyzed to determine iodide binding at the allosteric site.

3.9 Mutant rcPEPCK X-ray Diffraction

Table 9: Crystallographic Data and Model Statistics for Mutant rcPEPCK

	F284H 250mM KI	**F284W 250mM KI**
Wavelength (Å)	1.54	1.54
Space Group	P1 21 1	P1 21 1
Unit Cell Dimensions	a = 45.3 b = 118.7 c = 60.9 α = γ = 90.0° β = 111.5°	a = 45.1 b = 118.2 c = 60.7 α = γ = 90.0° β = 111.9°
Resolution Limits (Å)	59.34 – 2.09	28.90 – 2.34
No. of unique reflections	33311	22795
Completeness (%)	99.1 (93.1)	96.6 (89.7)
Redundancy	7.1 (6.9)	7.5 (6.7)
I/sigma	13.3 (2.4)	13.9 (1.8)
R_{merge}	0.10 (0.76)	0.09 (0.98)
No. of ASU molecules	1	1
R_{free}	0.26 (0.45)	0.28 (0.38)
R_{work}	0.22 (0.35)	0.22 (0.34)
Average B factor (Å^2)		
protein	50.8	52.0
water	48.7	46.6
Mn	47.1	52.3
I	71.6	67.1
Estimated coordinate error based on maximum likelihood (Å)	0.178	0.256
Bond length rmsd (Å)	0.003	0.002
Bond angle rmsd (deg)	1.224	1.234
Molprobity statistics (score, percentile, no. of Ramachandran outliers)	1.65, 95th, 2	1.89, 94th, 2

**Values in parentheses represent those in the highest resolution shell.*

Table 10: Anomalous peak height at the allosteric site with mutant rcPEPCK data added

[Iodide] (mM)	Mn^{2+} Anom. Peak Height ($e^-/Å^3$)	Allosteric Anom. Peak Height ($e^-/Å^3$)	*Norm. Anom. Peak Height ($e^-/Å^3$)
WT rcPEPCK			
10	16.23	6.26	0.386
25	17.28	10.41	0.602
50	15.8	11.54	0.730
100	11.56	10.72	0.927
250	11.26	12.02	**1.067**
500	13.7	13.68	0.999
F284H rcPEPCK			
250	21.83	5.73	**0.262**
F284W rcPEPCK			
250	10.91	0	**0**

**Peak heights were normalized by dividing by the anomalous peak height of their corresponding Mn cations.*

The F284H mutant shows a decreased anomalous signal compared to that of the wildtype at the same iodide concentration. At 250 mM potassium iodide, the anomalous signal at the allosteric site is approximately 4-fold greater for the wildtype than the histidine mutant (Table 10). No anomalous signal was observed for the allosteric site of the F284W mutant. Both of the mutants showed anomalous signal corresponding to iodide binding at the active site, comparable to what was found in the WT rcPEPCK structure.

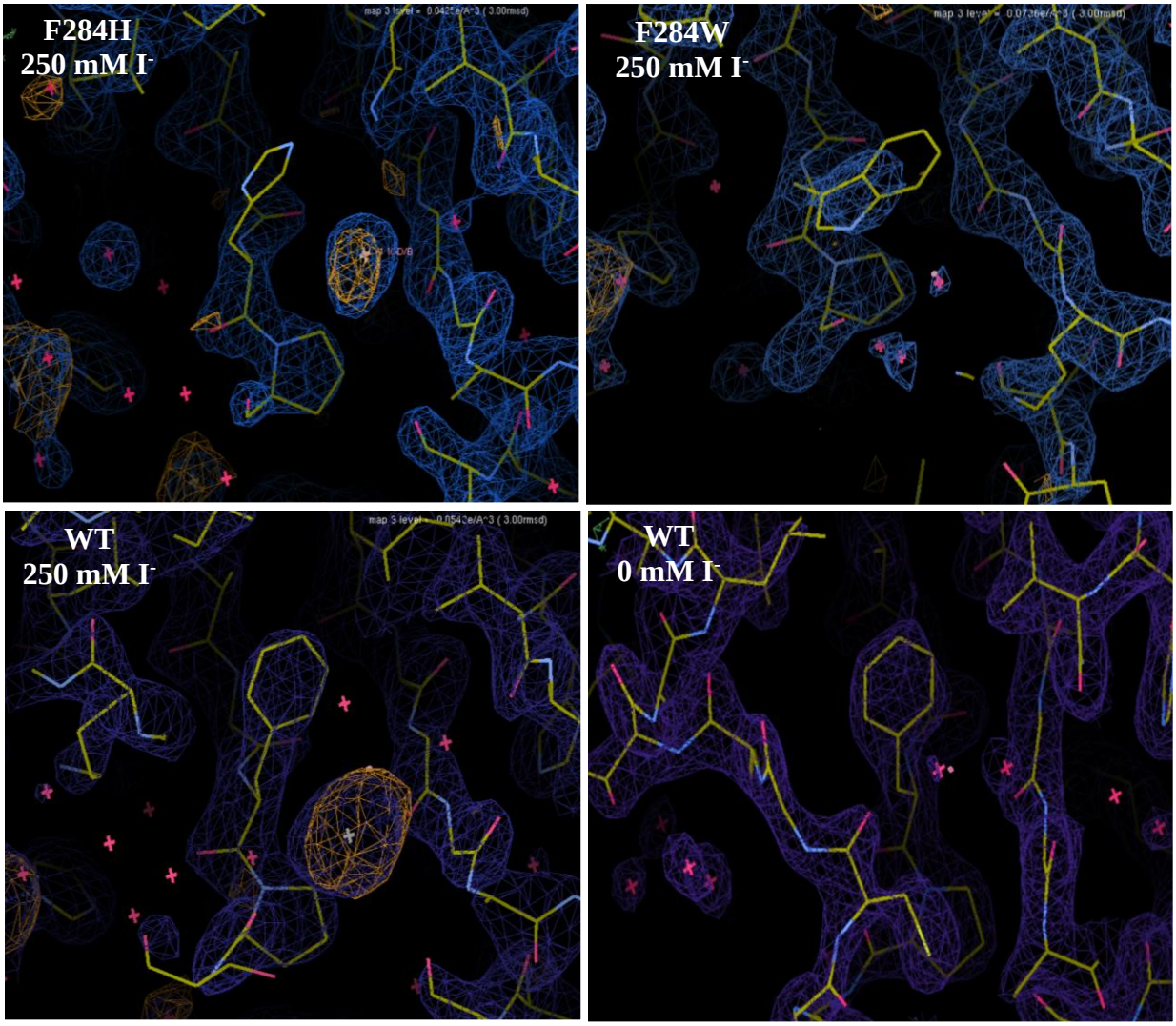

Figure 33: Anomalous signal at the allosteric site for WT and mutant rcPEPCK. Anomalous signal represented as orange electron density. Comparison of iodide binding to each of the allosteric mutants as well as the disordered conformation of the P-loop, most notable in the F284H and F284W mutants.

3.10 Mutant rcPEPCK Kinetic Characterization

Before inhibition assays could be performed on the F284H and F284W mutants, these new enzyme variants had to be characterized. It was hypothesized that due to the proximity of the allosteric site to the P-loop, it was likely that the K_M for GTP/GDP would have changed from that of the wildtype.

The K_M for the GTP and GDP nucleotides were determined (Table 11), and these kinetic parameters were used for the inhibition assays such that at least 4 times the K_M was added for each of the nucleotides. Mutation of residue 284 increased the K_M for GTP by 12-fold for both the histidine and tryptophan mutants, while increasing the K_M for GDP by 2.5-fold and 12-fold for histidine and tryptophan respectively.

Table 11: Kinetic characterization of F284H and F284W rcPEPCK mutants

a) OAA + GTP → PEP + GDP + CO_2					
	K_M (µM)			**k_{cat}/K_M (M^{-1} s^{-1})**	
enzyme	**OAA**	**GTP**	**k_{cat} (s^{-1})**	**OAA**	**GTP**
WT	39.6 ± 4.8	54.6 ± 6.0	22.3 ± 0.7	$5.6x10^5$	$4.1x10^5$
F284H	65.8 ± 10.6	645.7 ± 150	27.7 ± 1.3	$4.2x10^5$	$4.5x10^4$
F284W	89.2 ± 12.6	661.7 ± 154	28.3 ± 1.3	$3.2x10^5$	$4.4x10^4$
b) PEP + GDP + CO_2 → OAA + GTP					
	K_M (µM)			**k_{cat}/K_M (M^{-1} s^{-1})**	
enzyme	**PEP**	**GDP**	**k_{cat} (s^{-1})**	**PEP**	**GDP**
WT	206.3 ± 17.2	85.9 ± 9.3	15.0 ± 0.3	$7.3x10^4$	$1.8x10^5$
F284H	236.4 ± 25.1	219.9 ± 30.8	15.1 ± 0.4	$6.4x10^4$	$8.0x10^4$
F284W	126.6 ± 15.4	986.5 ± 136	4.0 ± 0.09	$3.1x10^4$	$5.2x10^3$

All kinetic experiments were performed at 25°C. PEPCK variants were characterized in a) the forward direction and b) the reverse direction of catalysis.

3.11 Mutant rcPEPCK Inhibition Kinetics

Table 12: Expanded table of inhibition constants for wildtype and mutant rcPEPCK

c) OAA + GTP → PEP + GDP + CO_2 (Chloride) – using OAA as the variable substrate		
enzyme	**K_M/Specific Activity K_I (mM)**	**1/Specific Activity K_I (mM)**
WT	120.5 ± 0.43	757.1 ± 0.43
F284H	171.8 ± 1.0	264.5 ± 0.01
F284W	95.1 ± 0.35	97.3 ± 0.01
d) PEP + GDP + CO_2 → OAA + GTP (Chloride) – using PEP as the variable substrate		
enzyme	**K_M/Specific Activity K_I (mM)**	**1/Specific Activity K_I (mM)**
WT	14.1 ± 3.7	290.3 ± 0.01
F284H	18.9 ± 2.7	412.0 ± 0.01
F284W	30.7 ± 6.9	95.0 ± 0.19
e) PEP + GDP + CO_2 → OAA + GTP (Iodide) – using PEP as the variable substrate		
enzyme	**K_M/Specific Activity K_I (mM)**	**1/Specific Activity K_I (mM)**
WT	33.8 ± 100	8.42 ± 0.04
f) Binding Isotherm for Allosteric Site		
	K_D (mM)	
WT	20.0 ± 3.8	

Inhibition assays on the PEPCK mutants showed that mutating the allosteric site does not have a significant effect on inhibition in the physiological direction of gluconeogenesis. However, introducing these mutations at position 284 does have an interesting effect on inhibition in the reverse direction. The F284H mutant does alleviate inhibition in the reverse direction, but only very minimally, especially when compared to the reduction of iodide binding revealed from the structural data. The F284W mutant had the weakest inhibition, with roughly half the inhibitory strength compared to the WT, but the kinetic data does not correlate with the complete lack of iodide binding seen in the structural data.

There is a notable discrepancy between the kinetic and structural data due to the use of two different anions: chloride for the kinetic inhibition assays, and iodide for the structural approach. To attempt to tie the data together, the kinetic inhibition assays were repeated on the WT rcPEPCK enzyme, this time using iodide. The inhibition constant was determined for iodide in the reverse direction, and was compared to its chloride counterpart. It was discovered that chloride is the stronger competitive inhibitor (K_I of 14.1 mM)(Figure H1) and despite being the smaller of the two anions, chloride is approximately twice as effective at inhibiting PEPCK activity compared to iodide (K_I of 33.8 mM)(Figure H7).

Chapter 4 Discussion

4.1 Kinetic characterization and anionic inhibition of WT rcPEPCK

Kinetic assays performed on the WT enzyme supported what numerous other studies had identified: PEPCK activity in the PEP → OAA direction, referred to as the reverse direction of catalysis, is significantly reduced compared to the OAA → PEP direction, which is considered the physiological direction of gluconeogenesis. This is demonstrated by the catalytic efficiency as seen in Table 5; there is an order of magnitude difference between the k_{cat}/K_M for OAA in the forward direction and PEP in the reverse direction. PEPCK activity in the forward direction is easily demonstrated *in vivo*, despite the difficulty in performing the forward direction assay *in vitro*. There are several intricacies involved with the assay, including obtaining pure substrates for enzymatic assay, but most notably being the spontaneous decarboxylation of OAA by the high concentration of metal cations required for PEPCK function.[48] This background rate is subtracted from the total reaction rate to obtain the true reaction rate for PEPCK.

The kinetic data also shows the difference in affinity PEPCK has for the OAA/PEP substrates. The K_M for OAA is lower than that of PEP by an order of magnitude, again demonstrating a preference for the forward direction over the reverse direction of catalysis. However, these values for the substrates likely only represent the apparent K_M, calculated based on the kinetic data. Despite the fact that the PEPCK-catalyzed reaction is thermodynamically reversible, PEPCK primarily catalyzes the conversion of OAA to PEP in higher eukaryotes.[3] The kinetic data shows that PEPCK does not act in a unidirectional manner *in vitro*, and will catalyze the reaction in either direction given the appropriate substrates, however, it is apparent that enzyme activity in the reverse direction of catalysis is inhibited by some mechanism. Our initial hypothesis concluded that there was some significant difference between the PEPCK assay *in vitro* and the intracellular environment *in vivo*. The kinetic assay has been optimized by only including the minimum substrates and buffers required for PEPCK activity. This includes the mandatory metal cations that act as PEPCK cofactors, Mg^{2+} and Mn^{2+}.[49,50] However, these cations are added as chloride salts,

which consequently has the disadvantage of adding 4 mM chloride to the assay mixture. It was hypothesized that this abundance of chloride in the kinetic assay leads to the inhibition of the WT rcPEPCK enzyme in the PEP → OAA direction *in vitro*, and would likely have an even stronger inhibitory effect on PEPCK *in vivo*, considering the high concentration of chloride as well as many other anions in a biological cell.[26,27]

To test the hypothesis of anionic inhibition, chloride was chosen as the anionic inhibitor due its abundance in biological systems. As one of the most ubiquitous anions of the halide family, chloride would be the most physiologically relevant anion to play a role in the regulation of PEPCK activity. Additional chloride was added to the standard PEPCK assay, and the competitive inhibition constant, K_I, was determined for chloride in both the forward and reverse directions of catalysis (Table 6). The K_I in the PEP → OAA was calculated to be approximately 14.1 mM of chloride, compared to the significantly weaker inhibition in the OAA → PEP direction, calculated to be approximately 120.5 mM. This is an entire order of magnitude difference in the inhibition constants, similar to the difference in the aforementioned catalytic efficiency between the forward and reverse directions of catalysis. The K_I for chloride in the forward or physiological direction of gluconeogenesis is quite high, and as such chloride inhibition does not significantly affect PEPCK activity in the OAA → PEP direction, whether it is *in vitro* or *in vivo*. Conversely, the K_I for chloride in the reverse direction is comparatively low, resulting in a stronger inhibition on PEPCK activity. Considering the average biological cell has upwards of 100 mM of chloride, it becomes apparent how PEPCK activity is regulated for the gluconeogenic pathway.[26,27] It is this difference in anionic inhibition between the forward and reverse directions of catalysis that likely allows for kinetic regulation, despite the fact that the PEPCK-catalyzed reaction is thermodynamically reversible.

4.2 Structural determination of anion binding to WT rcPEPCK via anomalous diffraction

X-ray crystallography, combined with the anomalous diffraction of iodide, was used to examine anion binding to PEPCK. Iodide was used as the anionic inhibitor as a proxy for chloride, due to its unique anomalous properties. WT rcPEPCK crystals were soaked in 500 mM potassium iodide and diffracted at our home source (CuKα = 1.54Å), then the resulting diffraction patterns were analyzed to generate both the WT structure and a corresponding anomalous difference map. Iodide was easily located at the active site, tightly bound at the OAA/PEP site as expected of a competitive inhibitor (Figure 19).

Further crystal soaking experiments revealed the presence of an allosteric site, located directly behind the P-loop, where the anomalous signal appeared to titrate with increasing iodide concentration (Figure 20-21). This contrasts the anomalous signal at the active site, which remains relatively constant over the range of concentration used for the iodide soaks, and only begins to decrease at the lowest iodide concentration used. The putative allosteric site does not appear to have the tetrahedral geometry of known anion-binding sites, so further analysis is needed.

The iodide bound to the allosteric site is unique due in its observed titration when compared to all other iodide anions found in the WT rcPEPCK structure (listed in Appendix I). There is a total of eighteen iodide anions found in the 500 mM KI wildtype structure, most of which are bound to the surface of the enzyme. The two iodide anions present in the active site are non-titratable, demonstrating a behaviour similar of that to the surface-bound iodides (Appendix I). Each of the iodides in the active site has an occupancy of approximately 0.5, indicating that there is only one iodide truly bound to the active site, and that the iodide is likely to be bound in either of these two positions located in the OAA/PEP site. This is an artifact of macromolecular X-ray diffraction, in that a dataset is the average of all of the molecules that comprise the crystalline lattice. It is interesting to note that one of these anomalous signals in the active site disappears in the 10 mM KI structure, indicating that at lower concentrations of iodide (likely on the micromolar scale) this anomalous signal could start to titrate. Overall, only the iodide bound to the allosteric site was observed to titrate over the range of iodide concentration used in both the kinetic assays

as well as the aforementioned crystal soaking experiments. Using the anomalous scattering of iodide to analyze occupancies of bound anions is a fairly recent method of using iodide soaking, that which was previously only used to obtain phase information.[51]

Generation of a binding isotherm using the anomalous peak height plotted against iodide concentration allowed us to calculate an approximate binding constant for the allosteric site (Figure 22). The K_D for iodide at the allosteric site was determined to be 20.0 mM. We can compare this binding constant to the inhibition constant from the kinetic assays: the K_D is remarkably similar to the K_I for chloride in the reverse direction of catalysis. This addresses several questions about the kinetic data, such as if the competitive inhibition seen from the PEPCK assays is a combination of anions binding to both the allosteric and active sites. The structural data provides evidence that the regulation of PEPCK in a biological system is due primarily to binding at the allosteric site, and not the active site, as one would initially expect of a competitive inhibitor. Without anions present in the crystallization conditions, the pocket is closed and the P-loop can undergo the conformational changes necessary to bind the nucleotide substrate. Binding to the allosteric site causes the P-loop to become disordered (Figure 24), directly affecting nucleotide binding. Disorder of the P-loop correlates to a change in apparent K_M for the nucleotide as well as the PEP substrate (Michaelis-Menten curves in Appendix C), due to the decreased binding of GDP and the rate of phosphoryl transfer between nucleotide and PEP substrate.

Interestingly, in the unbound state of WT rcPEPCK, the sulfhydryl group of C288 appears to occupy the allosteric pocket in nearly the same position as the iodide in the anion-bound state (Figure 25). This hyper-reactive cysteine is essential for catalysis and therefore PEPCK activity is known to be inhibited through reduction of the sulfhydryl group or substitution of the cysteine for another amino acid.[52] Perturbing the conformation of the P-loop and therefore the positioning of C288 likely contributes to the decrease in PEPCK activity seen in the chloride inhibition assays.

4.3 Structural solution of rcPEPCK mutants and determination of allosteric binding via anomalous diffraction

To determine if this is indeed an allosteric pocket despite not resembling known anion-binding sites, PEPCK mutants were created to examine the effect on anion binding and enzyme activity. Iodide is bound to the pocket by weak interactions with the peptide backbone, and aromatic residues greater than 4Å away (Figure 23). Due to the proximity to the active site, many of the amino acids that comprise the pocket are integral to enzyme function. F517 and R346 are part of the P-loop and involved in nucleotide binding respectively, while S462 is an integral part of the Ω-loop lid.[11,34] F284 was chosen for mutagenesis, because it has no previously known role for enzyme function (Figure 26). In order to conserve protein folding and enzyme function, phenylalanine was mutated to two other aromatic residues, histidine and tryptophan (Figure 27). Due to the difference in size between the histidine and tryptophan residues, it was hypothesized that the F284W mutant would have the more significant effect on anion binding compared to the more conservative F284H mutant.

The F284H and F284W rcPEPCK mutant crystals were grown using the same protocol as the wildtype. Initial screening of these mutant crystals yielded poor diffraction patterns, therefore seeding was used to improve nucleation and overall crystal quality. Crystals were soaked in 250 mM potassium iodide and diffracted at our home source. One immediate difference between the mutants and the WT was the conformation of the P-loop. Upon binding to the allosteric site, the P-loop changes to a slightly more disordered conformation in the wildtype, however, binding to the allosteric mutants F284H and F284W leads to a much higher state of disorder. As such, the P-loop is not modelled in the mutant PEPCK structures (Figure 33). Generation of anomalous difference maps yielded nine additional iodide anions that were not present in the wildtype structures, though these iodides were surface-binding and expected to be non-titratable (See Appendix I).

Examining the allosteric site of the F284H mutant shows a decreased anomalous peak height approximately one fourth of the anomalous signal found at the wildtype's allosteric site when soaked at the same iodide concentration (Table 12). This supports the hypothesis that the phenylalanine at position 284 has a role in anionic binding, even if only through weak interactions. Mutating phenylalanine to histidine, although the mutated residue retains aromaticity and similar size, decreases the electrostatic interactions with iodide in some way. It is possible that F284 binds iodide to the pocket through anion-π or anion-quadrupole interactions, which are known to occur between an anionic species and the electropositive edge of an aromatic ring.[53–55] Aromatic ring systems can have a quadrupole moment as a result of their π electrons interacting with nearby positively charged amino acids, leaving behind an electron-deficient aromatic ring.[56] Another of the allosteric residues, not chosen for mutagenesis, F517 also appears to be positioned edgewise for anion-π interaction with the bound iodide (Figure 23). Further research is needed to determine whether an anion-π interaction is plausible between the aromatic residues of the allosteric pocket and anionic ligands. Both the benzene ring of phenylalanine and the neutral imidazole ring of histidine act are able to act as aromatic systems. Along with their similar size, this explains how the F284H mutant retains some level of anionic binding, as demonstrated in the anomalous difference maps, though it is unclear why the difference in magnitude of the anomalous signals is so large. It is also important to note that there is also no discernable electron density surrounding the imidazole group, indicating that the histidine side chain is disordered. Conversely, analyzing the F284W mutant reveals a complete lack of anomalous signal at the allosteric site, and indeed the tryptophan ring is significantly larger than either histidine or phenylalanine. The electron density indicates that the tryptophan ring has moved towards the center of the allosteric pocket and serves to sterically occlude iodide from binding (Figure 33).

4.4 Kinetic characterization and anionic inhibition of PEPCK mutants

Both the F284H and F284W rcPEPCK mutants were characterized in order to determine their new kinetic parameters for GTP/GDP nucleotide binding, due to the conformational changes of the P-loop as revealed by the structural data. The F284H mutant had a slight change in the K_M for the nucleotides, while the F284W mutant had the most significant change, as expected. The K_M for GDP in the PEP → OAA direction had increased to nearly 1 mM, an increase by a factor of 5 relative to the wildtype. Using these adjusted kinetic parameters, the chloride inhibition assays were repeated for both of the allosteric mutants in the forward and reverse directions of catalysis. Compared to the wildtype, inhibition of the F284H mutant decreased only slightly in both the forward and reverse directions, as can be seen by the change in K_I (Table 16). This correlates to the structural data, where a decrease in anomalous signal demonstrated decreased anionic binding to the allosteric site of the F284H mutant. Interestingly, chloride inhibition of the F284W mutant was cut in half in the reverse direction compared to the wildtype (translated as an increase in K_I by a factor of 2), while inhibition increased slightly in the forward direction of catalysis (Table 16). This does not correlate as well to the structural data as the histidine mutant did. From the aforementioned structural data, the F284W mutant showed no iodide binding to the allosteric site, and indeed the tryptophan ring appeared to occupy the allosteric pocket entirely. This discrepancy could likely be attributed to the use of two different halides between the kinetic and structural approaches.

4.5 Comparison of the kinetic and structural approaches

The easiest way to examine the difference between chloride and iodide as anionic inhibitors was to repeat the kinetic inhibition assay on the wildtype enzyme, this time using iodide (Table 17). The resulting iodide inhibition constant (iodide K_I = 33.8 mM) of the wildtype in the reverse direction of catalysis was significantly different than previously determined for chloride (chloride K_I = 14.1 mM), and the data from the iodide re-plot shows a slight curvature, possibly indicating a partial inhibition via iodide. The kinetic inhibition assays show that chloride is roughly twice as potent as a competitive inhibitor than iodide. Aside from the obvious difference in electronegativity, due to chloride's smaller ionic radius when compared to the iodide anion, steric hindrance would also play a lesser role in binding to the allosteric pocket. This could help explain why the kinetic data for the histidine mutant was nearly identical to that of the wildtype, while the structural data showed a much larger difference in anion binding. This likely applies to the tryptophan mutant as well, explaining why the kinetic data shows chloride inhibition of the F284W mutant, despite the structural data lacking any anomalous signal at the allosteric site.

Another more difficult option would be to perform the structural approach using chloride as the inhibitor. However, like other more physiologically relevant atoms, chloride's absorption edge (K edge of chloride is 4.4Å)[40] is at a much longer wavelength that is unattainable at most beamlines.[57]

It is also important to mention another key difference between the kinetic and structural approaches, namely the environment PEPCK is exposed to. To reiterate an integral point from earlier, the kinetic assays have high concentrations of substrates, metals and salts that are necessary for enzyme function. This includes the nucleotides that affect the conformation of the P-loop upon binding to the active site. In comparison, x-ray crystallographic conditions include the bare minimum of a buffer, precipitation agent, and manganese cations to induce nucleation. The kinetic and structural approaches by themselves, while providing insightful information, do not yield a complete picture. The combination of the two experimental methods act as supporting evidence to analyze allosteric regulation of PEPCK.

Chapter 5 Conclusions and Future Work

Kinetic assays performed on the wildtype enzyme reinforced the fact that PEPCK activity is lower in the reverse direction of catalysis. Chloride inhibition assays demonstrated inhibition in the reverse direction to be significantly stronger than that of the forward direction by an order of magnitude. The resulting K_I in the reverse direction determined the mM range of iodide concentration which would then be used in the subsequent crystal soaking experiments. WT rcPEPCK crystals were soaked over the 0 to 500 mM iodide concentration range, and the resulting anomalous signal found at the allosteric site was used to generate a binding isotherm, yielding a K_D similar to that of the K_I from the kinetic data. A combination of the kinetic and structural data provides evidence to suggest that binding to the allosteric site regulates enzyme activity *in vivo*, and ensures that PEPCK primarily catalyzes the reaction in the OAA→PEP direction needed for the gluconeogenic pathway despite being a thermodynamically reversible reaction.

Analysis of the allosteric site reveals key residues that form the pocket. Mutagenesis of one of these residues, along with the complementary kinetic and structural approaches used for the wildtype, shows the role F284 plays in anion binding. It is hypothesized that non-covalent interactions with the protein backbone, and well as weak anion-π interactions with aromatic residues serve to bind anions to this pocket. Substituting for another amino acid, even another aromatic residue of similar size like histidine, affects anionic binding and therefore decreases the anionic inhibition of rcPEPCK.

Structural comparisons between the wildtype and mutant enzyme variants demonstrate how binding to the allosteric site might affect nucleotide binding and therefore enzyme function. The close proximity of the allosteric site to that of the GTP/GDP nucleotide binding site causes any ligand binding at the allosteric site to directly inhibit enzyme activity by impeding nucleotide binding. In this way, anions that bind to the allosteric site can be classified as competitive inhibitors, since they alter apparent the K_M and prevent the nucleotide from binding. Binding to the allosteric site causes the P-loop to become highly disordered, making it more difficult for the enzyme to adapt the correct conformation for nucleotide binding.

As with other reversible competitive inhibitors, inhibition can be overcome provided substrate is added at saturating conditions. Under high substrate concentrations, there is a greater probability that the nucleotide can bind to the active site, and the P-loop can adopt the appropriate conformation required for catalysis. The difference in affinity for the different nucleotides in the forward and reverse directions of catalysis can help explain why PEPCK inhibition is stronger in the reverse direction. The GTP nucleotide is preferred over GDP, as evidenced by the K_M's and binding affinities. Due to PEPCK's greater affinity for the GTP, inhibition in the forward direction is relatively insignificant compared to that of the reverse direction.

Combining a kinetic approach studying chloride inhibition, and a structural approach analyzing the binding of iodide via anomalous signal, we can hypothesize that the inhibition of PEPCK activity in the reverse direction can be mostly attributed to allosteric regulation. In this way, binding to the allosteric site is proposed to result in the unidirectional nature of the PEPCK-catalyzed reaction in higher eukaryotes, ensuring gluconeogenesis can occur.

Further research is necessary to determine at what micromolar concentration of iodide will the active site begin to titrate in comparison to the millimolar scale of the allosteric site. X-ray diffraction at a specialized beamline with a longer wavelength would allow for the anomalous diffraction of chloride and a direct comparison with the chloride inhibition assays.[57] Further kinetic assays on the wildtype should to be performed using other anions for a more detailed understanding of the cellular environment *in vivo*. Extended mutagenesis on the rat cytosolic enzyme and repeated experiments on other PEPCK isoforms could be done to observe the effects of anionic inhibition on enzymes involved in the key regulatory steps of metabolic pathways.

References

(1) Voet, D., Voet, J. G. (2011) Biochemistry 4th ed. John Wiley & Sons, Hoboken, New Jersey.

(2) Chiba, Y., Kamikawa, R., Nakada-Tsukui, K., Saito-Nakano, Y., and Nozaki, T. (2015) Discovery of PP-type phosphoenolpyruvate carboxykinase genes in Eukaryotes and Bacteria. *J. Biol. Chem. 290*, 23960–23970.

(3) Hanson, R. W., and Garber, A. J. (1972, October) Phosphoenolpyruvate carboxykinase. I. Its role in gluconeogenesis. *Am. J. Clin. Nutr.*

(4) Forest, C., Tordjman, J., Glorian, M., Duplus, E., Chauvet, G., Quette, J., Beale, E. G., and Antoine, B. (2003) Fatty acid recycling in adipocytes: A role for glyceroneogenesis and phosphoenolpyruvate carboxykinase. *Biochem. Soc. Trans. 31*, 1125–1129.

(5) Tannen, R. L. (1978) Ammonia metabolism. *Am. J. Physiol. 235*, 265–277.

(6) Granner, D., Andreone, T., Sasaki, K., and Beale, E. (1983) Inhibition of transcription of the phosphoenolpyruvate carboxykinase gene by insulin. *Nature 305*, 549–551.

(7) O'Brien, R. M., Lucas, P. C., Forest, C. D., Magnuson, M. A., Granner, D. K. (1990) Identification of a sequence in the PEPCK gene that mediates a negative effect of insulin on trancription. *Science (80-.). 249*, 533–537.

(8) Liu, J., Park, E. A., Gurney, A. L., Roesler, W. J., and Hanson, R. W. (1991) Cyclic AMP induction of phosphoenolpyruvate carboxykinase (GTP) gene transcription is mediated by multiple promoter elements. *J. Biol. Chem. 266*, 19095–19102.

(9) Xiong, Y., Lei, Q. Y., Zhao, S., and Guan, K. L. (2011) Regulation of glycolysis and gluconeogenesis by acetylation of PKM and PEPCK. *Cold Spring Harb. Symp. Quant. Biol. 76*, 285–289.

(10) Latorre-Muro, P., Baeza, J., Armstrong, E. A., Hurtado-Guerrero, R., Corzana, F., Wu, L. E., Sinclair, D. A., Lopez-Buesa, P., Carrodeguas, J. A., Denu, J. M. (2018) Dynamic acetylation of cytosolic phosphoenolpyruvate carboxykinase toggles enzyme activity between gluconeogenic and anaplerotic reactions. *Mol Cell. 71*, 718–732.

(11) Carlson, G. M., and Holyoak, T. (2009) Structural Insights into the Mechanism of Phosphoenolpyruvate Carboxykinase Catalysis. *J. Biol. Chem. 284*, 27037–27041.

(12) Cui, D. S., Broom, A., McLeod, M. J., Meiering, E. M., and Holyoak, T. (2017) Asymmetric anchoring is required for efficient Ω-loop opening and closing in cytosolic phosphoenolpyruvate carboxykinase. *Biochemistry 56*, 2106–2115.

(13) Case, C. L., and Mukhopadhyay, B. (2007) Kinetic characterization of recombinant human cytosolic phosphoenolpyruvate carboxykinase with and without a His10-tag. *Biochim. Biophys. Acta - Gen. Subj. 1770*, 1576–1584.

(14) Johnson, K. A., and Goody, R. S. (2011) The original Michaelis constant: Translation of the 1913 Michaelis-Menten Paper. *Biochemistry 50*, 8264–8269.

(15) Northrop, D. B. (1998) On the meaning of Km and V/K in enzyme kinetics. *J. Chem. Educ. 75*, 1153–1157.

(16) Waldrop, G. L. (2009, January) A qualitative approach to enzyme inhibition. *Biochem. Mol. Biol. Educ.*

(17) Monod, J. F. (1961) Teleonomic mechanisms in cellular metabolism, growth and differentiation. *Cold Spring Harb. Symp. Quant. Biol. 26*, 389–401.

(18) Nussinov, R., and Tsai, C. J. (2015, February 1) Allostery without a conformational change? Revisiting the paradigm. *Curr. Opin. Struct. Biol.* Elsevier Ltd.

(19) Gunasekaran, K., Ma, B., and Nussinov, R. (2004, November 15) Is allostery an intrinsic property of all dynamic proteins? *Proteins Struct. Funct. Genet.*

(20) Fenton, A. W. (2008) Allostery: an illustrated definition for the "second secret of life." *Trends Biochem Sci 23*, 420–425.

(21) Stiffin, R. M., Sullivan, S. M., Carlson, G. M., and Holyoak, T. (2008) Differential inhibition of cytosolic PEPCK by substrate analogues. Kinetic and structural characterization of inhibitor recognition. *Biochemistry 47*, 2099–2109.

(22) Izui, K., Matusda, Y., Kameshita, I., Katsuki, H., Woods, A. E. (1983) Phosphoenolpyruvate carboxylase of Escherichia coli. Inhibition by various analogs and homologs of phosphoenolpyruvate. *J. Biochem. 94*, 1789–1795.

(23) Robinson, B. H., and Oei, J. (1975) 3-Mercaptopicolinic acid, a preferential inhibitor of the cytosolic phosphoenolpyruvate carboxykinase. *FEBS Lett. 58*, 12–15.

(24) Makinen, A. L., and Nowak, T. (1983) 3-Mercaptopicolinate. A reversible active site inhibitor of avian liver phosphoenolpyruvate carboxykinase. *J. Biol. Chem. 258*, 11654–11662.

(25) Balan, M. D., McLeod, M. J., Lotosky, W. R., Ghaly, M., and Holyoak, T. (2015) Inhibition and Allosteric Regulation of Monomeric Phosphoenolpyruvate Carboxykinase by 3-Mercaptopicolinic Acid. *Biochemistry 54*, 5878–5887.

(26) Kretsinger, R. H., Uversky, V. N., Permyakov, E. A. (2013) Cellular Electrolyte Metabolism. *Encycl. Met.* Springer.

(27) Frausto de Silva, J. J. R., Williams, R. J. P. (2001) Sodium, potassium, and chlorine osmotic control, electrolytic equilibria, and currents. *Biol. Chem. Elem. Inorg. Chem. Life.* Oxford University Press.

(28) Krissinel, E., and Henrick, K. (2007) Inference of Macromolecular Assemblies from Crystalline State. *J. Mol. Biol. 372*, 774–797.

(29) Rossmann, M. G. (1990) The molecular replacement method. *Acta Crystallogr. Sect. A 46*, 73–82.

(30) Hendrickson, W. A. (1985) Analysis of protein structure from diffraction measurement at multiple wavelengths. *Trans. Am. Cryst. Assoc. 21*, 11–21.

(31) Smith, J. L. (1991) Determination of three-dimensional structure by multiwavelength anomalous diffraction. *Curr. Opin. Struct. Biol. 1*, 1002–1011.

(32) Hendrickson, W. A. (2014) Anomalous diffraction in crystallographic phase evaluation. *Q. Rev. Biophys.* Cambridge University Press.

(33) Rose, J. P., and Wang, B. C. (2016) SAD phasing: History, current impact and future opportunities. *Arch. Biochem. Biophys. 602*, 80–94.

(34) Sullivan, S. M., and Holyoak, T. (2007) Structures of rat cytosolic PEPCK: Insight into the mechanism of phosphorylation and decarboxylation of oxaloacetic acid. *Biochemistry 46*, 10078–10088.

(35) Troy A. Johnson, T. H. (2012) The Ω-Loop Lid Domain of Phosphoenolpyruvate Carboxykinase Is Essential for Catalytic Function. *Biochemistry 51*, 9547–9559.

(36) Holyoak, T., Sullivan, S. M., and Nowak, T. (2006) Structural insights into the mechanism of PEPCK catalysis. *Biochemistry 45*, 8254–8263.

(37) McNicholas, S., Potterton, E., Wilson, K. S., and Noble, M. E. M. (2011) Presenting your structures: The CCP4mg molecular-graphics software. *Acta Crystallogr. Sect. D Biol. Crystallogr. 67*, 386–394.

(38) Johnson, T. A., McLeod, M. J., and Holyoak, T. (2016) Utilization of Substrate Intrinsic Binding Energy for Conformational Change and Catalytic Function in Phosphoenolpyruvate Carboxykinase. *Biochemistry 55*, 575–587.

(39) Troy A. Johnson, T. H. (2010) Increasing the conformational entropy of the Ω-loop lid domain in PEPCK impairs catalysis and decreases catalytic fidelity. *Biochemistry 49*, 5176–5187.

(40) Brennan, S., Cowan, P. L. (1992) A suite of programs for calculating x-ray absorption, reflection and diffraction performance for a variety of materials at arbitrary wavelengths. *Rev. Sci. Instrum. 63*, 850.

(41) Dubnau, D. (1999) DNA Uptake in Bacteria. *Annu. Rev. Microbiol. 53*, 217–244.

(42) Lorenz, M. G., Wackernagel, W. (1994) Bacterial Gene Transfer by Natural Genetic Transformation in the Environment. *Microbiol. Rev. 58*, 563–602.

(43) Studier, F. W. (2005) Protein Production by Auto-Induction in High-Density Shaking Cultures. *Protein Expr. Purif. 41*, 207–234.

(44) Otwinowski, Z., Minor, W. (1997) Processing of x-ray diffraction data collected in oscillation mode. *Methods Enzym. 276*, 307–326.

(45) Collaborative Computational Project, Number 4. (1994) The CCP4 suite: programs for protein crystallography. *Acta Crystallogr. Sect. D Biol. Crystallogr. 50*, 760–763.

(46) Vagin, A., Teplyakov, A. (1997) MOLREP: an Automated Program for Molecular Replacement. *J. Appl. Crystallogr. 30*, 1022–1025.

(47) Emsley, P., Lohkamp, B., Scott, W. G., Cowtan, K. (2010) Features and development of Coot. *Acta Crystallogr. Sect. D*

Biol. Crystallogr. 66, 486–501.

(48) Tsai, C. S. (1967) Spontaneous decarboxylation of oxalacetic acid. *Can. J. Chem. 45*, 873–880.

(49) Colombo, G., Carlson, G. M., and Lardy, H. A. (1981) Phosphoenolpyruvate Carboxykinase (Guanosine 5'-Triphosphate) from Rat Liver Cytosol. Dual-Cation Requirement for the Carboxylation Reaction. *Biochemistry 20*, 2749–2757.

(50) Hebda, C. A., and Nowak, T. (1982) Phosphoenolpyruvate Carboxykinase. Mn2+ and Mn2+ Substrate Complexes *257*, 5515–5522.

(51) Rocchio, S., Duman, R., El Omari, K., Mykhaylyk, V., Orr, C., Yan, Z., Salmon, L., Wagner, A., Bardwell, J. C. A., Horowitz, S. (2019) Identifying dynamic , partially occupied residues using anomalous scattering research papers. *Acta Crystallogr. Sect. D Biol. Crystallogr. D75*, 1084–1095.

(52) Lewis, C. T., Seyer, J. M., and Carlson, G. M. (1989) Cysteine 288: An essential hyperreactive thiol of cytosolic phosphoenolpyruvate carboxykinase (GTP). *J. Biol. Chem. 264*, 27–33.

(53) Jackson, M. R., Beahm, R., Duvvuru, S., Narasimhan, C., Wu, J., Wang, H. N., Philip, V. M., Hinde, R. J., and Howell, E. E. (2007) A preference for edgewise interactions between aromatic rings and carboxylate anions: The biological relevance of anion-quadrupole interactions. *J. Phys. Chem. B 111*, 8242–8249.

(54) Berryman, O. B., Hof, F., Hynes, M. J., and Johnson, D. W. (2006) Anion-π interaction augments halide binding in solution. *Chem. Commun. 1*, 506–508.

(55) Philip, V., Harris, J., Adams, R., Nguyen, D., Spiers, J., Baudry, J., Howell, E. E., and Hinde, R. J. (2011) A survey of aspartate-phenylalanine and glutamate-phenylalanine interactions in the protein data bank: Searching for anion-π pairs. *Biochemistry 50*, 2939–2950.

(56) Chakravarty, S., Ung, A. R., Moore, B., Shore, J., and Alshamrani, M. (2018) A Comprehensive Analysis of Anion-Quadrupole Interactions in Protein Structures. *Biochemistry 57*, 1852–1867.

(57) Wagner, A., Duman, R., Henderson, K., and Mykhaylyk, V. (2016) In-vacuum long-wavelength macromolecular crystallography. *Acta Crystallogr. Sect. D Struct. Biol. 72*, 430–439.

Appendix A: PEPCK Expression Vector Map

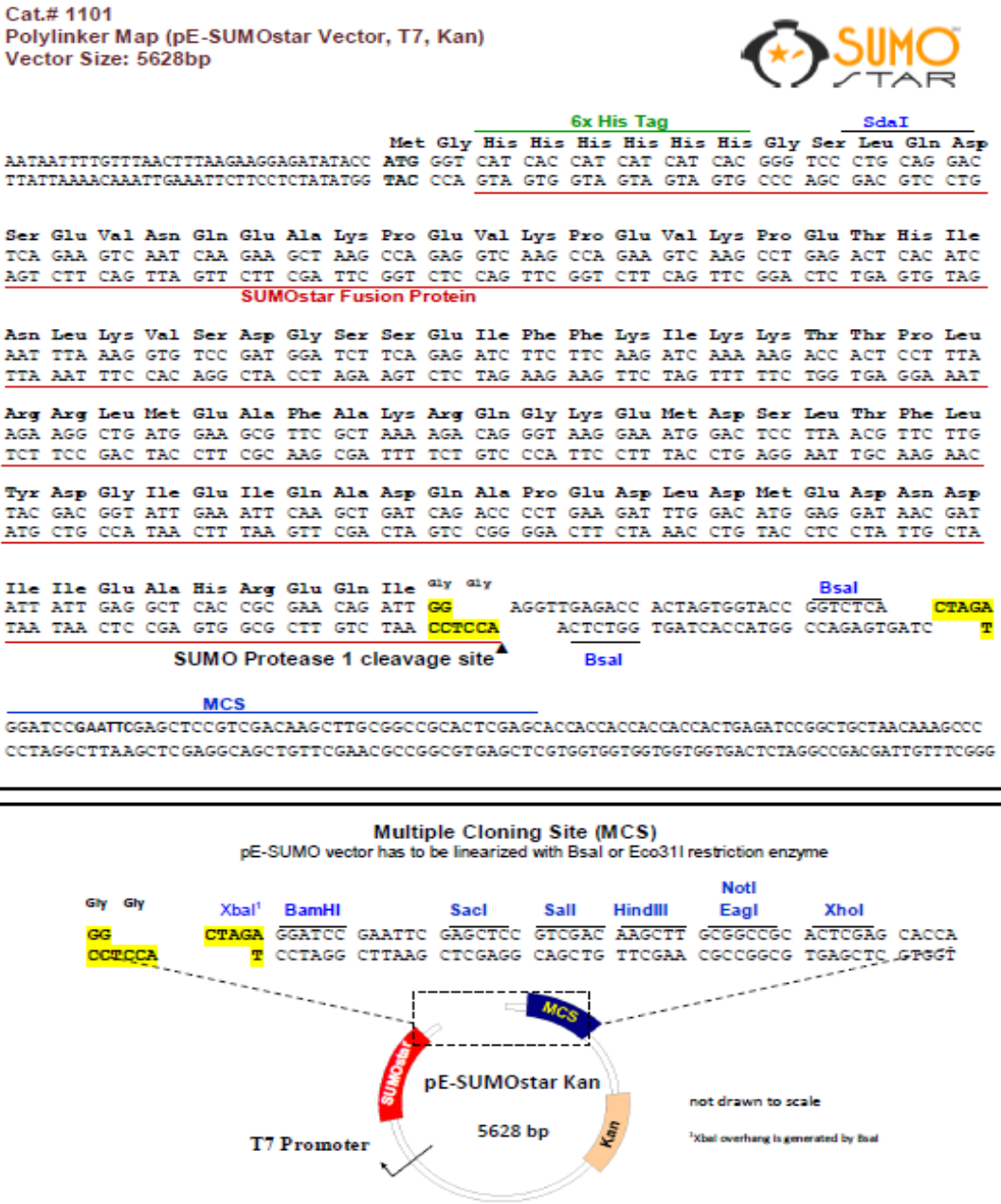

Figure A: Polylinker map for the pE-SUMOstar expression vector. The WT rcPEPCK gene (accession # NM_198780.3; NP_942075.1) was cloned into the pE-SUMOstar vector as described previously, transformed into the BL21 *E. coli* protein expression cell line and stored at -80°C as a common cell stock.

Appendix B: Kinetic Characterization of WT rcPEPCK

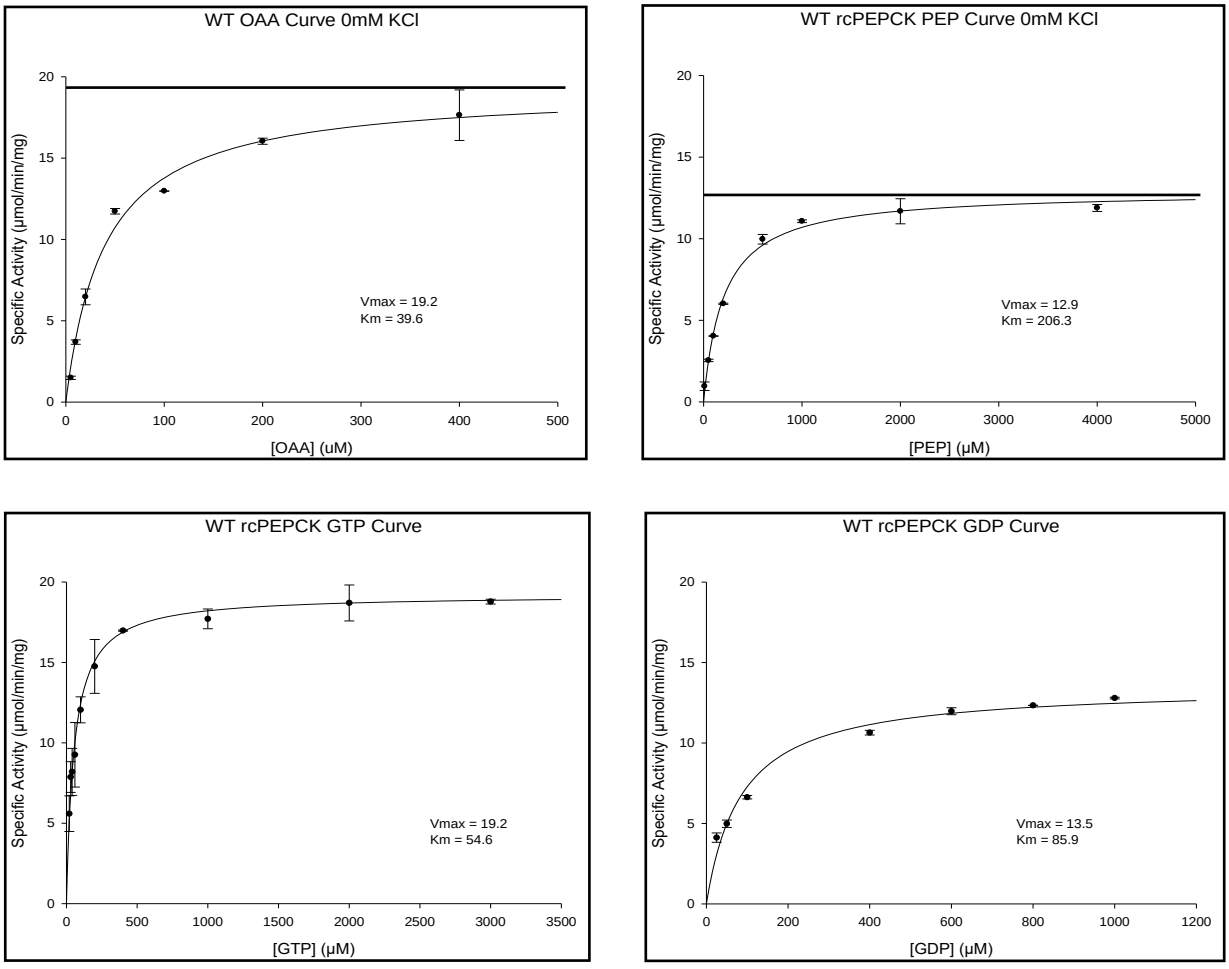

Figure B: Michaelis-Menten curves of the PEPCK-catalyzed reaction both in the OAA → PEP direction (top left), and the PEP → OAA direction (top right). Nucleotide curves of the PEPCK-catalyzed reaction both in the OAA → PEP direction (bottom left) and the PEP → OAA direction (bottom right).

Appendix C: Kinetic Inhibition of WT rcPEPCK by Chloride

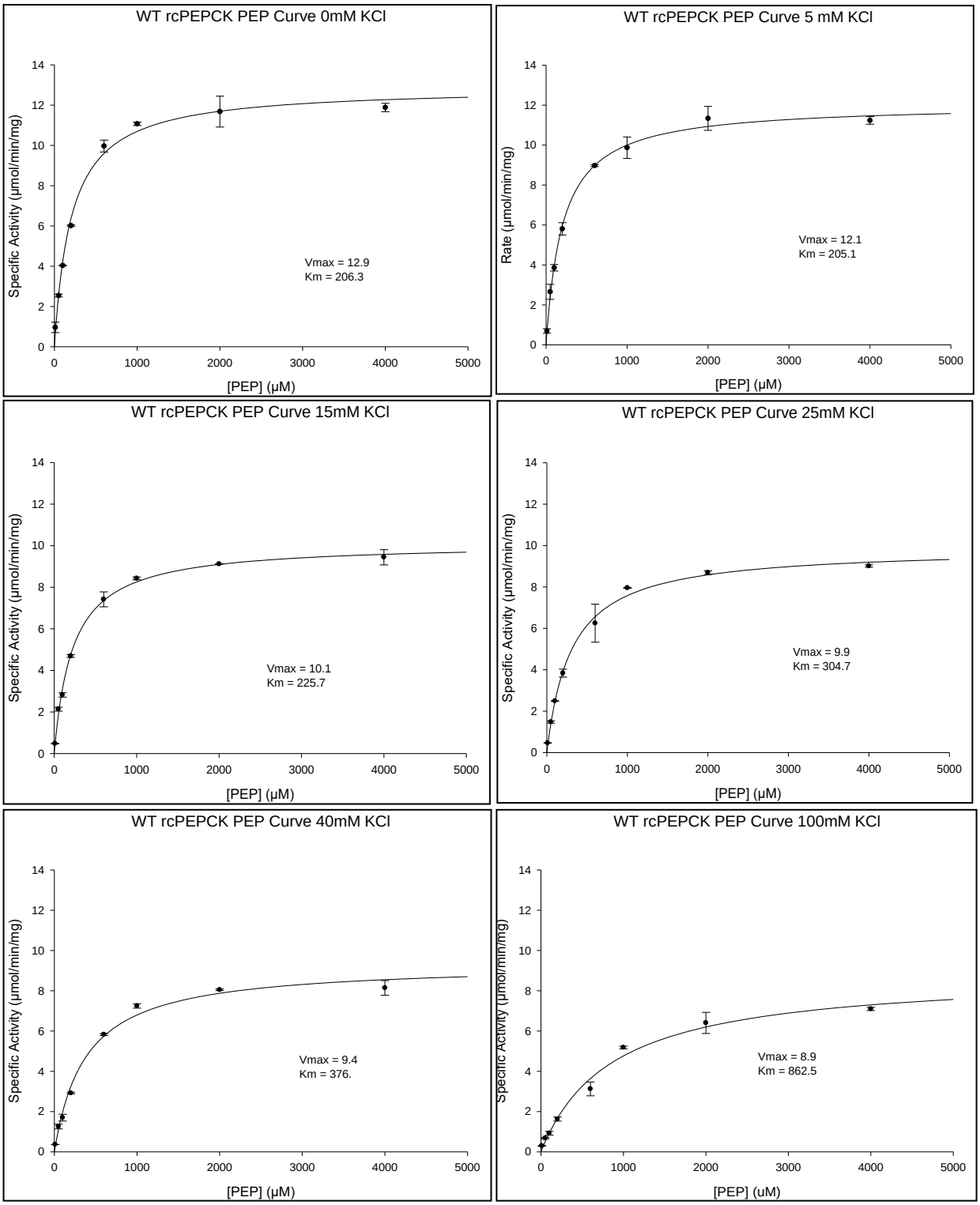

Figure C1: WT rcPEPCK reverse direction kinetic inhibition assays under increasing chloride concentrations.

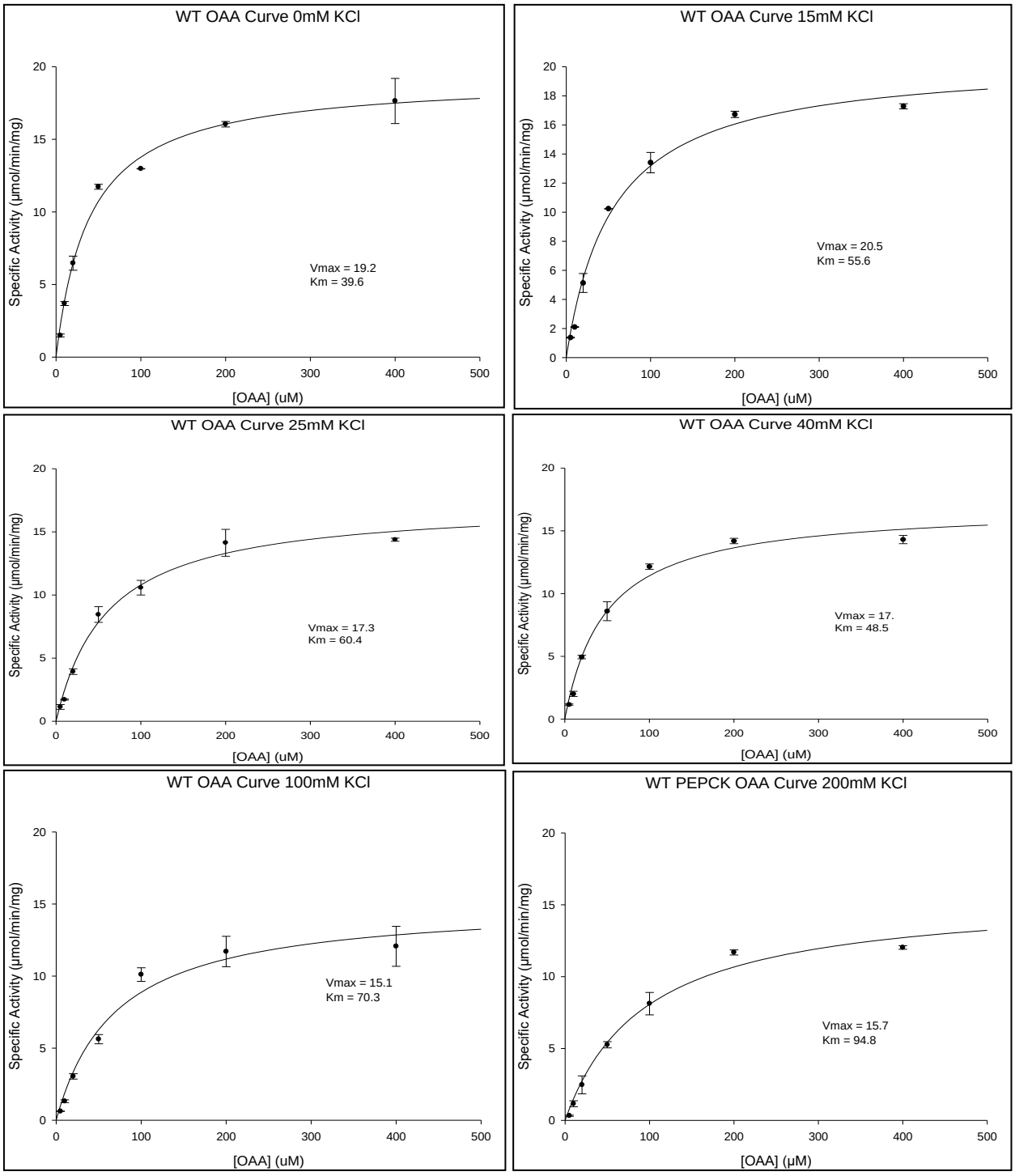

Figure C2: WT rcPEPCK forward direction kinetic inhibition assays under increasing chloride concentrations.

Appendix D: Reverse Direction Inhibition of WT rcPEPCK by Iodide

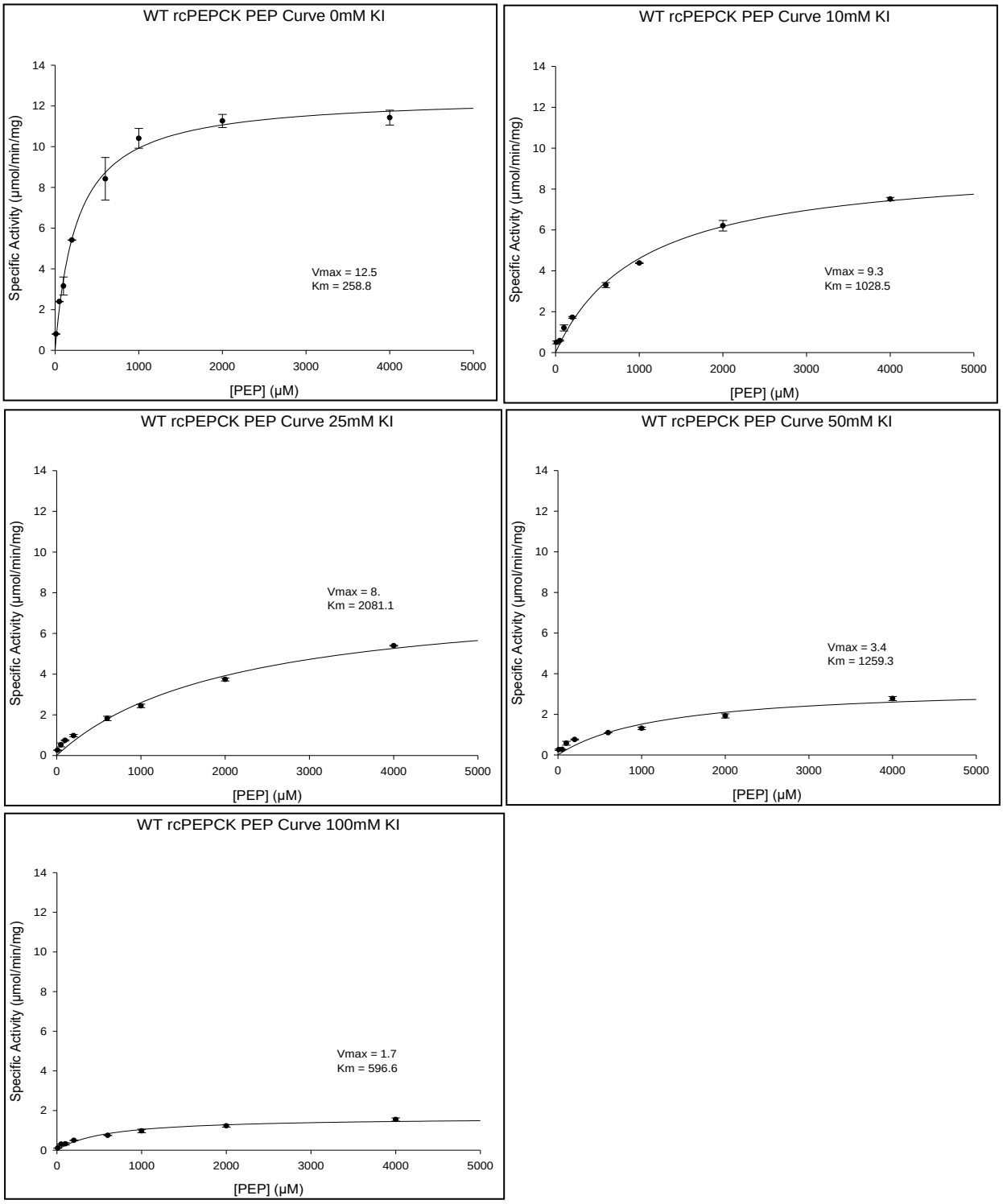

Figure D: WT rcPEPCK reverse direction kinetic inhibition assays under increasing iodide concentrations.

Appendix E: Kinetic Characterization of F284H and F284W rcPEPCK Mutants

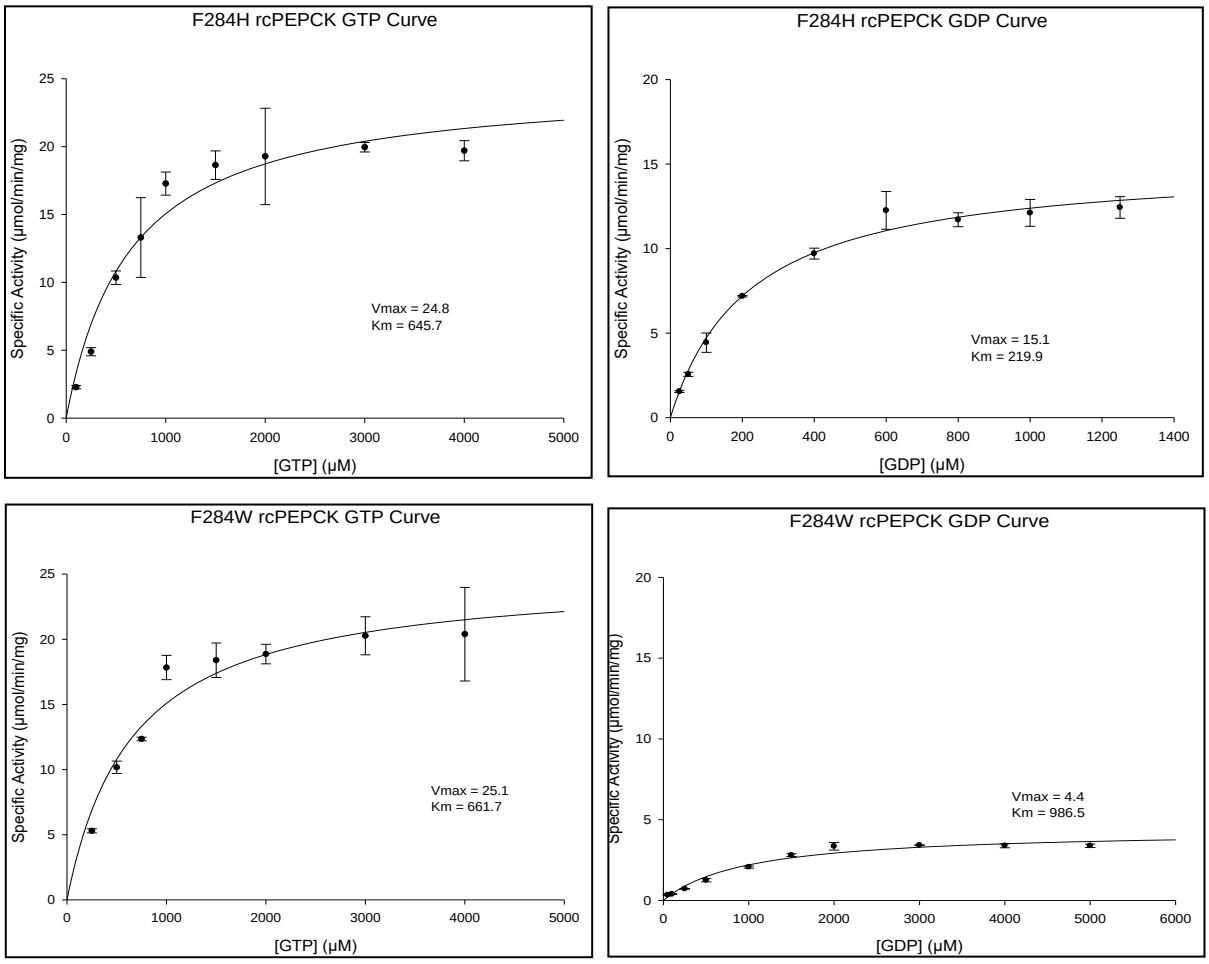

Figure E: Kinetic characterization and determination of KM for the GTP and GDP nucleotides for the F284H (top) and F284W (bottom) rcPEPCK mutants.

Appendix F: Kinetic Inhibition of F284H rcPEPCK by Chloride

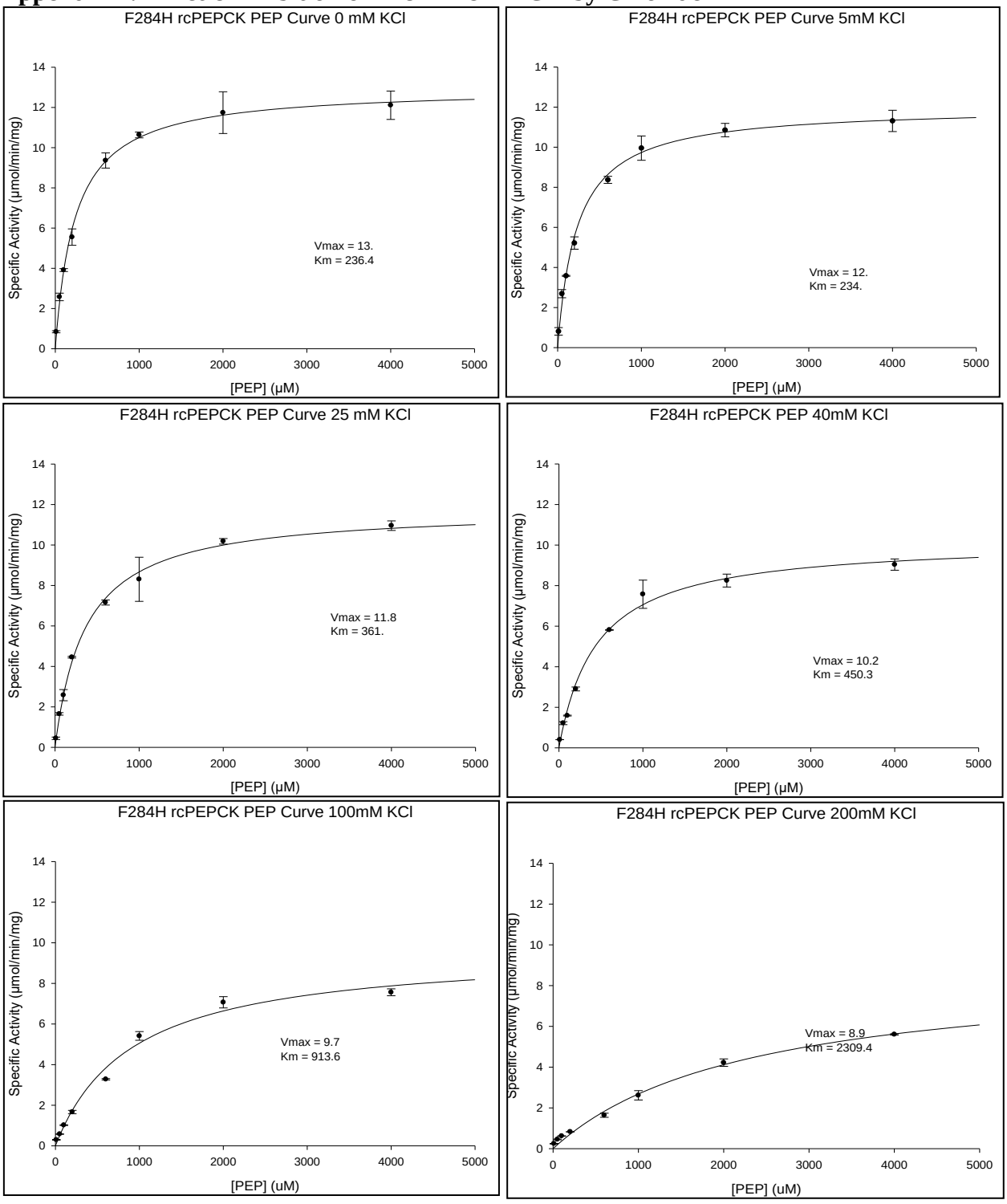

Figure F1: F284H rcPEPCK reverse direction kinetic inhibition assays under increasing chloride concentration.

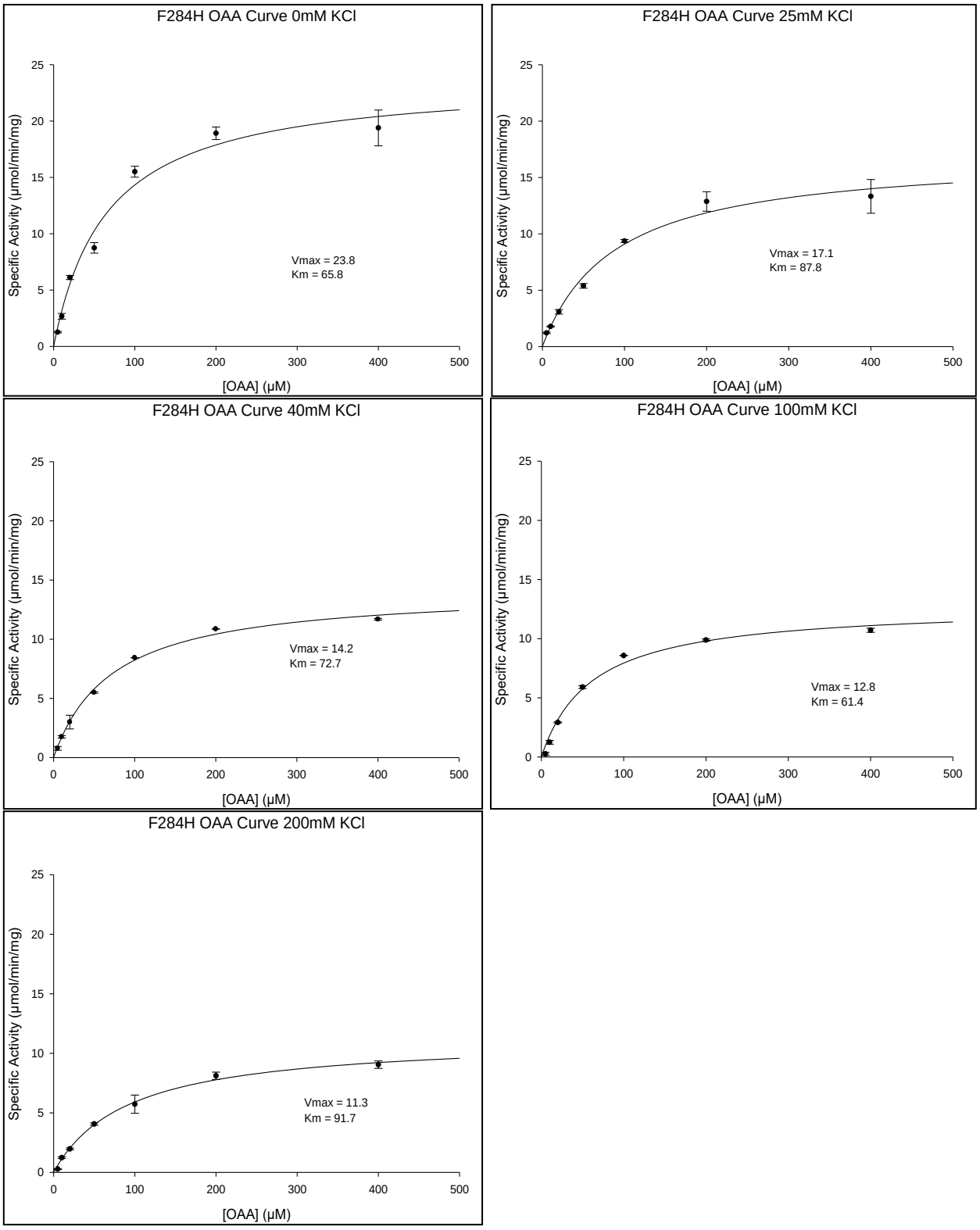

Figure F2: F284H rcPEPCK forward direction kinetic inhibition assays under increasing chloride concentration.

Appendix G: Kinetic Inhibition of F284W rcPEPCK by Chloride

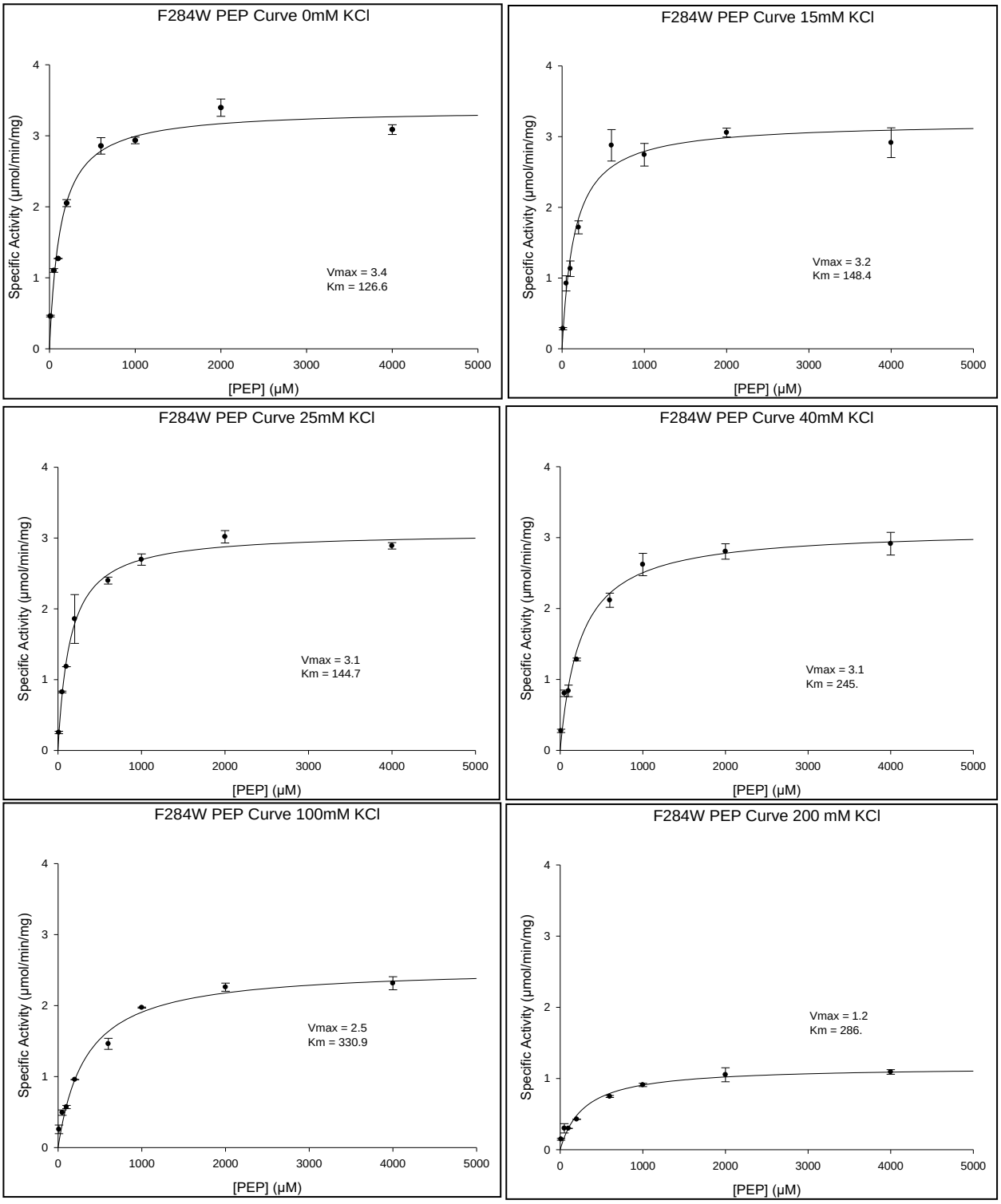

Figure G1: F284W rcPEPCK reverse direction kinetic inhibition assays under increasing chloride concentration.

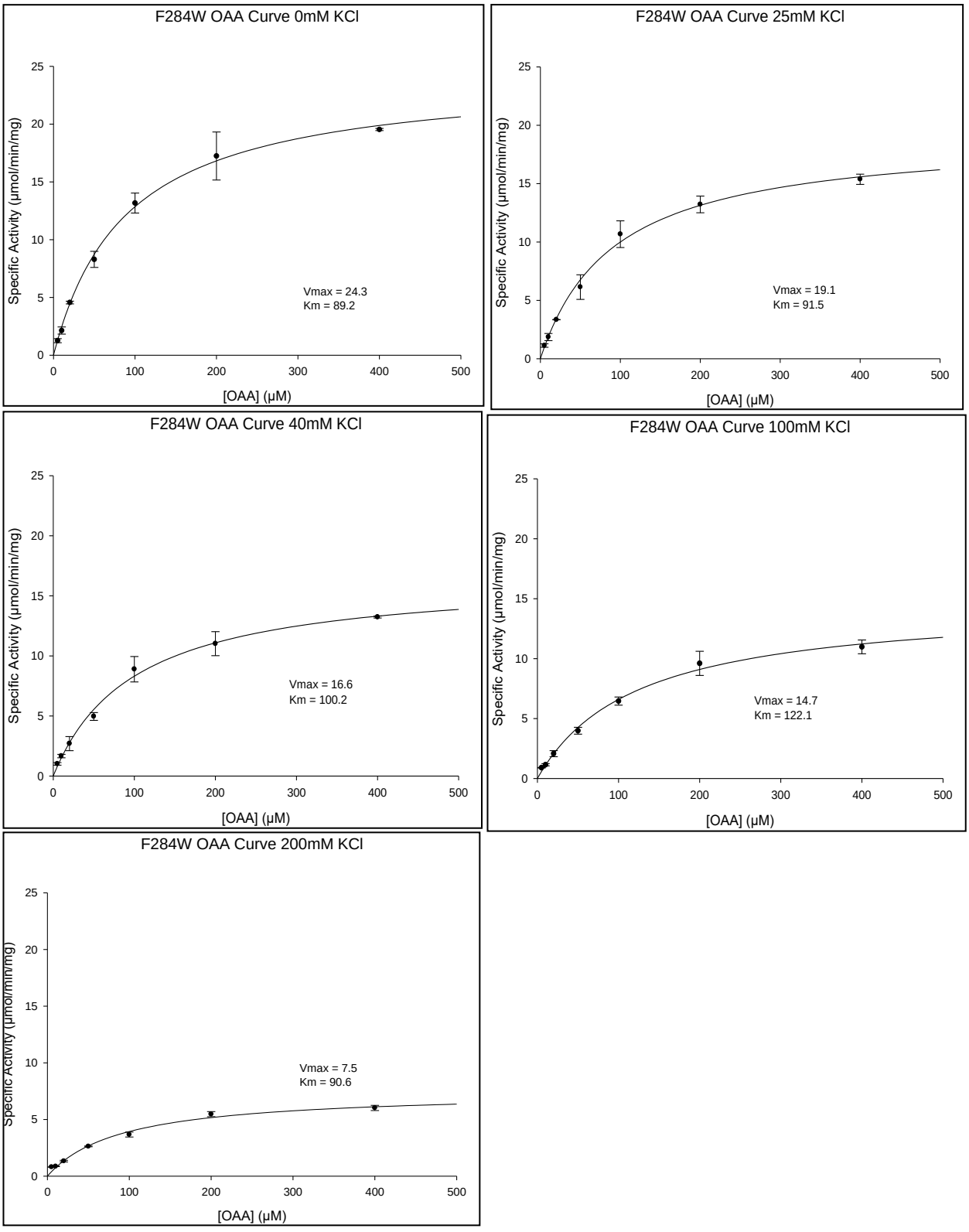

Figure G2: F284W rcPEPCK forward direction kinetic inhibition assays under increasing chloride concentration.

Appendix H: Kinetic parameters and competitive inhibition re-plots for wildtype and mutant rcPEPCK

Table H1: Kinetic parameters of WT rcPEPCK and inhibition constant of KCl

KCl (mM)	Specific Activity (µmol/min/mg)	K_M (µM)	1/Specific Activity	K_M/Spec. Act.
a) OAA + GTP → PEP + GDP + CO_2				
0	19.2	35.6	0.0521	1.854
5	19.6	46.0	0.0510	2.347
15	20.5	55.6	0.0488	2.712
25	17.3	60.4	0.0578	3.491
40	17	48.5	0.0588	2.853
100	15.1	70.3	0.0662	4.656
200	15.7	94.8	0.0637	6.038
b) PEP + GDP + CO_2 → OAA + GTP				
0	12.9	206.3	0.0775	15.992
5	12.1	205.1	0.0826	16.950
15	10.1	225.7	0.0990	22.347
25	9.9	304.7	0.1010	30.778
40	9.4	376.0	0.1064	40.000
100	8.9	862.5	0.1124	96.910

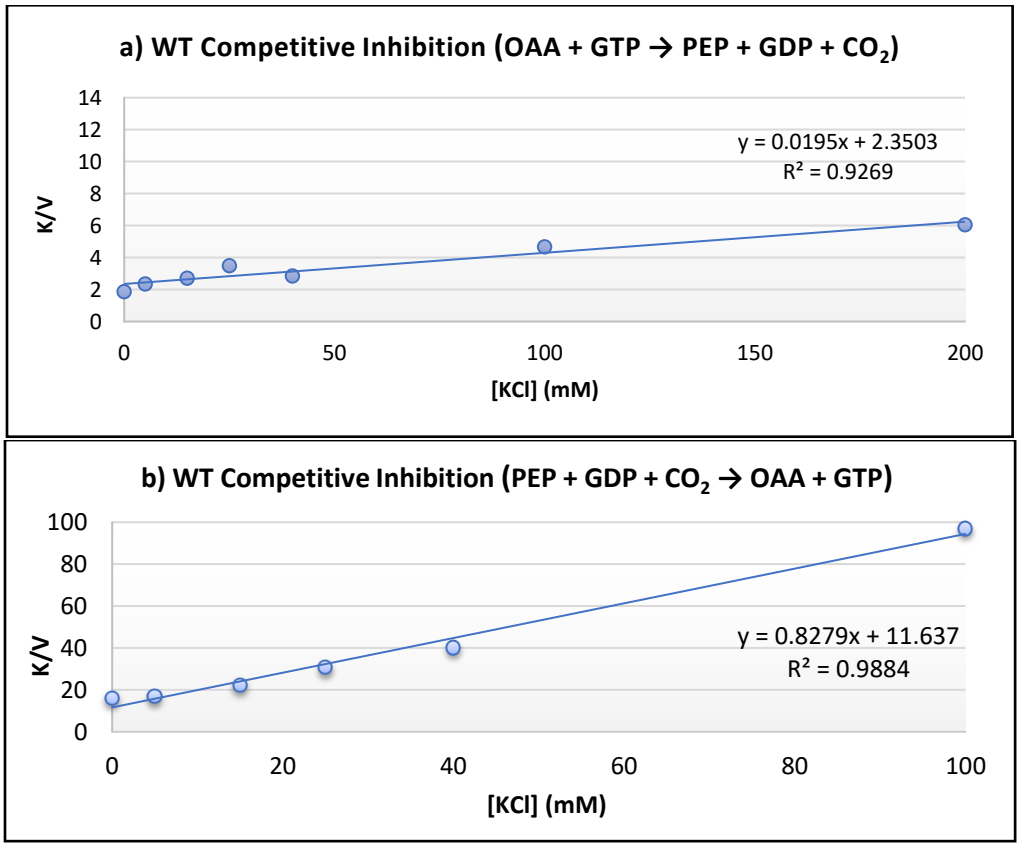

Figure H1: Kinetic re-plots of chloride concentration and ratio of K_M/Specific Activity for WT rcPEPCK.

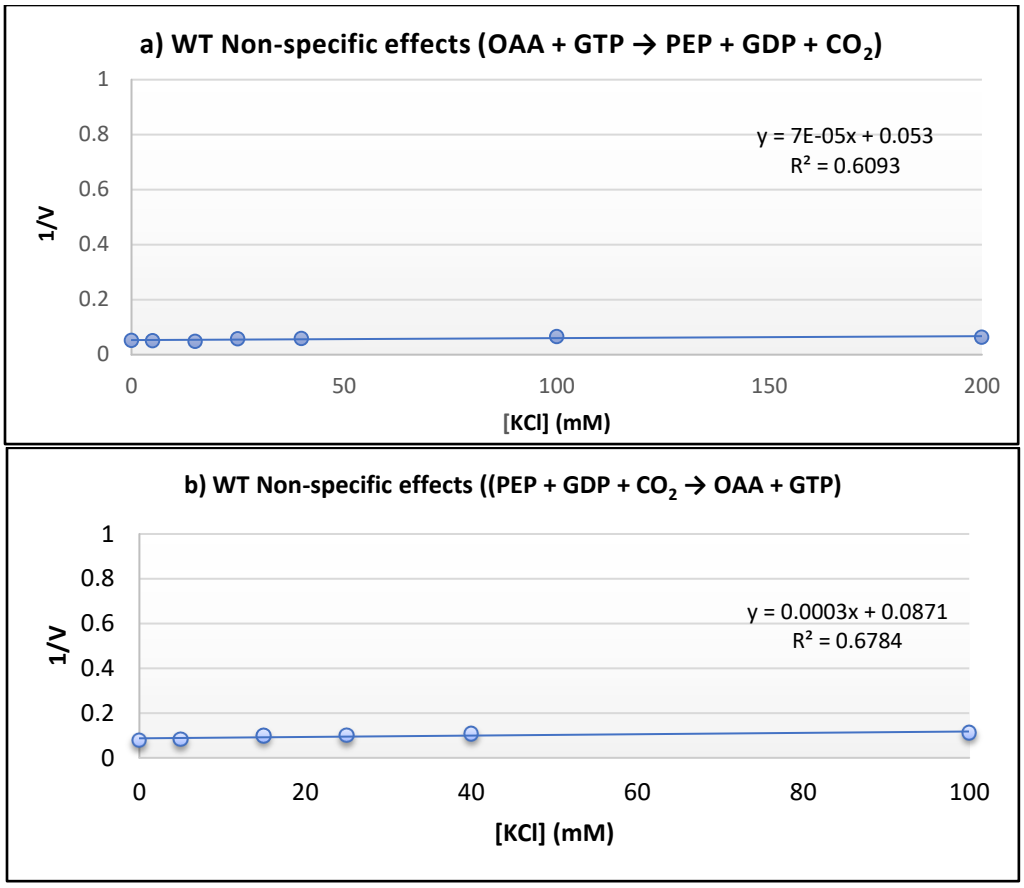

Figure H2: Kinetic re-plots of chloride concentration and ratio of 1/Specific Activity for WT rcPEPCK.

Table H2: Kinetic parameters of F284H rcPEPCK and inhibition constant of KCl

KCl (mM)	Specific Activity (µmol/min/mg)	K_M (µM)	1/Specific Activity	K_M/Spec. Act.
a) OAA + GTP → PEP + GDP + CO_2				
0	23.7	65.8	0.0422	2.776
25	17.1	87.8	0.0585	5.135
40	14.2	72.7	0.0704	5.120
100	12.8	61.4	0.0781	4.797
200	11.3	91.7	0.0885	8.115
b) PEP + GDP + CO_2 → OAA + GTP				
KCl (mM)	**Specific Activity (µmol/min/mg)**	**K_M (µM)**	**1/Specific Activity**	**K_M/Spec. Act.**
0	13	236.4	0.0769	18.185
5	12	234	0.0833	19.500
15	12.1	290.7	0.0826	24.025
25	11.8	361	0.0848	30.593
40	10.2	450.3	0.0980	44.147
100	9.7	913.6	0.1031	94.186
200	8.9	1500	0.1124	168.539

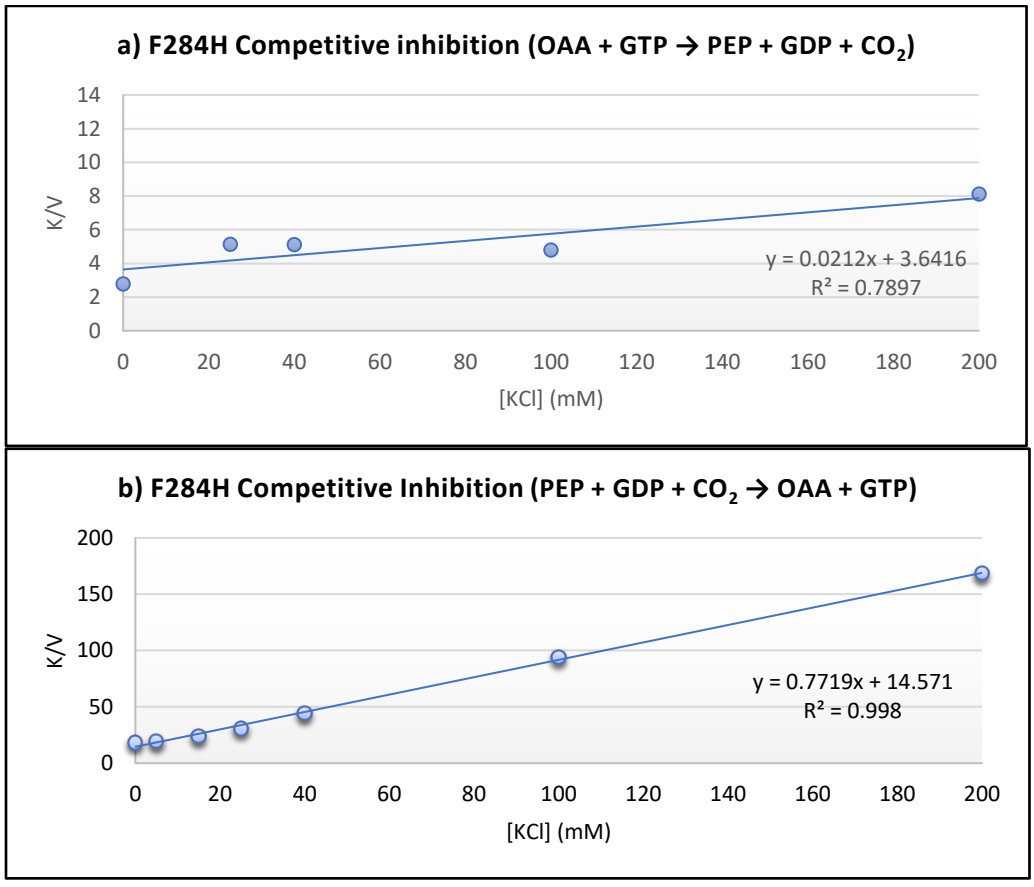

Figure H3: Kinetic re-plots of chloride concentration and ratio of K_M/Specific Activity for F284H rcPEPCK

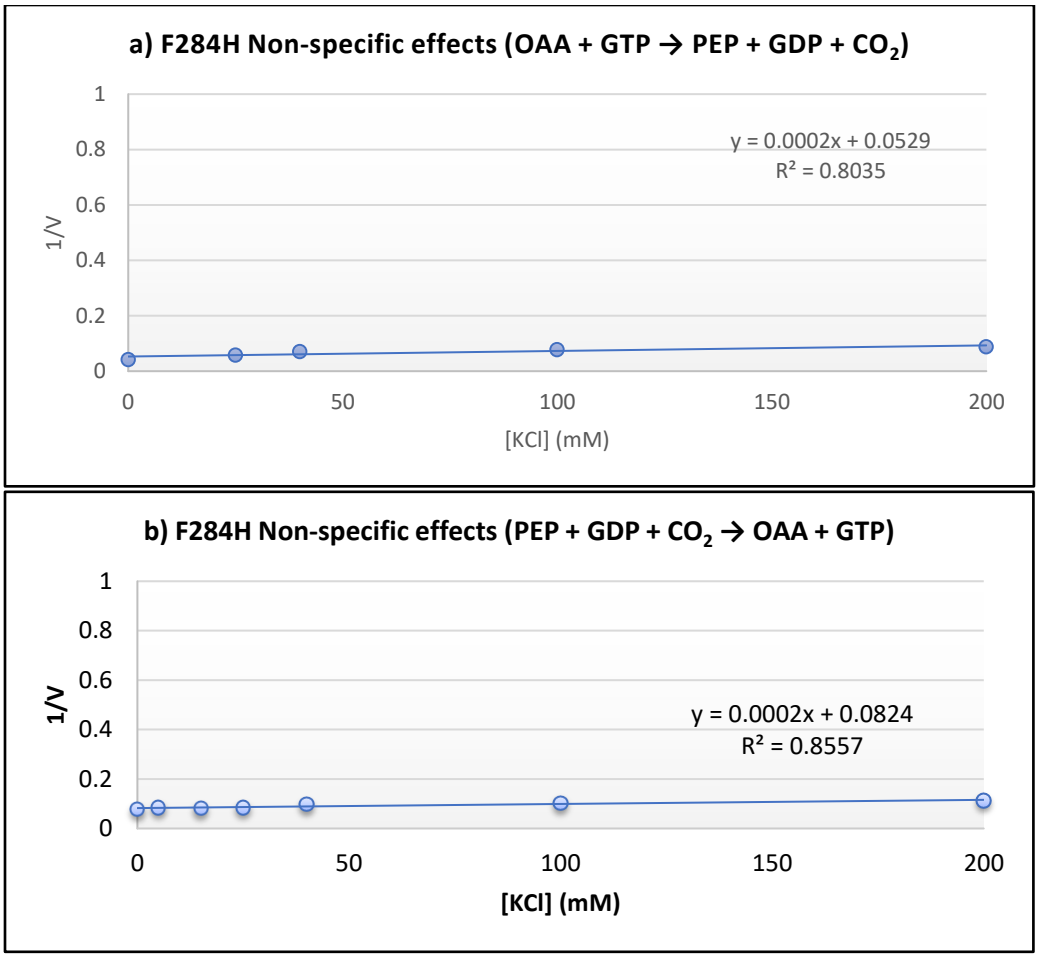

Figure H4: Kinetic re-plots of chloride concentration and ratio of 1/Specific Activity for F284H rcPEPCK.

Table H3: Kinetic parameters of F284W rcPEPCK and inhibition constant of KCl

KCl (mM)	Specific Activity (µmol/min/mg)	K_M (µM)	1/Specific Activity	K_M/Spec. Act.
a) OAA + GTP → PEP + GDP + CO_2				
0	24.3	89.2	0.0412	3.671
25	19.1	91.5	0.0524	4.791
40	16.6	100.2	0.0602	6.036
100	14.7	122.1	0.0680	8.306
200	7.5	90.6	0.1333	12.080
b) PEP + GDP + CO_2 → OAA + GTP				
KCl (mM)	**Specific Activity (µmol/min/mg)**	**K_M (µM)**	**1/Specific Activity**	**K_M/Spec. Act.**
0	3.4	126.6	0.2941	37.235
15	3.2	148.4	0.3125	46.375
25	3.1	144.7	0.3226	46.677
40	3.1	245	0.3326	79.0323
100	2.5	330.9	0.4000	132.360
200	1.2	286	0.8333	238.333

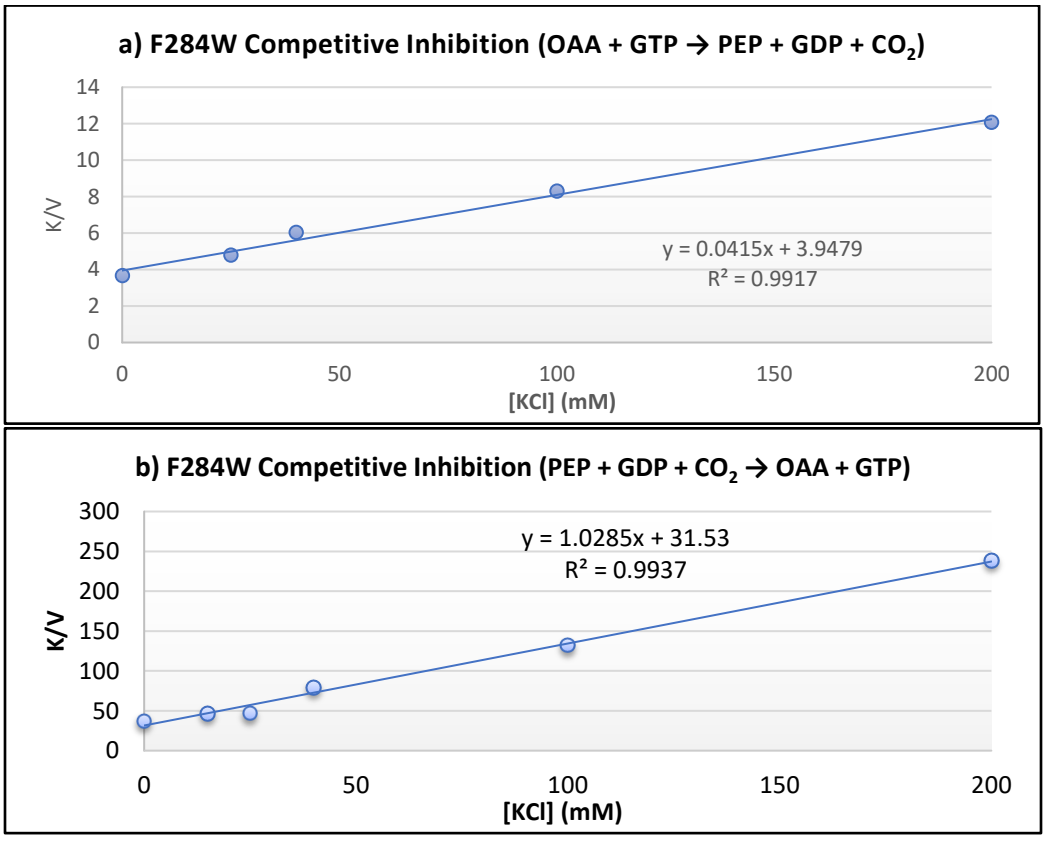

Figure H5: Kinetic re-plots of chloride concentration and ratio of K_M/Specific Activity for F284W rcPEPCK.

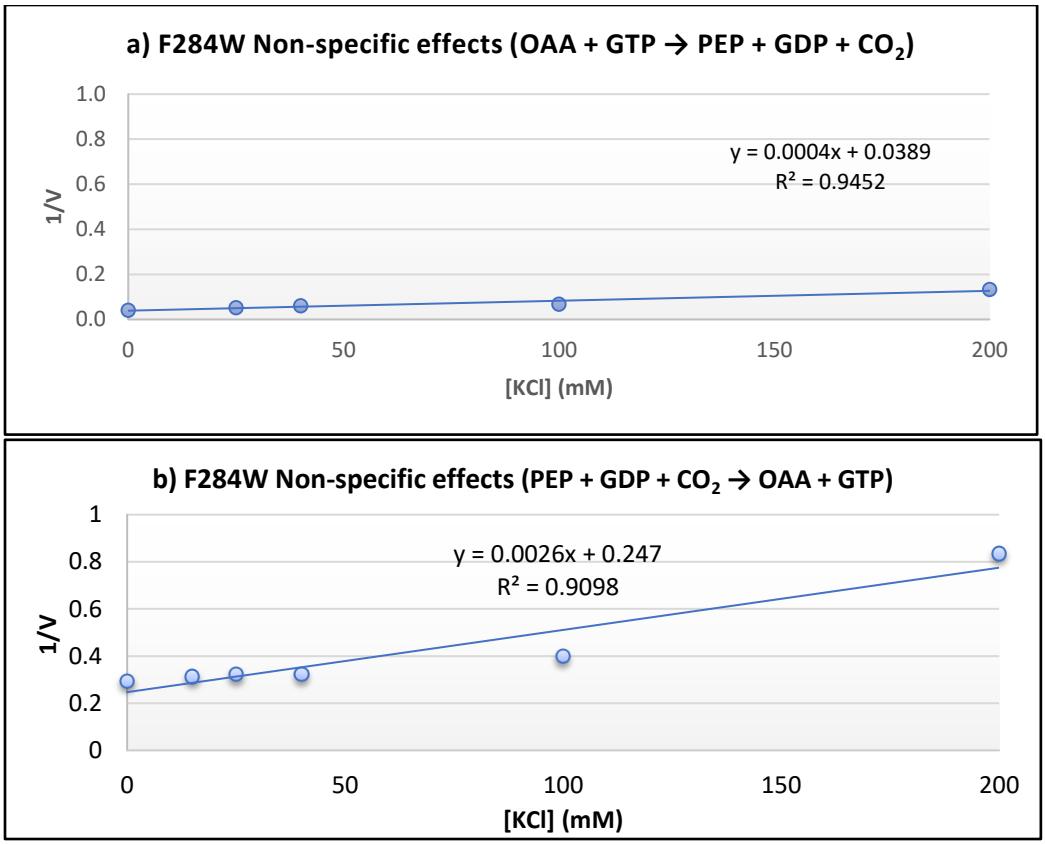

Figure H6: Kinetic re-plots of chloride concentration and ratio of 1/Specific Activity for F284W rcPEPCK.

Table H4: Kinetic parameters of WT rcPEPCK and inhibition constant of KI

PEP + GDP + CO_2 → OAA + GTP KCl (mM)	Specific Activity (µmol/min/mg)	K_M (µM)	1/Specific Activity	K_M/Spec. Act.
0	12.5	258.8	0.0800	20.704
10	9.3	1028.5	0.1075	110.591
25	8	2081.1	0.1250	260.138
50	3.4	1259.3	0.2941	370.382
100	1.7	596.6	0.5882	350.941

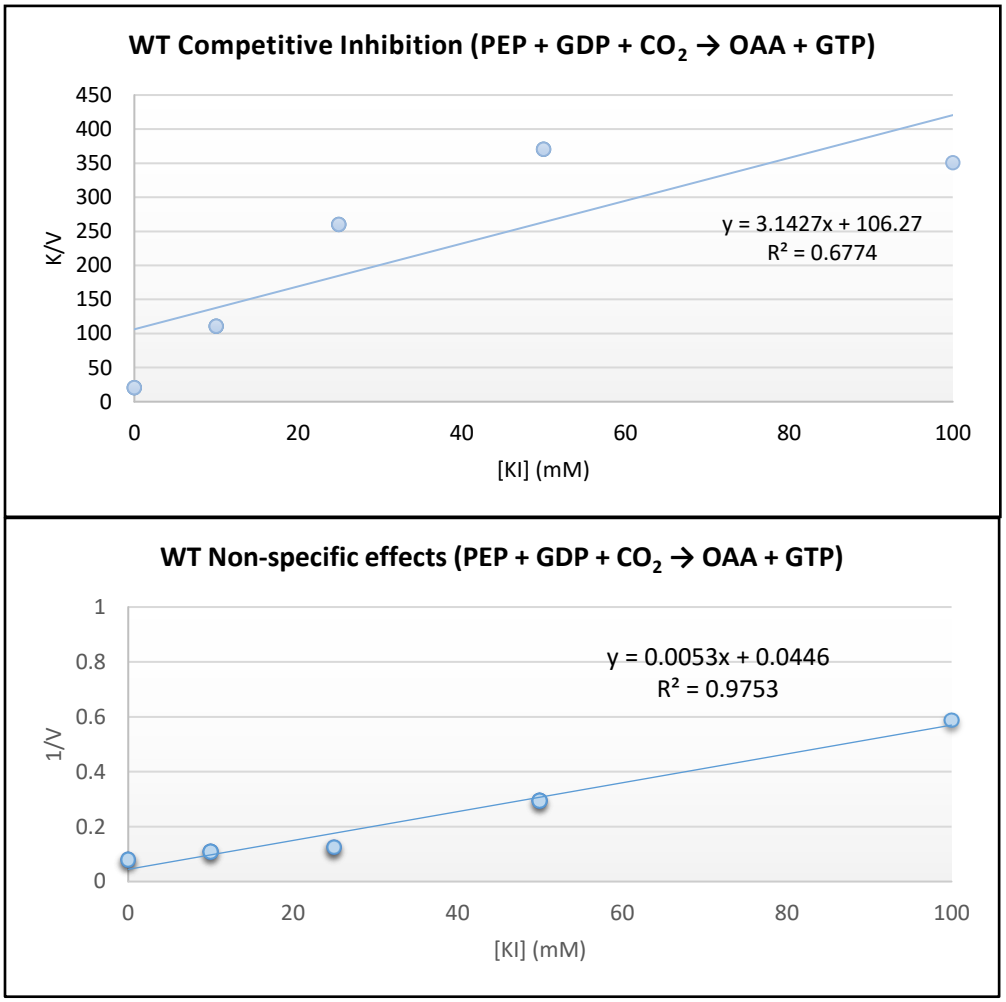

Figure H7: Kinetic re-plots of iodide concentration and ratio of 1/Specific Activity for WT rcPEPCK.

Appendix I: Anomalous peak heights for iodide ions bound to WT, F284H and F284W rcPEPCK

Table I1: Anomalous peak height raw data for WT rcPEPCK in $e^-/Å^3$ corresponding to crystals soaked from 10 to 500 mM KI. Iodides 1 and 2 are bound to the active site, while Iodide 3 represents the allosteric site. The remaining iodides have been numbered by decreasing peak height using the 500 mM KI structure as a reference.

Iodide #	500 mM KI	250 mM KI	100 mM KI	50 mM KI	25 mM KI	10 mM KI
Mn	**13.7**	**11.26**	**11.56**	**15.8**	**17.28**	**16.23**
1	14.87	17.41	11.27	19.91	13.05	11.91
2	11.71	8.33	7.72	5.79	6.93	
3	**13.68**	**12.02**	**10.72**	**11.54**	**10.41**	**6.26**
4	10.95	10.11	6.24	9.05	6.66	
5	10.9	10.23	5.9			
6	9.05	9.61	11.43	6.63	5.55	
7	8.77	6.51		6.03		
8	8.32	6.53				
9	7.65	6.31				
10	7.15	6.02		5.6	5.9	
11	7.09					
12	6.98					
13	6.58	5.39				
14	6.56					
15	6.02					
16	5.99	5.84				
17	5.97	6.15				
18	5.29	5.11				

Table I2: Normalized anomalous peak height data for WT rcPEPCK in $e^-/Å^3$ corresponding to crystals soaked from 10 to 500 mM KI. Iodides 1 and 2 are bound to the active site, while Iodide 3 represents the allosteric site. The remaining iodides have been numbered by decreasing peak height using the 500 mM KI structure as a reference. The data was normalized by dividing peak height of the iodide by the peak height of the corresponding Mn (M1) cation.

Iodide #	500 mM KI	250 mM KI	100 mM KI	50 mM KI	25 mM KI	10 mM KI
Mn	**1**	**1**	**1**	**1**	**1**	**1**
1	1.085	1.546	0.975	1.260	0.755	0.734
2	0.855	0.740	0.668	0.366	0.401	
3	**0.999**	**1.068**	**0.927**	**0.730**	**0.602**	**0.386**
4	0.799	0.898	0.540	0.573	0.385	
5	0.796	0.909	0.510			
6	0.661	0.853	0.989	0.420	0.321	
7	0.640	0.578		0.382		
8	0.607	0.580				
9	0.558	0.560				
10	0.522	0.535		0.354	0.341	
11	0.518					
12	0.510					
13	0.480	0.479				
14	0.479					
15	0.439					
16	0.437	0.519				
17	0.436	0.546				
18	0.386	0.454				

Table I3: Anomalous peak heights for F284H and F284W rcPEPCK in $e^{-}/Å^{3}$ corresponding to crystals soaked from 10 to 500 mM KI. Iodides 1 and 2 are bound to the active site, while Iodide 3 represents the allosteric site. The remaining iodides have been numbered by decreasing peak height using the WT 500 mM KI structure as a reference. The data was normalized by dividing peak height of the iodide by the peak height of the corresponding Mn (M1) cation.

	Raw Data		Normalized Data	
Iodide #	**F284H 250mM KI**	**F284W 250mM KI**	**F284H 250mM KI**	**F284W250mM KI**
Mn	**21.83**	**10.91**	**1**	**1**
1	11.49	6.66	0.526	0.610
2	24.49	11.43	1.122	1.048
3	5.73		0.262	
4	12.92	9.22	0.592	0.845
5	10.83	6.2	0.496	0.568
6	10.88	7.36	0.498	0.675
7	7.33	7.69	0.336	0.705
8				
9	6.53	4.42	0.299	0.405
10				
11	5.99	5.86	0.274	0.537
12	5.48	4.02	0.251	0.368
13	6.03		0.276	
14				
15	5.68	4.73	0.260	0.434
16	7.30	5.11	0.334	0.468
17	7.03	4.12	0.322	0.378
18	4.24		0.194	
19	7.05		0.323	
20	6.99	4.28	0.320	0.392
21	5.58		0.256	
22	5.29	4.34	0.242	0.398
23	5.00		0.229	
24	5.00		0.229	
25	4.66	4.29	0.213	0.393
26		5.10		0.467
27		5.29		0.485

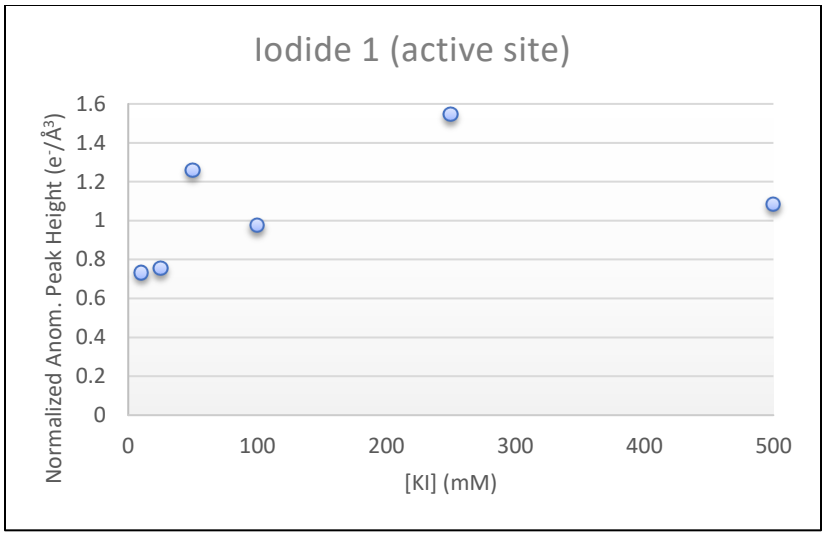

Figure I1: Plot of normalized anomalous peak height for iodide 1 located in the active site.

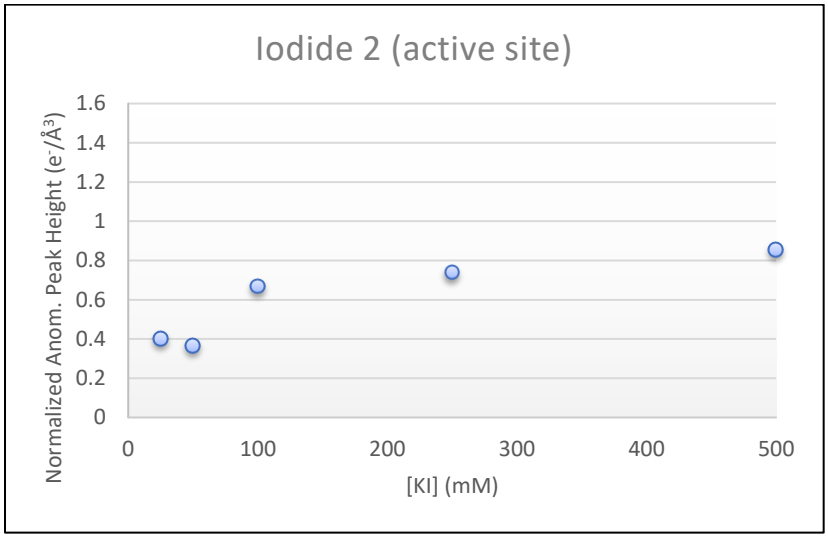

Figure I2: Plot of normalized anomalous peak height for iodide 2 located in the active site.

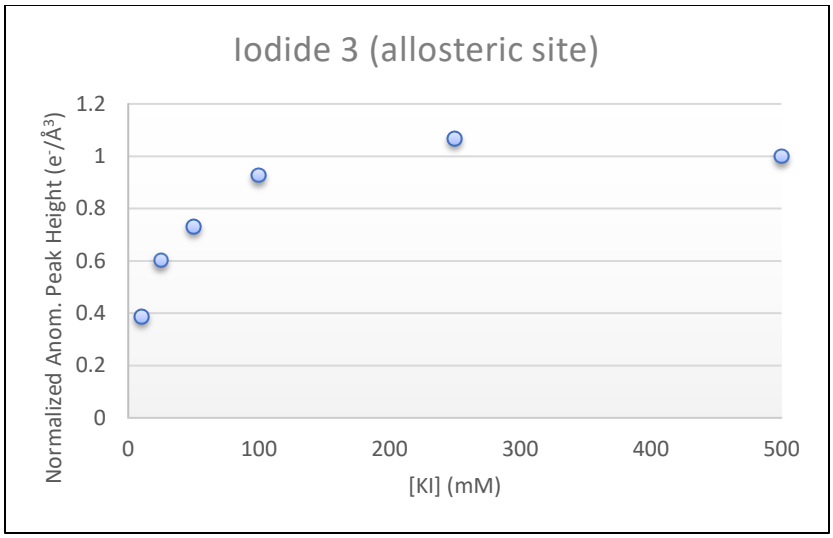

Figure I3: Plot of normalized anomalous peak height for iodide 3 located in the allosteric site.

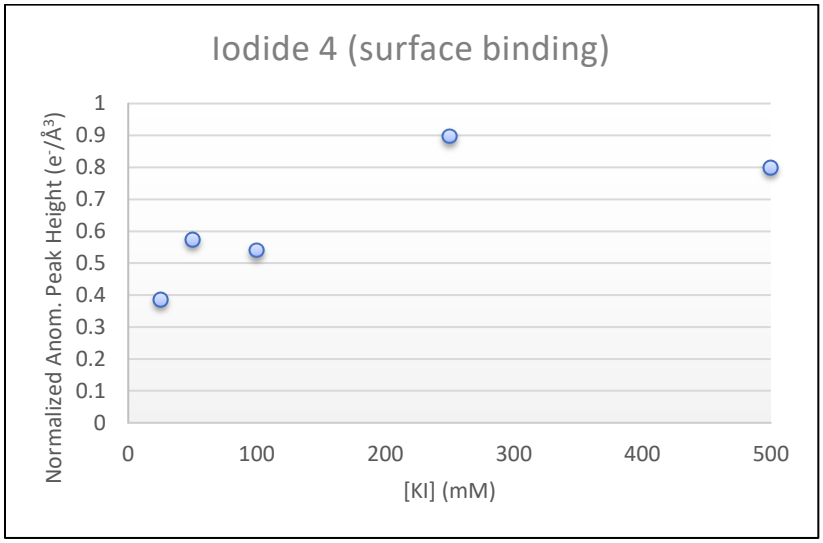

Figure I4: Plot of normalized anomalous peak height for iodide 4 located on the surface of PEPCK.

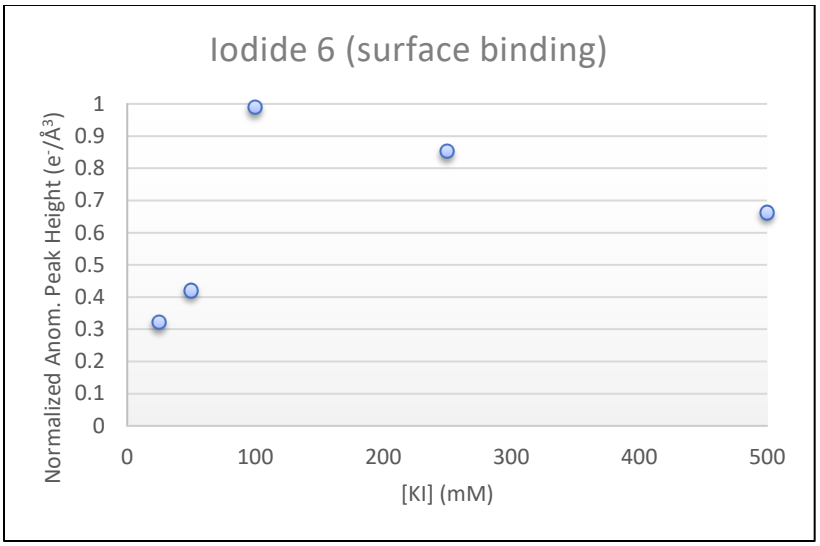

Figure I5: Plot of normalized anomalous peak height for iodide 6 located on the surface of PEPCK.